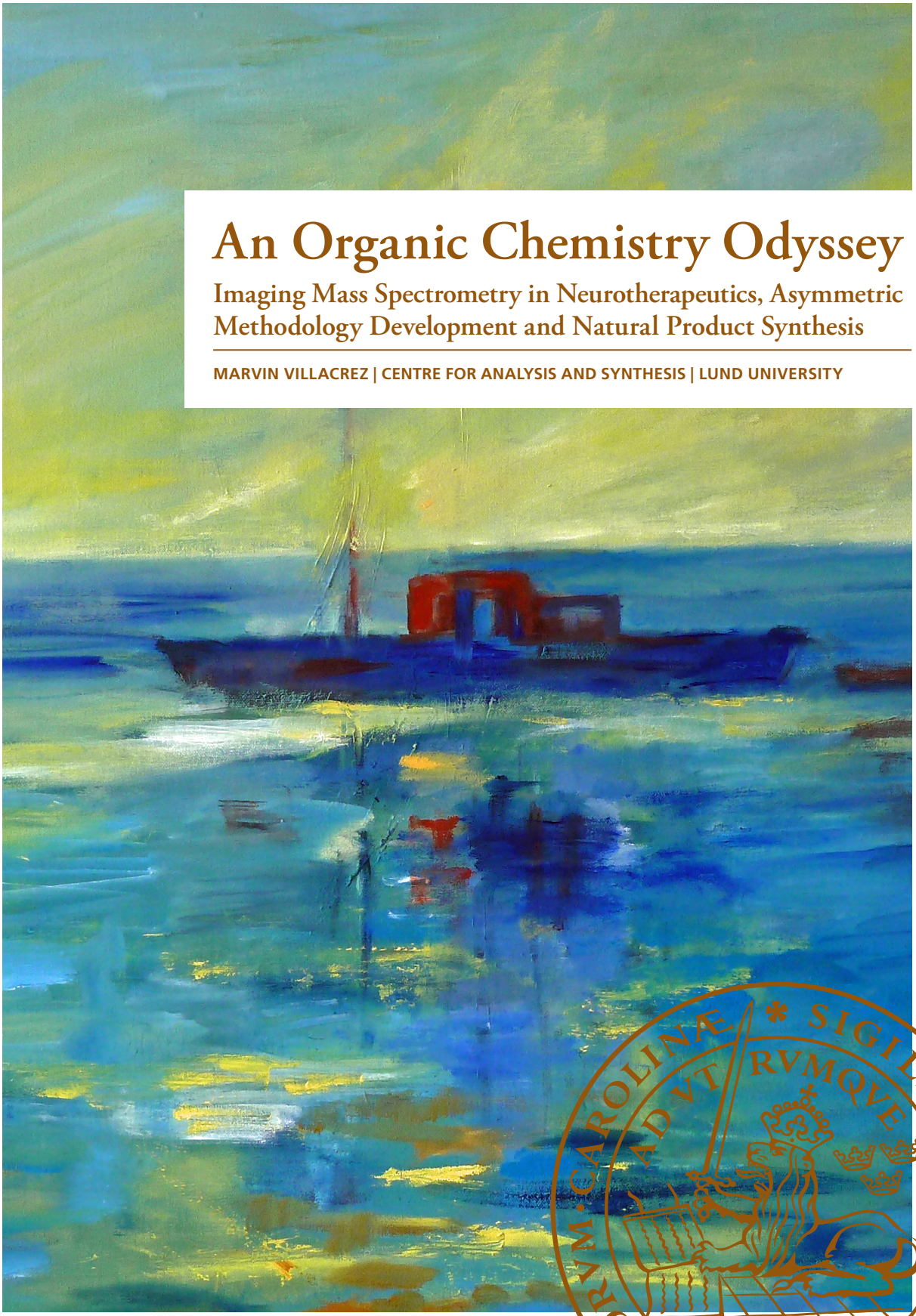

An Organic Chemistry Odyssey

Imaging Mass Spectrometry in Neurotherapeutics, Asymmetric Methodology Development and Natural Product Synthesis

MARVIN VILLACREZ | CENTRE FOR ANALYSIS AND SYNTHESIS | LUND UNIVERSITY

An Organic Chemistry Odyssey

An Organic Chemistry Odyssey

Imaging Mass Spectrometry in Neurotherapeutics, Asymmetric Methodology Development and Natural Product Synthesis

Marvin Villacrez

LUND
UNIVERSITY

DOCTORAL DISSERTATION

by due permission of the faculty of Science, Lund University, Sweden.
To be defended at Kemicentrum.

Lecture Hall K:C, 14.00. Friday, May 17, 2024

Faculty opponent
Prof. Luke Odell, Uppsala University, Sweden

Organization	**Document name**
LUND UNIVERSITY Centre for Analysis and Synthesis	Doctoral Thesis
	Date of issue 2024-05-17
Author: Marvin Villacrez	

Title and subtitle: An Organic Chemistry Odyssey – Imaging Mass Spectrometry in Neurotherapeutics, Asymmetric Methodology Development and Natural Product Synthesis

Abstract: The development of imaging technologies and brain models is crucial for advancements in neurotherapeutic drug discovery and development. They assume a critical role in evaluating essential parameters such as drug blood-brain barrier (BBB) permeation, distribution, and metabolism, all of which are vital for the development of safe and effective medications. In the first part of this thesis, we explore how the antipsychotic drug clozapine (CLO) and its two primary metabolites, *N*-desmethylclozapine (NDMC) and clozapine-*N*-oxide (CNO), permeate the blood-brain barrier and how they are distributed as well as metabolised within the brain. This investigation is conducted primarily in a desert locusts (*Schistocerca gregaria*) *ex vivo* brain model by employing Imaging Mass Spectrometry (IMS), specifically Matrix Assisted Laser Desorption Ionization Imaging Mass Spectrometry (MALDI-IMS) as imaging tool. IMS leverages the capabilities of traditional Mass Spectrometry (MS) but in a two-dimensional format, enabling the creation of ion intensity maps that disclose the precise spatial distribution of molecules within analysed samples. Notably, IMS achieves mapping without the need for molecular imaging probes.

Our study was carried out by subjecting isolated desert locust brains to incubation in solutions containing the studied drugs for durations of 15 and 45 minutes. This unique *ex vivo* approach allowed us to investigate the isolated behaviour of the drugs within the brain, free from the influence of systemic contamination.

Obtained ion intensity maps revealed that CLO exhibits a notable capacity to traverse the BBB. After a 15-minute incubation period, the drug was primarily located at the brain tissue's periphery. However, following a 45-minute incubation, it was distributed throughout the entire brain. The maps also reveal that CLO is readily metabolised to NDMC within the brain, with its distribution mirroring that of CLO. Interestingly, these findings diverge significantly from the NDMC administration studies. In the maps derived from these experiments, it becomes apparent that NDMC exhibits a constrained ability to penetrate the BBB, as its distribution remains predominantly limited to the tissue edges even after 45 minutes of incubation. Regarding CNO incubation experiments, the resulting maps clearly illustrate its highly restricted ability to penetrate the BBB, demonstrating an even lower BBB permeability than that observed for NDMC. Furthermore, the maps show the presence of both CLO and NDMC, indicating that CNO is susceptible to brain metabolism. This discovery holds significant implications in the context of CNO's use in the Designer Receptors Activated only by Designer Drugs (DREADD) technique, where it is employed with the assumption of its pharmacological inactivity. The presence of CLO and NDMC, both of which exhibit pharmacological activity on dopamine, serotonin, and muscarine receptors, could potentially have influenced the interpretation of results in previously conducted DREADD studies. This suggests the necessity for a reevaluation of the outcomes of these experiments.

The ion intensity maps generated in this study are groundbreaking and showcase the potential of our IMS desert locust brain model platform for application in both pharmaceutical research and neuroscience.

The second part of this thesis targets the development of small-molecule compounds. It presents an efficient enantioselective approach for the synthesis of vicinal amino alcohols and our attempts towards the total synthesis of Aspidophylline A. By using asymmetric transfer hydrogenation (ATH) on β-amido-α-keto esters undergoing dynamic kinetic resolution (DKR); we managed to synthesise various *anti*-β-amido-α-hydroxy esters in high yields and excellent diastereo- and enantioselectivities. The protocol developed for the hydrogenations uses HCO_2H:NEt_3 (2:5) as a hydrogen source and RuCl[(*R,R*)-FsDPEN](*p*-cymene) as a catalyst, both commercially available.

Our work on Aspidophylline A has brought us to the synthesis of an advanced tricyclic intermediate.

Key words: Imaging Mass Spectrometry, Clozapine, Drug metabolism, Drug distribution Blood-brain barrier, Asymmetric transfer hydrogenation, Dynamic kinetic resolution, Natural product synthesis.

Classification system and/or index terms (if any)

Supplementary bibliographical information		**Language:** English
ISSN and key title		**ISBN** 978-91-8096-034-2 (printed) 978-91-8096-035-9 (e-version)
Recipient's notes	**Number of pages** 86	Price
	Security classification	

Signature Date 2024-03-25

An Organic Chemistry Odyssey

Imaging Mass Spectrometry in Neurotherapeutics, Asymmetric Methodology Development and Natural Product Synthesis

Marvin Villacrez

LUND
UNIVERSITY

Department of Chemistry
Centre for Analysis and Synthesis
Lund University
P.O. Box 124
SE-221 00 Lund University
Sweden

ISBN 978-91-8096-034-2 (Printed)
ISBN 978-91-8096-035-9 (Digital)

Printed in Sweden by Media-Tryck, Lund University
Lund 2024

To my Parents and Life Companion Gabby,

without whose never-ending support, love, and encouragement
this thesis would never have been completed.

List of Publications

I. **Evaluation of Drug Exposure and Metabolism in Locust and Zebrafish Brains Using Mass Spectrometry Imaging.**

M. Villacrez, K. Hellman, T. Ono, Y. Sugihara, M. Rezeli, F. Ek, G. Marko-Varga and R. Olsson

ACS Chemical Neuroscience. 2018, (9)8, 1994-2000

II. **Enantioselective synthesis of *anti*-β-amido-α-hydroxy esters via asymmetric transfer hydrogenation coupled with dynamic kinetic resolution.**

M. Villacrez and P. Somfai

Tetrahedron Lett. 2013, (54)38, 5266-5268

III. **A Rapid Construction of an Advanced Tricyclic Intermediate for the Total Synthesis of Aspidophylline A.**

M. Villacrez and P. Somfai

Manuscript in preparation.

Contribution to the Publications

I. I contributed to the design and planning of drug administration experiments and executed the main portion of the MALDI-IMS experiments. Furthermore, I conducted the majority of the data analysis and drafted the manuscript.

II. I participated in both the design and planning phases of the experiments, and subsequently conducted all of them. Furthermore, I conducted all compound analyses, specifically setting up and operating an HPLC apparatus for chiral analysis.

III. I conducted all experiments as well as analyses and was actively involved in planning and designing alternative synthetic routes. I also composed the initial draft of the manuscript.

Abbreviations

ATH	Asymmetric Transfer Hydrogenation
ATH/DKR	Asymmetric Transfer Hydrogenation Coupled with Dynamic Kinetic Resolution
BMEC	Brain microvascular endothelial cell
CHCA	α-cyano-4-hydroxy cinnamic acid
CLO	Clozapine
CNO	Clozapine-*N*-oxide
CNS	Central Nervous System
CYP	Cytochrome p450
DKR	Dynamic Kinetic Resolution
DMP	Dess-Martin Periodane
DPAE	2-amino-1,2-diphenylethanol
DPEN	1,2-diphenylethane-1,2-diamine
ee	Enantiomeric excess
GABA	Gamma-Aminobutyric Acid Receptor
H&E	Haematoxylin and Eosin Stain
IMS	Imaging Mass Spectrometry
LC-MS	Liquid Chromatography Mass Spectrometry
MALDI	Matrix Assisted Laser Desorption Ionisation
MALDI-IMS	Matrix Assisted Laser Desorption Ionisation Imaging Mass Spectrometry
NDMC	*N*-desmethylclozapine
TH	Transfer hydrogenation
TsDPEN	*N*-p-Tosyl-1,2-diphenylethylenediamine
Ts_2O	*p*-Toluenesulfonic Anhydride

Preface

In the dynamic field of drug discovery and development, the journey from initial concept to medication is fundamentally a collaborative endeavour. Central to this challenging pursuit, organic chemistry emerges as a foundational pillar. It offers the universal language of arrows and bonds that unite the diverse array of sciences essential in this quest, encompassing medicine, biology, pharmacology, physics, bioinformatics, and material sciences, among many others. Organic chemists, as masters of the discipline, not only bridge the fields through their mastery of the language but also bring the knowledge and craftsmanship essential to the design and manufacturing of medications. Now, in an era of unprecedented technological advancements, the significance of organic chemists in pharmaceutical research has never been greater.

This thesis stands as a testament to the enduring significance of organic chemistry in pharmaceutical research. It consists of two parts. In the first part, we engage in the collaborative spirit of science to explore the fate of the gold standard antipsychotic, CLO, in an isolated brain. Our objective was to gain insights into its brain dynamics, with the broader goal of developing an IMS-brain platform for advancing research in neuropharmacology and neuroscience (*Paper 1).* The second part delves into the core principles of organic chemistry, focusing on developing small molecule compounds, the backbone of modern pharmacology (*Paper 2, manuscript 1*). For a more comprehensive account of the second part, I kindly refer you to ref. 1.[1]

Table of Contents

1. Imaging Mass Spectrometry in Neurotherapeutics

The 20th century was marked by remarkable scientific and technological progress, leading to the development of Central Nervous System (CNS) medications that completely reshaped the treatment landscape for neurological disorders. However, a major limitation of the majority of these medications lies in their focus on providing symptomatic relief or slowing disease progression, rather than offering definitive cures. In addition, their wide-ranging side effects significantly impact patient quality of life. As a result, many patients on CNS drug treatments gain only limited benefits, creating an urgent need for more effective neuropharmaceuticals. Unfortunately, this demand is expected to surge exponentially in the near future, driven mainly by the global rise in life expectancy. Despite the critical situation, the CNS drug discovery and development sector has experienced a notable slowdown in innovation in recent years.[2-5]

For a neurotherapeutic agent to elicit its effects, it must reach the intended target within the brain at adequate concentrations. Should it fail to meet these essential requirements, its efficacy is compromised. However, even if the drug meets these basic criteria, it can still produce secondary pharmacological or toxic effects, potentially compromising its safety profile. Challenges in developing drugs that strike an optimal balance between efficacy and safety contribute significantly to the limited innovation in neurotherapeutics.[6, 7]
The BBB (figure 1.1) plays a central role in issues related to drug efficacy. It acts as the brain's chemical gatekeeper, preventing undesirable solutes (*e.g.*, toxins and pathogens) carried in the blood from entering the brain whilst allowing passage to life's essentials (*e.g.*, amino acids, glucose, and oxygen)[8].

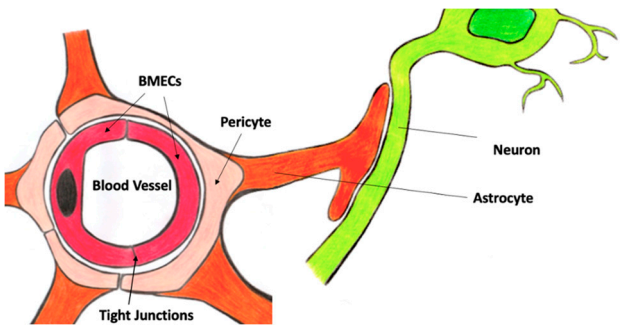

Figure 1.1: The BBB is primarily constituted by brain microvascular endothelial cells (BMECs), pericytes, astrocytes, neurons, and tight junction protein complexes. The tight junctions effectively restrict the passage of drugs to the brain by sealing the intercellular spaces between BMECs.

Non-endogenous compounds, such as drugs, typically encounter restricted passage through the BBB, limiting their ability to reach therapeutic concentrations in the brain, thereby impacting their efficacy[9, 10]. Challenges in efficacy can also stem from a drug's neuropharmacokinetic (neuro*PK*) profile, encompassing its absorption, distribution, metabolism, and elimination. Of particular concern are distribution and metabolism, as these processes also can introduce safety concerns through drug distribution to unintended brain regions or the generation of toxic metabolites[11, 12].

Assessing a drug's ability to permeate the BBB and its neuro*PK* profile is critically important in modern CNS drug discovery and development. To this end, imaging techniques such as immunohistochemistry, Positron Emission Tomography (PET), and autoradiography play a key role[13-15]. They provide spatiotemporal information in a visual manner on how drugs traverse the BBB, distribute within the brain, and undergo metabolism.[16]. Despite these techniques' undeniable contribution to neurotherapeutics, their use is to a great extent limited by their reliance on molecular imaging probes, introducing limitations such as restricted image resolution, dynamic range, and sensitivity[17]. The use of imaging probes also requires prior analyte knowledge and precludes the simultaneous assessment of multiple analytes.[18] This presents a significant challenge in drug metabolism studies, given that a single drug can be metabolised into a wide array of compounds, many of which typically are unknown[19]. Moreover, discerning between the parent drug and metabolites that retain the imaging probe introduces yet another layer of complexity.

Addressing these limitations, IMS emerges as a powerful technique used to visualise the spatial distribution of molecules within a sample (figure 1.2). Owing to its foundations in MS, the technique offers the unique ability to target molecules (*e.g.,* drugs, drug metabolites, glycans, lipids, peptides and biomacromolecules) by using their molecular masses as fingerprints. IMS can perform this directly within tissues or cells, without the requirement for molecular imaging probes.

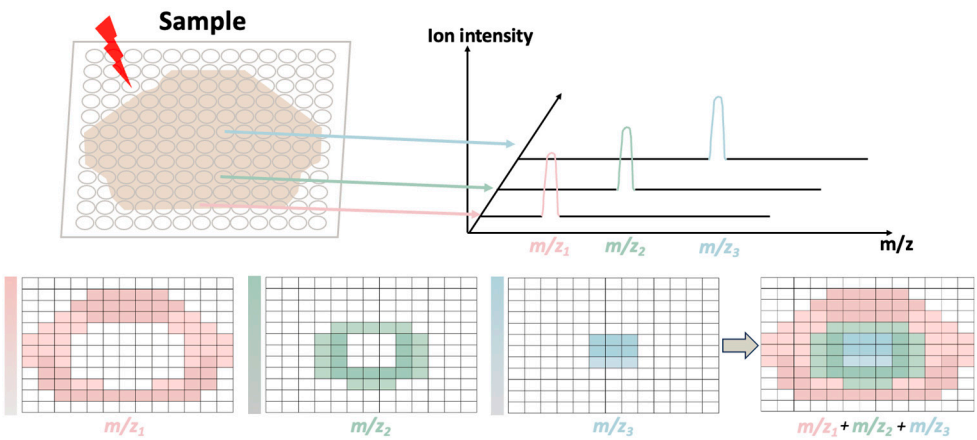

Figure 1.2: In IMS, MS data is integrated with spatial coordinates from analysed tissue samples, enabling the creation of ion intensity maps that visually depict the distribution of analytes.

Bypassing the need for molecular imaging probes enables the detection of previously unknown analytes and the simultaneous mapping of multiple compounds. IMS also offers high sensitivity and an extensive dynamic range, features essential for detecting both trace and abundant drugs. Additionally, it is a non-destructive technique, preserving sample integrity for further analysis.[20-22]

With its remarkable mapping capabilities, IMS has rapidly found a central role in neurotherapeutics. For instance, Liu and co-workers used the technique to uncover novel insights into ketamine's potential mechanism of action as an antidepressant[23]. Furthermore, in a landmark study conducted in 2013, ion intensity maps were able to illuminate the diverse effects of tumour vasculature on drug BBB permeation, providing novel perspectives on brain drug delivery[24]. IMS particularly excels in drug metabolism studies for its capability to simultaneously analyse the wide range of metabolites generated upon drug administration. This is highlighted in a study by Castellino's team on the antiretroviral drug candidate Fosdevirine, responsible for causing seizures in trial subjects. IMS was instrumental in identifying early unknown metabolites, one of which accumulated in myelinated axons, thus yielding novel insights into the possible mechanisms underlying epilepsy-related seizures[25, 26]. Moreover, within the novel field of personalised medicine, IMS is increasingly considered a valuable tool. It has been used for mapping the distribution of chemotherapeutics and corresponding metabolites in brain tumours. The generated ion intensity maps have disclosed patient-exclusive drug penetration and metabolic patterns, allowing for a safer and more efficient treatment approach[27, 28].

This research project is dedicated to exploiting the benefits of IMS to investigate the distribution, metabolism, and permeation across the BBB of CLO, NDMC, and CNO in an isolated neural system.

1.2 Background

IMS is built upon the principles of MS, an analytical technique able to separate ionised atoms and molecules by exploiting differences in the ratios of their charges to their respective masses (m/z)[29]. In an IMS experiment, the sample is ionised at a discrete point, known as a pixel, where a mass spectrum is recorded. This procedure resembles a conventional MS experiment. However, following the acquisition of the first pixel, the tissue sample is repositioned to ionise another part of the sample, where data collection resumes to generate a new pixel. This process iterates until the desired number of pixels has been collected. The recorded MS data is finally compiled to produce an ion intensity map that depicts the distribution of analytes in the scanned tissue sample (figure 1.2).[30, 31]

IMS incorporates a range of platforms, each characterised by unique ionisation sources that offer similar but slightly different properties in terms of speed,

sensitivity, chemical scope and image resolution[32]. The most common ionisation sources are MALDI, secondary ion mass spectrometry (SIMS), and desorption electrospray ionisation (DESI). SIMS-IMS is renowned for its exceptional resolution, allowing for subcellular studies, yet this advantage is counterbalanced by high costs and tedious sample preparations. Of all three platforms, DESI-IMS requires the least sample preparation, but this asset typically comes with limited image resolution. When the identification of a broad spectrum of compounds is required, with a proper balance of resolution and cost-effectiveness, MALDI-IMS is often regarded superior.[32-34]

MALDI-IMS was introduced in the late 1990s. The technique relies on irradiation energy from a UV or IR laser and a chemical matrix that absorbs photons at the laser's wavelength. The matrix plays a crucial role in the desorption/ionisation of analytes and their subsequent transportation to the mass analyser.[35, 36]
MALDI-IMS has primarily gained popularity for being a soft ionisation technique, meaning that analyte ionisation occurs with minimal fragmentation. This attribute is particularly appealing in drug metabolism studies, where the detection and identification of a broad range of metabolites typically presents a formidable challenge. Furthermore, MALDI's soft ionisation enables the examination of biomacromolecules, a critical aspect in neurotherapeutics given these compounds' role in physiological and pathological conditions.[37, 38]
In the early stages of MALDI-IMS development, image resolution was primarily hindered by the size of the laser irradiation area. However, recent technological advancements have enabled laser areas as small as 1-10 µm. Given the average diameter of mammalian brain cell soma is around 20 µm, these technical improvements have significantly advanced MALDI-IMS in neurotherapeutics.[39-42]

IMS has been successfully employed for studying drug metabolism[43], drug-drug interactions[44], mapping the distribution of neurotransmitters[45], and the impact of drugs on biochemical pathways within mammalian brains[46]. Unfortunately, the use of mammals in research is resource-intensive, time-consuming and raises ethical concerns[47, 48]. In response, brain organoids have emerged as a recent alternative[49]. These miniature, simplified versions of the human brain offer a valuable platform for testing potential neurotherapeutic interventions in a more efficient and ethically acceptable manner. Yet, the lack of a BBB in these brain models limits their usefulness in CNS drug research.
In recent years, insects and zebrafish have become viable options[50, 51]. Insects offer several advantages as experimental animals compared to mammals, including short life cycles, low cost for rearing and few ethical concerns, facilitating high throughput screening of lead compounds[52-54]. Zebrafish, also possess unique features such as external development, optical transparency during embryogenesis, high fecundity, short generation times and limited ethical implications[55, 56]. Most importantly, both insects[57-59] and zebrafish[60-62] own a well-developed BBB, structurally and functionally homologous to their human counterpart (figure 1.3).

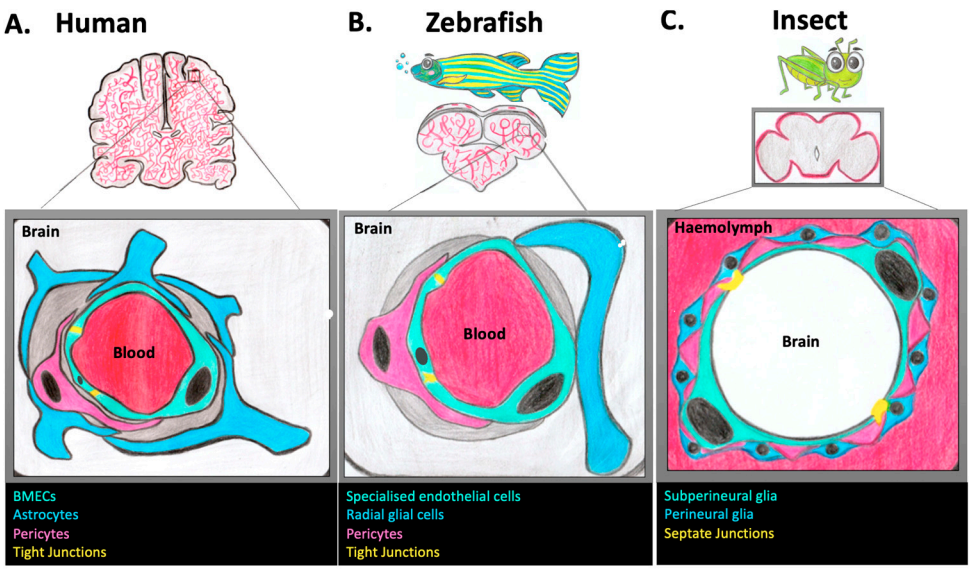

Figure 1.3: The human BBB (**A**) compared to its counterparts in zebrafish and insects. In zebrafish (**B**), the major BBB constituents are specialised endothelial cells (green), tight junctions (yellow), pericyte cells (pink), and radial glial cells (blue). The insect BBB (**C**) main components are perineural cells (blue) and subperineural glial cells (green). The latter are tightly connected in between by septate junctions (yellow), which share close similarities with tight junctions.

Although the use of insects initially might seem of limited use in neurotherapeutics due to the vast differences between insects and mammals, numerous neurotransmitters are shared between species. These include acetylcholine, GABA, glutamate, serotonin, dopamine, and tyramine[63, 64]. Insects also possess octopamine, which exhibits functional similarities to norepinephrine in mammals[65]. In addition, the interaction between P-glycoprotein and CYP3A4, renowned for its role in eliminating xenobiotics from the brain, has been corroborated as conserved across species[66]. These neurochemical resemblances suggest the presence of shared endogenous synthetic pathways and protective mechanisms against foreign substances between species, underscoring the potential of using insect brains in neurotherapeutics[67].
Zebrafish also hold notable neurochemical commonalities with mammals, including shared neurotransmitters, and enzymes for synthesis and metabolism[68-70].

The similarities between vertebrate and invertebrate brains make both insects and zebrafish attractive options for studying drug dynamics in neurotherapeutics. However, insects boast an open circulatory system, endowing them with a unique advantage over vertebrates. The open circulatory system allows insects to withstand severe physical trauma. A decapitated insect body can live up to several days after losing its head, dying only because, without a head, it cannot eat or drink. Not only can the body survive decapitation, but the isolated head can also thrive. Studies on

decapitated insects have reported that the isolated heads can continue to exhibit basic reflexive behaviours and sensory responses for several hours to a few days after decapitation. If the head is fed, it can survive up to several weeks.[71-74] With precise surgical techniques, the insect brain can be detached and removed without impairing its function for at least one hour[75, 76]. In stark contrast, removing the brains of vertebrates results in an immediate cessation of neural activity due to their closed circulatory system. Insects thus offer a direct avenue for exposing the brain to particular drugs, presenting an exclusive opportunity to investigate drug BBB permeation, distribution, and metabolism in the brain without the concern of peripheral contamination.

In this project, IMS is employed to investigate the spatiotemporal dynamics of CLO and its two main metabolites, NDMC and CNO (scheme 1.1). Our work centres around the desert locust *ex vivo* BBB/brain model developed by Nielsen and colleagues in 2013[75, 76]. Using this model, BBB permeation, distribution and Cytochrome p450 (CYP) for these compounds were assessed in a previously conducted in-house study[66]. However, this study, involving brain homogenates analysed with Liquid Chromatography-Mass Spectrometry (LC-MS), did not provide any spatiotemporal information on how CLO, NDMC and CNO behave within the brain. To address this gap, this project substitutes LC-MS for MALDI-IMS intending to obtain visual information on the permeation of these compounds through the BBB as well as their distribution and metabolic patterns within the brain. Additionally, our investigation was enriched with a proof-of-concept study on zebrafish (*Danio rerio*), aimed at studying where the drug accumulates within the fish brain.

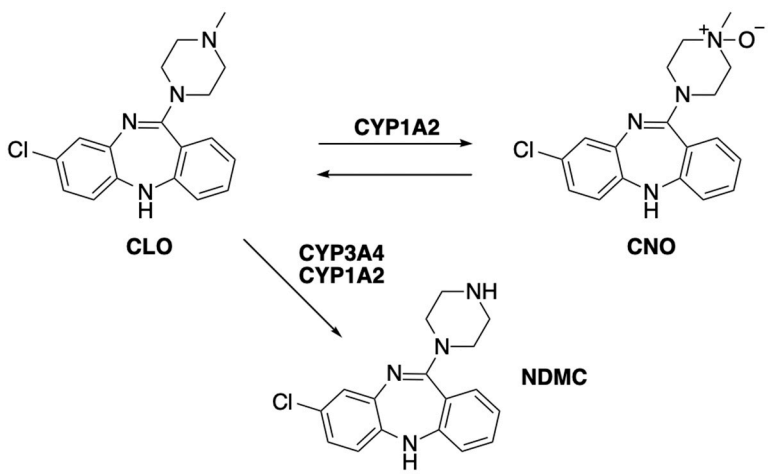

Scheme 1.1: Structures of CLO, NDMC and CNO. CLO is primarily converted to NDMC through an *N*-demethylation reaction, catalysed mainly by CYP3A4 and CYP1A2. CYP1A2 is also the key enzyme in the oxygen insertion process that forms CNO from CLO.[77]

1.3 Aim and Motivation

Developing drugs that have both an optimal neuro*PK* profile and a good ability to cross the BBB is a significant challenge. One of the main reasons for this is the lack of advanced analytical tools to thoroughly study the interaction between drugs and the BBB, as well as their fate within the brain[78-80]. Furthermore, the limitations of existing brain models present an additional obstacle in this process[81-83]. This thesis aims to leverage the advantages of MALDI-IMS as well as the desert locust *ex vivo* model and create an IMS-insect brain tool to drive advancements in neurotherapeutics. To evaluate this tool, our focus was directed towards the study of antipsychotics. Remarkably, since the introduction of chlorpromazine (the first antipsychotic developed) over sixty years ago, no drug that does not block dopamine receptors has been approved for the treatment of psychotic disorders. Given the global impact of psychotic disorders, which rank among the most burdensome and costly mental health illnesses, the scarcity of innovation within this field is concerning.[84-86]

Among several interesting drugs, CLO was selected because, although it ranks as the top antipsychotic of choice, its mechanism of action remains elusive. It is widely accepted that its mild dopamine-2 receptor affinity and a high affinity for serotonin 5_{HT2A} receptors are responsible for part of its pharmacological effects[87]. However, recent studies have begun to challenge this perspective. Two research teams, independently of each other, have proposed a mechanism where NDMC is responsible for the effects of CLO-based therapies[88]. NDMC stands out for its unique ability to bind to dopamine-2 and dopamine-3 receptors, exerting a weak partial agonist activity at these sites similar to that of the novel third-generation antipsychotics aripiprazole and bifeprunox[89]. NDMC's remarkable pharmacological profile suggests the possibility that CLO may function as a prodrug, with NDMC serving as the true active compound. To evaluate NDMC's potential role as an active substance, it underwent a phase IIb trial but demonstrated no efficacy compared to placebo. Peripheral dose-dependent side effects ruled out the option of assessing higher NDMC doses, leaving its precise role in therapies based on CLO unclear.

Beyond pharmacological applications, CLO is of interest for its second major metabolite, CNO, a widely employed ligand in DREADD technology[90]. DREADDs are specially engineered receptors that can be selectively activated by ligands, enabling precise manipulation of neural activity. This technique was notably demonstrated in 2007 by Roth and colleagues[91], who implanted DREADDs into mouse brains, which, when activated by CNO, facilitated precise exploration of diverse neurological and psychiatric conditions. The study established the foundation for the widespread use of CNO in DREADD studies. However, ever since, CNO has been the subject of debate and scrutiny due to concerns about its ability to cross the BBB and its integrity as an inert ligand.[92, 93]

1.4 Experimental Procedure and Sample Preparation

After dissecting the insect brains, we exposed them to the desired drugs for 15 and 45 minutes. Test solutions were prepared at 3 µM, a common practice in similar *ex vivo* studies[66, 75, 76]. However, for CNO experiments, a concentration of 10 µM was required. Through extensive literature research, we found that the most commonly utilised matrices in MALDI-IMS studies of small molecule compounds are 2,5-dihydroxybenzoic acid, sinapic acid, and α-cyano-4-hydroxycinnamic acid (CHCA). After rigorous evaluation of all three matrices, we ultimately selected CHCA for allowing simultaneous ionisation of the three analytes. Following numerous trial-and-error experiments and significant time investment, we successfully developed an instrumental protocol for assessing CLO, NDMC, and CNO simultaneously in brain tissues (See Appendix).

Regarding sample preparation, it was imperative to optimise procedures to preserve the native spatial distribution and molecular identity of the analytes in the brain samples. While protocols involving heat stabilisation of tissue samples were initially contemplated, flash-freezing emerged as our preferred method, as this technique swiftly halts all post-mortem processes and prepares the brain for sectioning.[94-96]

At the beginning of our investigation, sample preparation steps were evaluated on zebrafish brains. Despite the small size of the zebrafish brain, obtaining brain tissue samples in a reproducible manner was successfully achieved with hands-on experience. The desert locust brain, in contrast, provided significant handling challenges, owing to its limited size (averaging a volume of approximately 2 x 1.5 x 1 mm^3) and its gelatinous texture. In addition, its tooth-like shape (figure 1.4) predisposed it to deformation. While we expected challenges during sectioning, difficulties arose as early as flash-freezing. Achieving consistent brain morphology after freezing proved to be a challenging task, primarily because the insect brain was susceptible to significant deformation upon contact with surfaces and dissection instruments.

Figure 1.4: Desert locust brain shape from a coronal plane perspective.

In MALDI-IMS experiments, tissue sections are typically obtained through a frozen sectioning procedure. However, before sectioning can proceed, the sample must be securely attached to the cutting equipment. To this end, adhesives are commonly used. Unfortunately, these adhesives are polymer-based, giving rise to ion suppression effects in our experiments. To overcome this issue, we opted to use

Millipore water/ice as the adherent medium, but attachment difficulties remained. Finally, due to the cryostat's temperature hovering around -20°C, a feasible adherent was found in saturated NaCl Millipore solution. The transformation of brine into ice occurred at a measured pace, allowing for controlled and reasonably reproducible brain attachment. It must be stressed, however, that the use of brine was not free from issues and only by gaining handling experience was its use as an adherent satisfactory.

The thickness of the tissue sections was yet another critical parameter to evaluate. While thin sections (< 12 µm) were too fragile to handle, thicker sections (> 20 µm), adversely affected both the quantity of tissues that could be collected and the intensity of ion signals. We opted to collect tissue sections with a thickness of 14-18 µm. Without any additional treatment beyond tissue drying, tissue sections were mounted onto microscope slides for the application of the matrix. We evaluated the most inexpensive matrix application method first, consisting of using a painter's airbrush. This time-consuming approach required high demands on individual savoir-faire to obtain acceptable and reproducible results. Satisfactory matrix coating was obtained first after acquiring considerable experience, however, while the method was reproducible between applications by the same operator, person-to-person variability was high. Because of this, we decided to introduce the use of an automated sprayer to obtain reproducible results. While the sprayer indeed is capable of generating excellent coatings and highly reproducible results, the optimisation of the many instrumental parameters was very time-consuming.

1.5 Results

The ion intensity maps obtained from brains incubated with 3 µM CLO solution for 15 minutes demonstrate permeation of the drug through the BBB (figure 1.5**A**.) The presence of NDMC can also be observed (figure 1.5**B**), with its distribution pattern resembling that of CLO. Upon extending the incubation to 45 minutes, CLO is distributed throughout the brain tissue sample, with the highest relative concentration located along the edges (figure 1.5**C**). The presence of *in situ* generated NDMC after 45 minutes can be observed in figure 1.5**D**. CNO could not be detected in either of the CLO experiments.

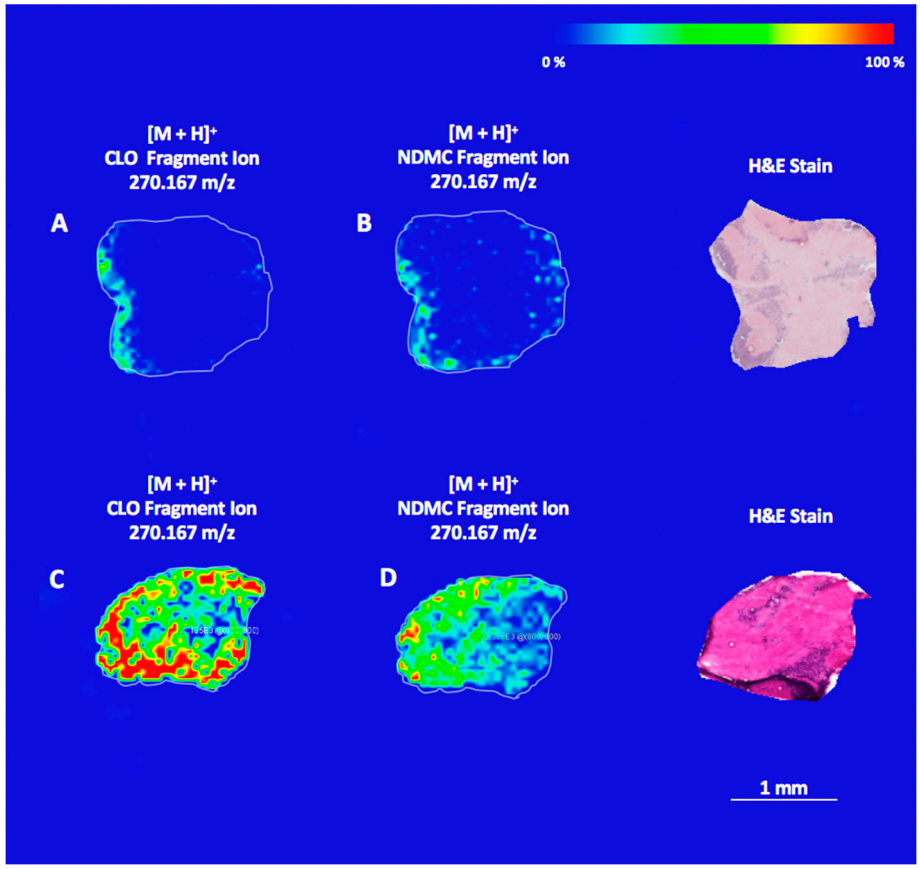

Figure 1.5: Ion intensity maps for incubation of brains with CLO. The drug permeates the BBB after 15 minutes of incubation (**A**) and is predominantly found along one edge of the brain. Metabolism to NDMC (**B**) is evident. Incubation for 45 minutes (**C**) reveals the distributions for CLO throughout the entire brain section with a similar distribution for NDMC (**D**). The colour-coded gradient bar shows the relative concentrations of the analysed compound. Scale bar = 1 mm. H&E staining was performed on analysed tissue samples.

Figure 1.6 illustrates brain incubation in a 3 µM NDMC solution. The 15-minute incubation is shown in figure 1.6**A**, and the 45-minute experiment in figure 1.6**B**. Neither CLO nor CNO were detected in these experiments.

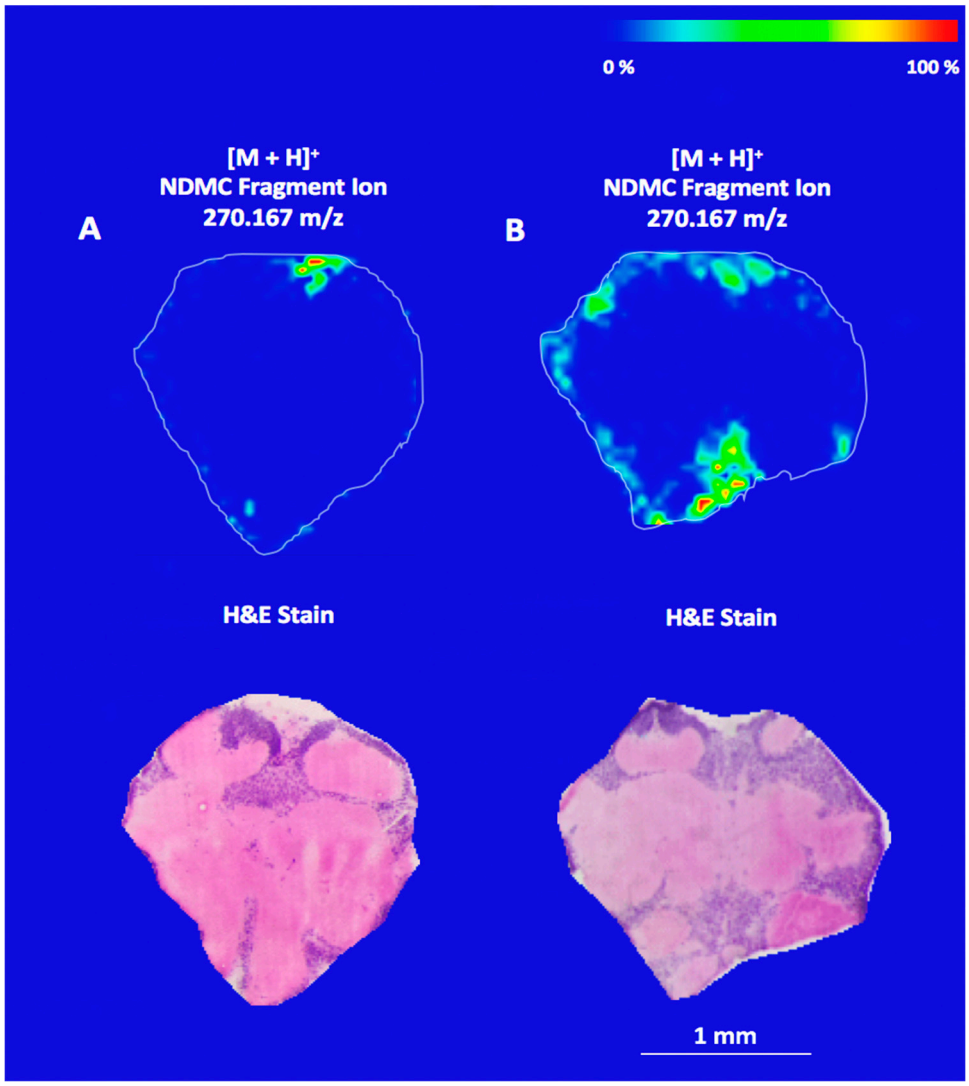

Figure 1.6: Ion intensity maps for brains incubated with NDMC for 15 minutes (**A**) reveal a limited drug penetration through the BBB. Extending the incubation time to 45 minutes (**B**) shows that NDMC permeates the BBB to a greater extent. The colour-coded gradient bar shows the relative concentrations of the analysed compound. Scale bar = 1 mm. H&E staining was performed on analysed tissue samples.

In the CNO experiments, the drug concentration was set to 10 µM, as none of the analytes were identifiable at lower concentrations. No compounds were detected in the 15-minute experiment. However, when incubation was set to 45 minutes, it became evident that CNO exhibits limited BBB permeability (figure 1.7**A**). Additionally, both CLO and NDMC were detected, as shown in figure 1.7**B** and 1.7**C**, respectively. All three compounds were primarily confined to the edges of the brain.

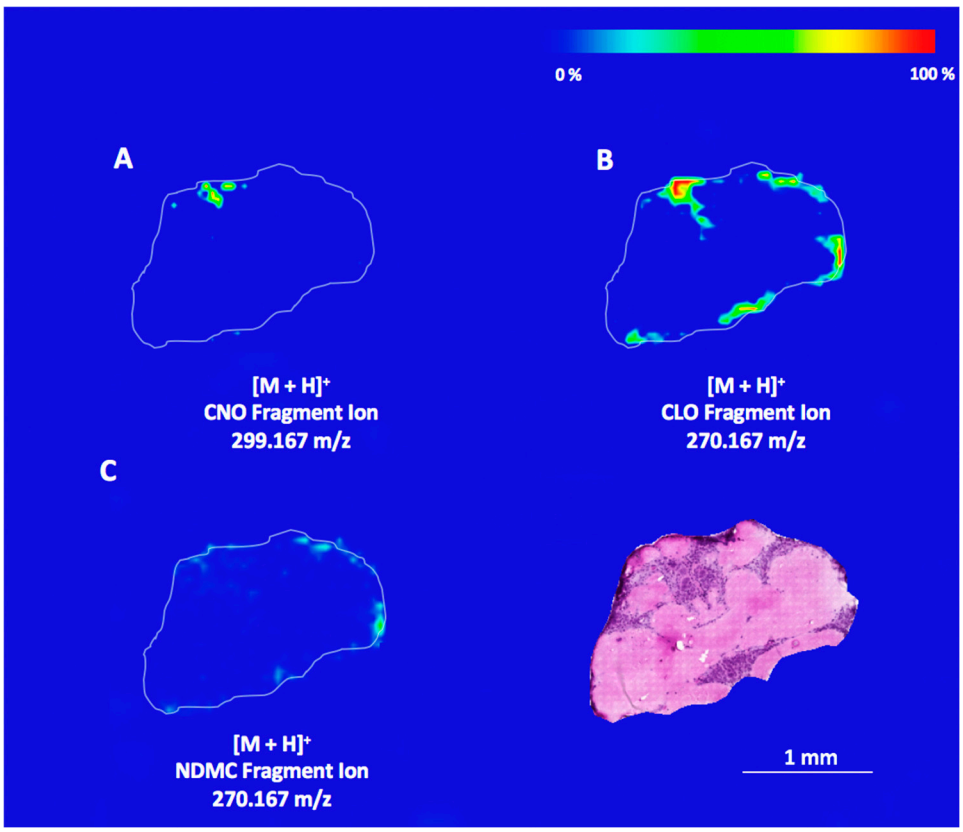

Figure 1.7: Ion intensity maps for brains incubated with CNO for 45 minutes Only a scarce amount of CNO was observed after 45 minutes of incubation at 10 µM (**A**). CLO was detected (**B**) as well as NDMC (**C**). The colour-coded gradient bar shows the relative concentrations of the analysed compounds. Scale bar = 1 mm. H&E staining was performed on analysed tissue samples.

Our study was amplified with a proof-of-concept study where adult zebrafishes were exposed to a 10 µM CLO aquatic environment. After 10 minutes of drug exposure, the zebrafish demonstrated behavioural and movement impairment. Noteworthy was how the shoal was dispelled, and individual fish were constantly at the top of the tank and repeatedly breaching the surface, while the fish in the control tank

showed no such activity. The disturbed *in vivo* activity indicated that a minimum effective concentration of CLO had been achieved. Unfortunately, we ran out of time at this stage, and we could only analyse the dissected brains after 10 minutes of CLO exposure. From figure 1.8, we can deduce high concentrations of CLO in the ventricular cavity (VCa) and optic tectum (TeO).

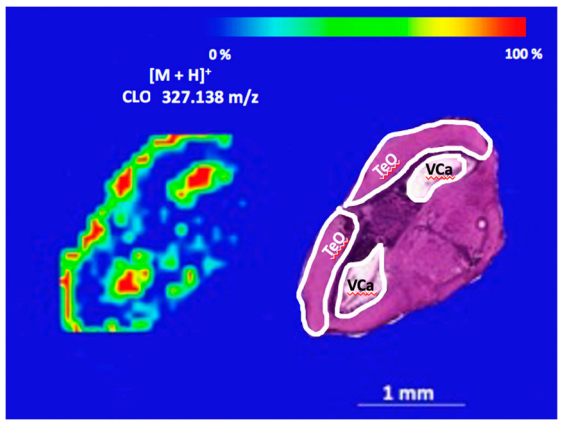

Figure 1.8: Brain tissue for zebrafish exposed to 10 µM of CLO for 10 minutes. Correlating the MALDI ion intensity maps with H&E histology stains reveals that CLO is abundant in the VCa and the TeO. The colour-coded gradient bar shows the relative concentrations of the analysed compound. Scale bar = 1 mm

1.6 Discussion

A distinct contrast in BBB permeability and distribution patterns was observed between CLO and NDMC. In the 15-minute NDMC experiment, figure 1.6**A**, the drug exhibited only minimal presence within the tissue section, with its distribution predominantly confined to the periphery even after 45 minutes, figure 1.6**B**. In contrast, CLO was localised at the tissue edge after 15 minutes, figure 1.5**A**, and over 45 minutes, figure 1.5**C**, the drug was spread throughout the entire tissue sample, implying a higher BBB permeability for CLO. Regarding drug metabolism, the maps reveal a significant difference in NDMC's distribution when derived from CLO metabolism versus its direct administration. Especially, in the 45-minute CLO experiment, NDMC is found distributed throughout the brain tissue, contrasting sharply with its edge-concentrated presence when directly administrated. These observations align with the outcomes of the phase IIb studies on NDMC, where its limited BBB permeability was posited as a potential factor in the inability to administer higher doses.

Unfortunately, we were unable to confirm the presence of CNO in the CLO experiments, making it essential to consider and address technical issues that might

have influenced this outcome. During the optimisation of the experimental protocol, CNO was the most difficult compound to detect. Adjusting the laser energy level allowed us to detect CNO, but regrettably, this compromised the detection of CLO and NDMC. Consequently, we settled on laser energy of 14 μJ for all experiments, as this level represented a compromise strategy to attain acceptable simultaneous ionisation of all three compounds. Additionally, it is crucial to recognise that the nature of MALDI-IMS renders it susceptible to localised ion suppression effects. This means that when CNO is co-localised with CLO and NDMC, it can lead to its reduced ionisation. Since our earlier LC-MS investigations revealed CNO to be present at significantly lower concentrations than both CLO and NDMC under identical experimental conditions, ion suppression is a likely explanation for the ostensible absence of CNO.

Having addressed the technical challenges in detecting CNO, we can now delve deeper into the CLO experiments in figure 1.5. Notably, the presence of NDMC in regions where CLO is absent can be observed. These observations could stem from the technical issues recently mentioned. Alternatively, we posit that these observations may be rationalised by three potential factors: 1) fast metabolism of CLO in certain brain compartments due to high or specific CYP expression, 2) different diffusion rates and 3) different efflux rates between CLO and NDMC.

Focusing now on the CNO experiment, the ion intensity map displayed in figure 1.7**A** confirms its penetration through the BBB. However, its limited presence and the requirement of a 10 μM administration concentration implies that CNO is not an efficient BBB permeant. What also stands out is the appearance of CLO and NDMC, as shown in figure 1.7**B** and figure 1.7**C**, respectively. This indicates that CNO is susceptible to brain metabolism, questioning its previously assumed inertness in DREADD experiments. If CLO is produced in concentrations high enough to influence neural receptors, its pharmacological properties could potentially lead to complex and unintended effects beyond those mediated by CNO acting at DREADDs. The complexity deepens when considering NDMC, which exhibits distinct neuropharmacological activity compared to CLO. Given its potentially unique actions, NDMC might have had a more significant impact on DREADD studies than CLO. Obviously, this takes us into the realm of speculation, and more research is needed before jumping to conclusions.

In the proof-of-concept experiments conducted on zebrafish, the ion intensity map in figure 1.8 discloses a noticeable accumulation of CLO in both the VCa and the TeO. The TeO, analogous to the superior colliculus in mammals, serves as a crucial processing centre for sensory information. We hypothesise that the accumulation of CLO within the TeO may be linked to the observed impairments in behaviour and movements, although further research is essential to investigate this potential correlation. Additionally, we observed the accumulation of CLO within the VCa. The observed accumulation potentially corroborates the hypothesis of a less developed BBB at the VCa in zebrafish.

This study underscores our platform's potential for studying the spatiotemporal dynamics of drugs. However, a key limitation was the MALDI-IMS sensitivity. In the previous in-house study using LC-MS, experiments at concentrations as low as 1 µM were able to be conducted, and CNO was reliably detected in both CLO and CNO experiments, highlighting the superior sensitivity of LC-MS. Besides instrumental limitations, considerable challenges with sample preparation need to be tackled for our approach to gain relevance in neurotherapeutics. From the moment the desert locust brain is detached from the skull, it poses handling difficulties due to its minute size and peculiar shape. First, it is difficult to avoid affecting its morphology when held with a pincer, and the deformation will carry over to the sectioning stage because of snap-freezing. Moreover, preparing the small brain for subsequent sectioning poses challenges, and the method of using brine to attach the brain is suboptimal due to the adverse effects of salts in MS. Moreover, the insect brains are fragile and proved difficult to section without embedding support. Consequently, we assessed the use of the embedding material Optimal Cutting Temperature (OCT) compound, documented in various MALDI-IMS studies. However, its use ended up introducing contaminants into our experiments due to OCT's polymeric nature, thus complicating analyte detection. The lack of suitable embedding support made it extremely challenging to achieve consistent sectioning of the desert locust brain, representing the most significant limitation of our study.

1.7 Conclusions

Before concluding our work, it is crucial to stress that our findings were derived from studies on animal brains. This requires a cautious interpretation of the results. That being said, our insect experiments have yielded intriguing results. The stark differences observed in BBB permeation and brain distribution between NDMC and CLO administration experiments are remarkable. Moreover, administering CLO leads to widespread distribution of NDMC throughout the brain, unlike direct NDMC administration. These findings suggest that CLO can potentially act as a prodrug for NDMC, but further investigation is required to validate these findings. In addition, our research challenges the notion of CNO as a suitable ligand in DREADD studies, suggesting that observed effects might have resulted from *in situ* generation of CLO or NDMC.

Broadly, our study confirms the potential of using IMS in tandem with the *ex vivo* brain model to expedite preclinical BBB permeation and neuro*PK* lead screenings. However, our approach is still in its infancy and requires further development, in particular regarding sample preparation.

1.8 Future Perspectives

Our findings highlight the potential of our IMS/ insect brain tool. However, a pivotal factor in extending and refining our study lies in the identification of an appropriate embedding material for brain sectioning. Such a material would not only facilitate the replication of our initial experiments, potentially yielding more precise results, but also expand the scope of our research to include the examination of additional compounds. Moreover, a suitable embedding material would enable us to section the brain from edge to edge, thereby allowing us to create comprehensive 3D ion intensity maps of the desert locust brain. These 3D maps would not only allow us to study BBB permeation and neuro*PK* more comprehensibly but also delve into the neurochemistry of the brain by targeting neurotransmitters, lipids, glycans, proteins, and peptides. The creation of such 3D brain maps would undoubtedly make a significant impact in the field of neurotherapeutics and insect neuroscience. Finding the right embedding support is therefore a top priority for broadening the scope of our future research.

2. Asymmetric Methodology Development and Towards the Total Synthesis of Aspidophylline A

The discovery and development of new pharmaceuticals is a tremendously complex undertaking that requires general and specific knowledge of a wide range of scientific areas such as pharmacy, medicine, and chemistry. The role of organic chemistry in the pharmaceutical industry continues to be one of the main drivers in the drug discovery process, and developments in modern drug discovery go hand in hand with developments in organic synthesis methodology.

2.1 ATH/DKR for high Enantioselectivy in the Synthesis of Vicinal Amino Alcohols *(Paper II)*

Hydrogenation reactions are among the most fundamental transformations in organic synthesis[97] and often used in the reduction of many functionalities including alkenes,[98] ketones,[99-101] and imines [102-104]. Direct hydrogenation with a pressure of H_2 gas and transfer hydrogenation (TH) are the two employed strategies for hydrogenation, and both utilise transition-metal catalysts involving first-, second-, and third-row transition metals of groups 8, 9, 10, and 11. However, while direct hydrogenation uses molecular hydrogen to achieve reduction, TH uses hydrogen sources other than H_2 (*g*), such as secondary alcohols and formate. TH becomes an attractive alternative to direct hydrogenation for a couple of reasons, 1) the method does not require hazardous pressurised H_2 gas nor elaborate experimental setups, 2) the hydrogen sources are normally readily available, low-cost, and easy to handle, 3) the metal catalysts involved are normally readily accessible and robust. [105, 106]

A remarkable milestone in the field was the introduction of chiral ligands to achieve enantioselective hydrogenations. In particular, the catalyst derived from the chiral monotosylated diamine 1,2-diphenylethane-1,2-diamine (TsDPEN) and the resultant Ru complex (Ru-TsDPEN) has received considerable attention due to its versatile application in a wide range of enantioselective reactions.[107-110] The Ru-TsDPEN catalyst, developed by Noyori and co-workers (scheme 2.1), can catalyse

reactions with high enantioselectivity, up to 99% ee, and is one of the most popular catalyst for asymmetric transfer hydrogenation (ATH) reactions.[111]

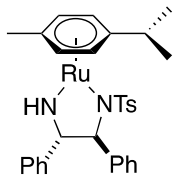

Scheme 2.1: Noyori's Ru-TsDPEN catalyst.

Recently, the field of metal-catalysed ATH has been boosted by applying dynamic kinetic resolution (DKR).[112] In DKR a racemic substrate possesses a configurationally labile stereogenic centre that undergoes racemization during the reaction (scheme 2.2). In this case, S_R is converted with a rate constant of k_R to diastereomers P_{RR} and P_{RS} while S_S is converted to P_{SR} and P_{SS} with a different rate constant, k_s. If $k_{rac}>k_r>>k_s$ the enantioselective synthesis of one diastereomer is possible and can be obtained in 100 % theoretical yield from racemic starting material. Hence, the asymmetric transfer hydrogenation assisted by dynamic kinetic resolution (ATH/DKR) can be used as an efficient technique for establishing the stereochemistry of two adjacent stereogenic centres.[113-115]

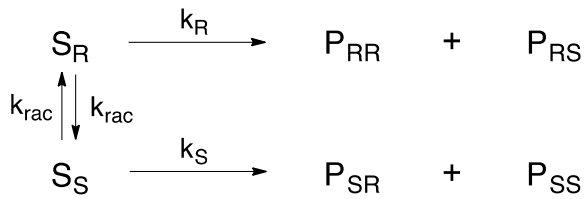

Scheme 2.2: Dynamic kinetic resolution.

Modern applications of ATH/DKR include, transformations β-ketoamides,[116] α-substituded-β-ketoesters,[116-118] cyclic α-oxy-β-ketoamides,[119] 1,3-diketones,[120-122] 1,2-diketones[123, 124], α-ketophosphonates,[125] 2-substituted-cycloalkanones,[126-128] β-ketosulfones[129]. The approach has emerged as a powerful and practical tool for reduction reactions in both academia and industry, due to its operational simplicity, high reaction rate and enantioselectivity and broad substrate scope. [130, 131]

Enantioselective synthesis of *anti*-α-amido-β-hydroxy esters

The β-amino-α-hydroxy ester functionality, and the related vicinal amino alcohol moiety, are found in various biologically active natural products. The importance of 1,2-amino alcohols is also well recognised in asymmetric synthesis, where the need for chiral auxiliaries and ligands is continuously increasing. Not surprisingly, the asymmetric synthesis of these structures has received considerable attention.

It has been shown that asymmetric transfer hydrogenation (ATH) coupled with dynamic kinetic resolution DKR can be applied to the formation of α-substituted-β-hydroxy esters. Previous reports on ATH/DKR on α-substituted compounds include α-methoxy-β-keto esters[132], α-alkyl-β-keto amides[116], and *N*-Cbz protected α-amido-β-keto ester[118]. The enantioselective synthesis of *anti*-β-hydroxy-α-amido esters using ATH/DKR has earlier been developed in our research group. The approach relies on the stereochemical lability of the α-stereocenter in **2.1** scheme 2.3, allowing for two stereocentres to be introduced in the asymmetric reduction. [113-115]

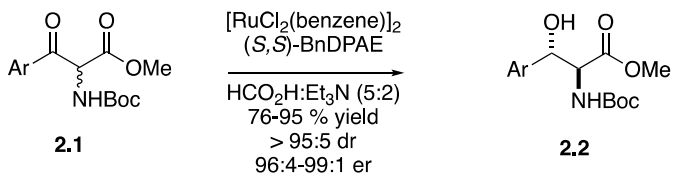

Scheme 2.3: ATH/DKR reactions for the reduction of α-amido-β-keto esters.

Excellent results in terms of yield, diastereo- and enantioselectivities were achieved for a wide range of α-amido-β-keto esters. We rationalised that the high diastereoselectivity resulted from an intramolecular hydrogen bonding in the substrate and became interested if the same methodology could achieve a *syn* diastereoselectivity if applied to a substrate unable to form an intramolecular hydrogen bond. In theory, enantioenriched *syn* α-amido-β-hydroxy esters could be obtained from α-azido-β-keto esters using a similar ATH/DKR approach.[133-137]

To test our hypothesis, we initiated our studies by preparing α-bromo-β-keto ester **2.4** under solvent-free conditions from commercially available keto ester **2.3** and *N*-bromosuccinimide (NBS) (scheme 2.4).[138] Our intension was to transform intermediate **2.4** to the corresponding α-azido-β-keto ester **2.5** through an S_N2 substitution with NaN_3 in DMF.

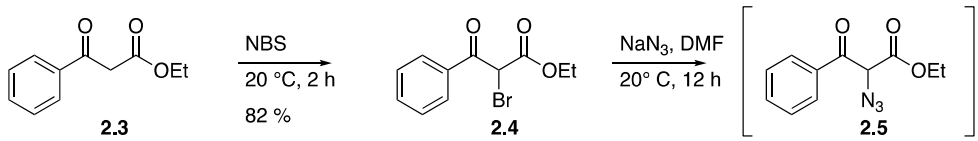

Scheme 2.4: Attempt to prepare azide 2.5 Synthesis of *α*-bromo-*β*-keto ester **2.4**.

However, despite the successful bromination, the rapid and spontaneous decomposition of compound **2.5** during the work-up phase hindered further investigation. We suspect that the formation of bubbles in the reaction mixture indicates the evolution of nitrogen gas. If this is the case, there is a possibility that an α-imino ketone intermediate was generated, although its precise formation within the mixture was not confirmed. Recently, an iron-catalysed alkylazidation of dehydroamino acids using peroxides as alkyl radical precursors has been presented by Waser and co-workers[139].

We redirect our attention to the synthesis of β-amido-α-keto esters, a regioisomer of the previously investigated α-amido-β-keto esters. In theory, enantioenriched β-amido-α-hydroxy esters could be obtained by using a similar ATH/DKR approach to that used for obtaining *anti*-β-hydroxy-α-amido esters. Encouraged by the asymmetric synthesis of diverse glycolic acid scaffolds via ATH/DKR of α-keto esters[140], we began our studies by generating a suitable β-amido-α-hydroxy ester to be evaluated under ATH/DKR conditions. The α-diazo ester **2.6a** was oxidized to the desired keto ester **2.7a** using oxone (scheme 2.5).[130]

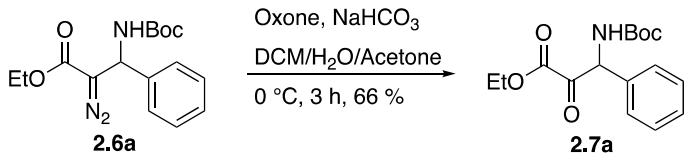

Scheme 2.5: Synthesis of β-amido-α-hydroxy ester **2.7a**.

With substrate **2.7a** in hand, we initiated the ATH/DKR investigations by screening reaction conditions and catalysts (table 2.1).

Table 2.1: Optimization of ATH/DKR reaction conditions.[a]

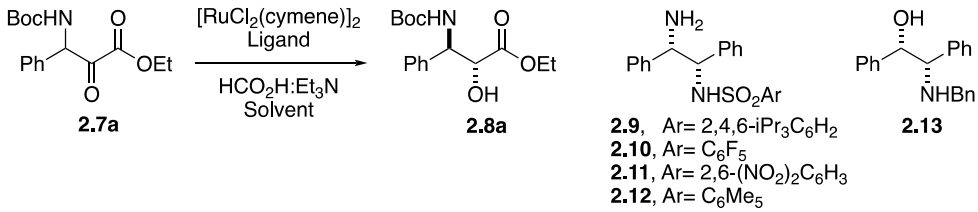

2.7a **2.8a**

2.9, Ar= 2,4,6-$iPr_3C_6H_2$
2.10, Ar= C_6F_5
2.11, Ar= 2,6-$(NO_2)_2C_6H_3$
2.12, Ar= C_6Me_5

2.13

Entry	Ligand	Solvent	Yield[b]	Time	dr[b]	er[c]
1	**2.9**	DMF	95 %	1h	>20:1	94:6
2	**2.10**[d]	DMF	95 %	1h	>20:1	95:5
3	**2.11**	DMF	73 %	5h	>20:1	78:22
4	**2.12**	DMF	97 %	1h	>20:1	81:19
5	**2.13**	DMF	88 %	0.5 h	>20:1	83:17
6	**2.10**[d]	Toluene	90 %	1 h	>20:1	90:10
7	**2.10**[d]	DMSO	94 %	1 h	>20:1	94:6
8	**2.10**[d]	Et_3N:HCO_2H(2:5)	93 %	1 h	>20:1	92:8
9[e]	**2.10**[d]	H_2O:CH_2Cl_2	95 %	1 h	3:1	n.d.[f]

[a]Reactions performed by heating $[Ru(p\text{-cymene})Cl_2]_2$ (0.05 eq.) and the ligand (0.15 eq.) in 2-propanol (0.1M) at 80 °C for 1 h. After cooling to rt the solvent was removed and the catalyst was added to a solution of **2.7a** (1 eq., 0.1 M) and HCOOH/Et_3N (5:2, 5 eq.). [b]Yield and *dr* determined by ^1H NMR spectroscopy of the crude reaction mixture. [c]Determined by chiral HPLC analysis of the crude reaction mixture. [d]Commercially available catalyst RuCl[(*R,R*)-FsDPEN](*p*-cymene) (0.05 eq.), purchased from Sigma-Aldrich, was added to a solution of **2.7a** (1 eq., 0.1 M) and HCO_2H/Et_3N (5:2, 5 eq.). [e]Reaction performed using emulsion conditions, see ref 53. [f]Not determined.

Substrate **2.7a** was screened using a series of catalyst complexes based on the (*p*-cymene)RuCl(ligand) framework. Chiral ligands **2.9-2.12** were manufactured based on the (*S,S*)-1,2-diphenylethane-1,2-diamine (DPEN) framework and differed by the aryl group attached to the sulfonamide. Chiral ligand **2.13** was prepared by a reductive amination between (*S,S*)-(-)-2-amino-1,2-diphenylethanol and benzaldehyde. Ester **2.8a** was obtained in good yields and excellent diastereoselectivity, favouring *anti* stereochemistry in all observed reactions. We rationalised that the diastereofacial selectivity was the result of the formation of an intramolecular hydrogen bond between the *N*-H and carbonyl moiety (figure 2.1). This conformation is believed to facilitate the hydride addition from the sterically least hindered side of the carbonyl group, thus leading to the observed *anti* diastereomer while the polar Felkin–Ahn model predicts the wrong diastereoselectivity.

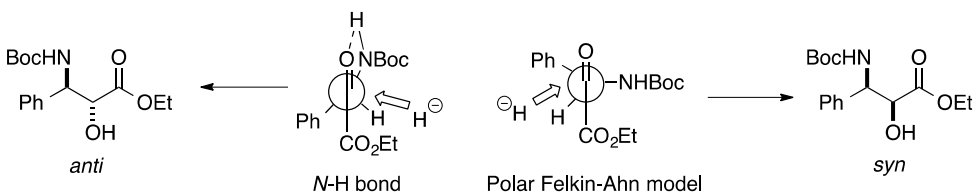

Figure 2.1: Models offering different relative stereochemistry.

The enantioselectivity was determined by chiral HPLC analysis and revealed a wide range of variations in enantiomeric ratios (*er)* for the experiments performed in DMF (Entries 1-5). The optimal reaction conditions used the pentafluorinated DPEN derivative **2.10** as ligand affording **2.8a** in excellent 95:5 *er* (Entry 2). The influence of the solvent system on the ATH/DKR reaction was also investigated. Unfortunately, solvent systems other than DMF resulted in inferior results, (Entries 6-9), with the emulsion showing exceptionally poor diastereomeric ratios (*dr)* (Entry 9). Another observation was the decrease in *dr* from 20:1 (*anti:syn*) to 3:1 (*anti:syn*) when the reaction was left overnight. This is probably due to an epimerisation process with the low *dr's* representing the equilibrium ratio. Finally, we were surprised by the large difference in the observed reaction rates (1 h) compared to the ATH/DKR of the regioisomeric α-amido-β-keto esters (5-7 days). We hypothesise that the difference in reactivity can be attributed to an increased electrophilicity of the α-carbonyl carbon due to the induction effect exerted by the vicinal electron-withdrawing ester functionality.[141] With the optimised conditions in hand we set out to investigate the scope of the reaction (table 2.2).

Table 2.2: Substrate scope of the ATH/DKR reaction.[a]

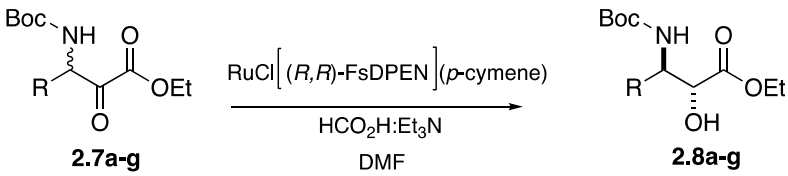

2.7a-g **2.8a-g**

Entry	R	Yield[b]	**2.7/2.8**	dr[b]	er[c]
1	Ph	95 %	**a**	>20:1	95:5
2	*p*-MeO-C_6H_5	96 %	**b**	>20:1	98:2
3	*m*-Br-C_6H_5	68 %	**c**	>20:1	62:38
4	*p*-F-C_6H_5	89 %	**d**	>20:1	99:1
5	*p*-Me-C_6H_5	96 %	**e**	>20:1	94:6
6	3-thiophene	92 %	**f**	>20:1	94:6
7	*o*-Br-C_6H_5	78 %	**g**	>20:1	94:6

[a]Catalyst RuCl[(*R,R*)-FsDPEN](*p*-cymene) (0.05 eq.), was added to a solution of **2.7a-g** (1 eq., 0.1 M) and HCOOH/Et_3N (5:2, 5 eq.). [b]Yield and *dr* determined by ^{1}H NMR spectroscopy of the crude reaction mixture. [c]Determined by chiral HPLC analysis of the crude reaction mixture.

The results presented in table 2.2 show a reliable performance of the ATH/DKR methodology for α-amido-β-keto esters. The only exception is found in compound **2.7c**, unfortunately offering **2.8c** in moderate yield and poor *er* (Entry 3).

Conclusions

We have developed a method for the ATH/DKR transformation of β-amido-α-keto esters into β-amido-α-hydroxy esters. Our method provides the corresponding *anti*-β-amido-α-hydroxy esters in high yields, *dr*'s and *er*'s by using commercially available ligand–catalyst complex, thus making it easy and operationally straightforward to perform.

2.2 Towards the Enantioselective Synthesis of Aspidophylline A *(Manuscript I)*

Our recent advancements in the carbopalladation-carbonylation domino sequence inspired our core strategy for the synthesis of Aspidophylline A (figure 2.2).[142, 143] Aspidophylline A was isolated in 2007 by Kam and co-workers from the Malayan stem-bark *Kopsia Singaporensis*. The remarkable structural features of Aspidophylline A, coupled with its notable bioactivities, have rendered it an attractive target molecule for the synthetic community. [144]

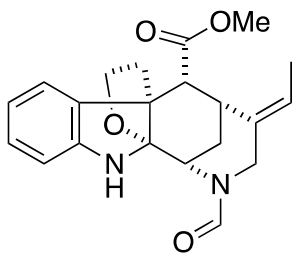

2.9

Figure 2.2: Aspidophylline A.

Retrosynthetic Analysis

A noteworthy feature of Aspidophylline A is its intricate pentacyclic framework, entailing a bridged [3.3.1] bicycle and five stereogenic centres, including an all-carbon quaternary one. The target compound was planned to be derived from tetracyclic intermediate **2.10** (scheme 2.6) after formylation of the piperidine nitrogen and oxygen-carbon bond formation yielding tetrahydrofuran ring **E**. The key transformation in the total synthesis was envisioned to be a domino carbopalladation–carbonylation sequence, converting compound **2.11** to **2.10** by installing **D** ring followed by *syn* insertion of carbon monoxide. We envisioned that intermediate **2.11** could be synthesized from species **2.12** after *N*-alkylation.

Formation of the tricyclic framework **2.12** was projected to occur by implementation of a regioselective S_N2 aminolysis ring-opening reaction[145] of aziridine **2.14** to afford diamine **2.13**, followed by an intramolecular Heck reaction[146]. We aimed to introduce the precise stereochemistry in the final target compound by executing an asymmetric regioselective aziridination on diene **2.15** to yield bicyclic compound **2.14**.

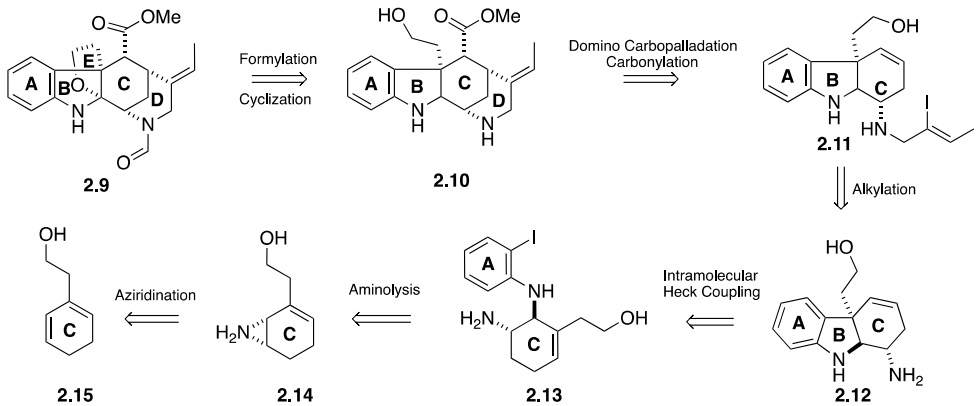

Scheme 2.6: Retrosynthetic scheme for the total synthesis of Aspidophylline A.

With a retrosynthetic approach in hand, we launched our studies towards the synthesis of Aspidophylline A by identifying a feasible synthetic route to conjugated diene **2.15**.

Progress of the Synthesis

The protected analogue **2.19** of 1,3-diene **2.15** was synthesized by tandem enyne metathesis[147-150] between 1,5-cyclooctadiene **2.18** and alkyne **2.17** (scheme 2.7).[151] Alkyne **2.17** was obtained after protection of commercially available alcohol **2.16**.

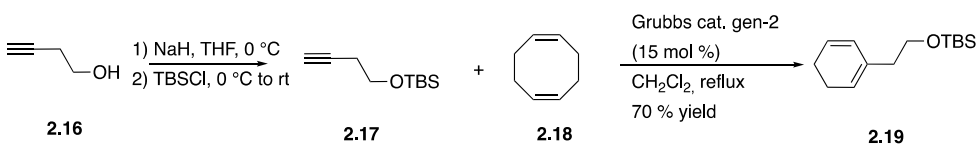

Scheme 2.7: Synthesis of protected diene **2.19**.

With species **2.19** in hand, we continued the synthesis towards Aspidophylline A (scheme 2.8). Our synthetic route offered rapid access to the tricyclic scaffold **2.23**. Compound **2.19** was transformed into the bicyclic aziridine **2.21** by using

aziridination chemistry developed by Komatsu[152]. The olefin aziridination reaction offered a non-typical insertion of the nitrogen into the least substituted double bond, *i.e.,* the bond expected to possess the lowest reactivity towards metal nitrene complexes like **2.20**. No regioisomer of **2.21** was found in the reaction mixture despite modest yields of 48 %. Without further optimisation, we continued with the synthesis via ring opening[145] of aziridine **2.21** with 2-iodoaniline in DMF, a reaction offering near quantitative yield of the vicinal diamine **2.22.** The tricyclic compound **2.23** was prepared through Heck coupling in high yields.

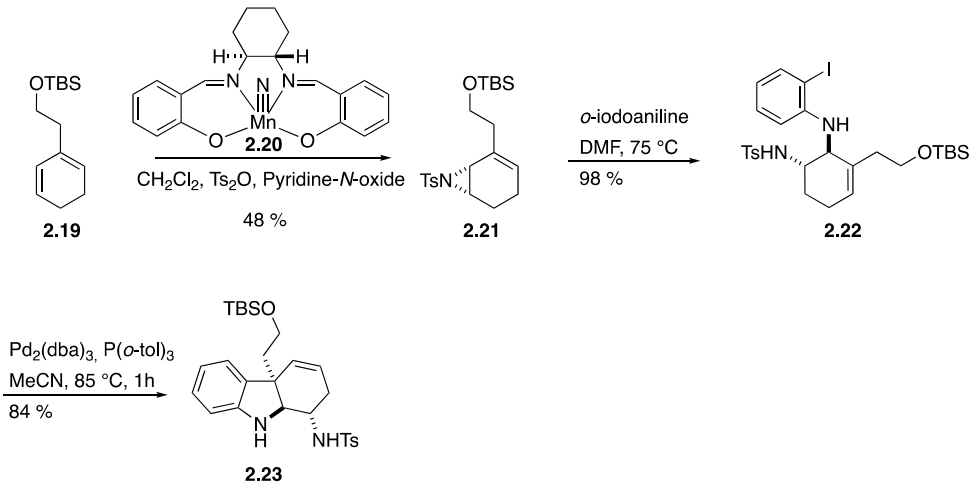

Scheme 2.8: A three-step approach to compound **2.23** starting from diene **2.19**.

Our aim to promptly evaluate the carbopalladation–carbonylation key step was hindered by the unexpected chemoselectivity in the projected *N*-alkylation step. Unfortunately, the sulphonamide nitrogen proved to be the least reactive nitrogen upon treatment with allylic bromide **2.25**[153]. After protection of intermediate **2.23** with 4-methoxybenzyl chloride (scheme 2.9) to yield compound **2.24**, several known procedures for *N*-alkylation of sulphonamides were evaluated for the synthesis of **2.26**. (Table 2.3).[154-157]

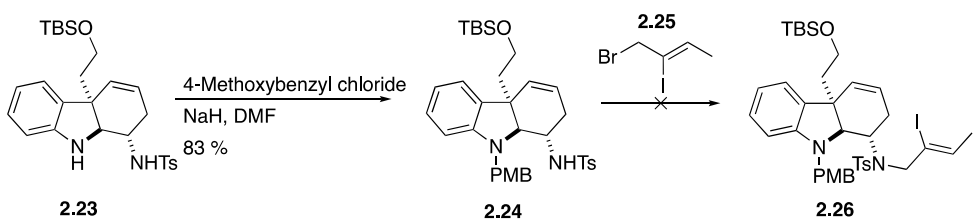

Scheme 2.9: Attempts to prepare compound **2.26**.

Table 2.3: Screening of reaction conditions for the alkylation of compound 2.24.

Entry	Base	Solvent	Temperature	Result
1	K_2CO_3	DMF	rt	no rxn
2	Cs_2CO_3	MeCN	rt	no rxn
3	Cs_2CO_3	MeCN	50 °C	decomp.
4	*t*-BuOK	THF	0 °C	decomp.
5	NaH	DMF	0 °C	decomp.
6	LDA	THF	-78 °C to rt	decomp.

Alkali metal carbonates were not basic enough to perform the desired *N*-deprotonation at room temperature (Entries 1-2). Both the addition of allylic bromide **2.25** or methyl iodide caused no alkylation of **2.24**. The addition of 18-crown-6-ether (0.1 eq.) to the reaction mixture proved also to be unsuccessful. Before turning our attention towards stronger bases, the influence of the temperature was studied using caesium carbonate as base (Entry 3). However, the colour of the reaction mixture went from yellow to black even before alkene **2.25** was added and TLC as well as NMR analysis indicated decomposition of the starting material. Due to the lack of deprotonation, we decided to use stronger deprotonating agents. Unfortunately, the use of *t*-BuOK, NaH and lithium diisopropylamide (LDA) prompted decomposition of compound **2.24**. Consequently, an alternative strategy for the introduction of the *N*-alkyl moiety had to be developed (scheme 2.10). It was envisioned that tetracycle **2.28** could be obtained after the introduction of furan ring **E** and alkylation with **2.25**, thus, allowing us to pursue the critical carbopalladation–carbonylation sequence. If successful, this approach can potentially provide the pentacyclic framework **2.29** only in need of formylation to conclude the total synthesis.

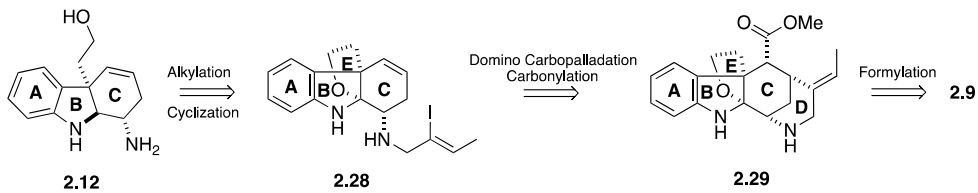

Scheme 2.10: Diversification of initial route towards Aspidophylline A.

We therefore continued our total synthesis by pursuing imine **2.30** which we intended to obtain by oxidation of sulphonamide **2.23** (scheme 2.11). We envisioned that access to the imine would give us the freedom to try out the essential alkylation before a cyclization or vice versa, but unfortunately, no imine was ever recovered (Table 2.4).

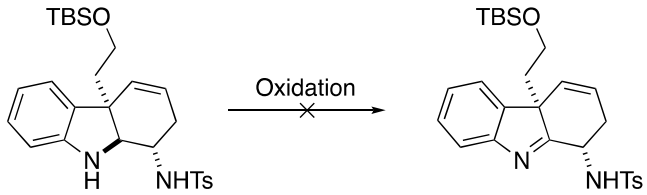

2.23 **2.30**

Scheme 2.11: Attempted oxidation of sulphonamide **2.23** to furnish imine **2.30**.

Table 2.4: Oxidation of compound 2.23.

Entry	Oxidation Source	Solvent	Temperature	Yield
1	DMP	CH_2Cl_2	0 °C	decomp.
2	MnO_2	CH_2Cl_2	0 °C	decomp.
3	$KMnO_4$	Benzene	rt	decomp.
4	$KMnO_4$	Benzene	0 °C	decomp.
5	Swern Oxidation	CH_2Cl_2	-78 °C to rt	undesired
6	PhIO	CH_2Cl_2	rt	62 %[a]

[a] Aminal **2.31** was obtained.

The first attempt was executed with commercially available Dess–Martin periodinane (DMP) and resulted in slow decomposition of starting material (Entry 1). Subjection to manganese-based oxidants resulted in immediate decomposition of the starting material (Entries 2-4). Swern oxidation delivered a clean reaction to a yet unknown compound (Entry 5). However, treatment with iodosobenzene at room temperature for one hour generated hemiaminal **2.31** instead of the anticipated imine (entry 6) and scheme 2.12.[158] Next, compound **2.31** will be exposed to acidic conditions in an attempt to access tetracycle **2.32**. We hypothesize that acidic reaction conditions will result in desylilation and *in-situ* imine formation followed by cyclization to give intermediate **2.32**.

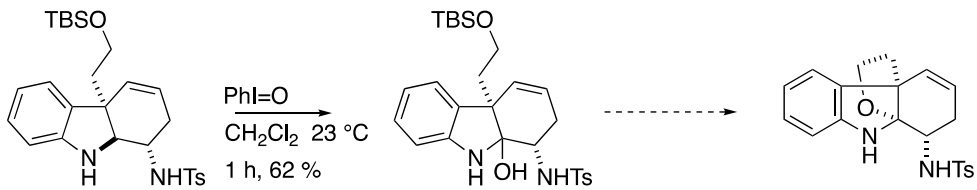

2.23 **2.31** **2.32**

Scheme 2.12: Obtained hemiaminal **2.31** will be used to furnish intermediate **2.32**.

Compound **2.23** was also transformed into amine **2.33**, upon treatment with naphthalene and sodium (scheme 2.13). This deprotection increases our synthetic

options for alkyl installation by enabling the potential use of reductive amination to render diene **2.34**.

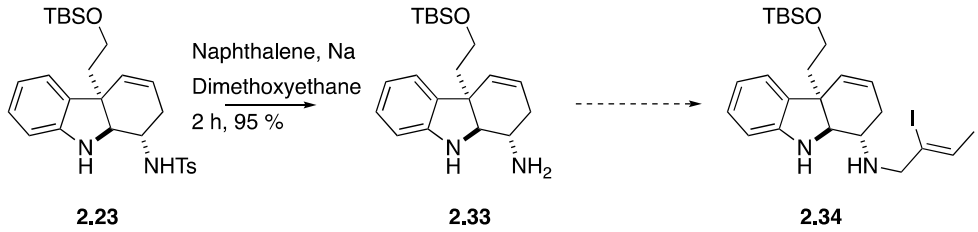

2.23 **2.33** **2.34**

Scheme 2.13: Amine **2.33** can potentially be transformed into diene **2.34** by alkylation or reductive amination.

Conclusions

To date, we have developed a 5-step route to the A/B/C tricyclic scaffold **2.31** present in Aspidophylline A **2.9**. A key feature of our approach is the straightforward installation of the correct relative stereochemistry of Aspidophylline A through the regioselective opening of aziridine **2.21**. Our synthetic route also provides rapid access to several advanced intermediates where the critical carbopalladation-carbonylation can be evaluated.

3. Concluding Remarks

This thesis presents a comprehensive exploration of two distinct yet interconnected domains, IMS in neurotherapeutics and organic synthesis, each offering unique advancements in their respective fields.

In the first part of this thesis, we delved into the dynamics of the antipsychotic drug CLO and its two main metabolites, NDMC and CNO in the brain. Through the innovative use of IMS and a desert locust *ex vivo* BBB/brain model, we were able to visualise and understand the neural distribution of these compounds without the need for molecular imaging probes. Our study sheds light on the limited penetration of CNO through the BBB and its neural metabolism to CLO and NDMC, observations that may carry significant implications for CNO's use in DREADD technology. Furthermore, while directly administered NDMC exhibited limited distribution, NDMC generated from *in situ* CYP-metabolism on CLO, was distributed throughout the brain. Our findings emphasise the need for a thorough understanding of drug dynamics in the brain for optimising drug delivery strategies, ensuring effective targeting, and minimising potential adverse effects. With this understanding, the effectiveness and safety of neurotherapeutic interventions can be improved.

Transitioning to the second part of this thesis, with our developed ATH/DKR strategy, we achieved remarkable yields, diastereo-, and enantioselectivities in the synthesis of aromatic *anti*-β-amido-α-hydroxy esters. Our methodology holds promise for the efficient synthesis of biologically active compounds in drug discovery and development. Our work on Aspidophylline A led to the synthesis of an advanced tricyclic intermediate, laying the groundwork for the total synthesis of this biologically intriguing natural compound.

The collaborative efforts highlighted in this thesis exemplify the importance of interdisciplinary collaboration in advancing pharmaceutical research. Our research is poised not only to expedite the pace of innovation but also to enable the exploration of uncharted territories in neurotherapeutic research, potentially enhancing the well-being and quality of life of individuals.

Acknowledgements

I would like to express my warmest and most sincere gratitude to my supervisor, Prof. Peter Somfai, for his invaluable guidance and support throughout my doctoral journey. Your steady commitment to excellence, profound expertise in chemistry, and dedication to fostering my intellectual growth have been instrumental throughout my Ph.D. journey. Thank you for believing in me and for embodying not only exceptional chemistry prowess but also genuine kindness.

I am also deeply grateful to Professors Roger Olsson and György Marko-Varga for providing me with the unique opportunity to pursue my dream of working in the field of neuroscience. A special thanks to you Prof. Olsson for your joyful mentorship and your consistent readiness to share your knowledge and expertise.

I wish to extend my heartfelt gratitude to Prof. Kenneth Wärnmark for being such an inspiring chemistry lecturer and for welcoming me into his research group as a diploma worker. Your mentorship was instrumental in becoming a chemist.

I also would like to extend my gratitude to all the workers of the CAS and the Department of Experimental Medical Science for fostering a great working environment. A special thanks to Maria Levin for her consistently kind attitude, which has made every interaction a pleasant experience.

I am also immensely grateful to my elementary school teachers, Bo Petersson and Gunilla Jönsson, who instilled in me the belief that I could one day become a scientist. Additionally, I owe a debt of gratitude to my first chemistry teacher, Kjell Magnusson, for introducing me to the world of chemistry in such a captivating way.

I am also deeply thankful to my high school chemistry teacher and distinguished artist, Lena Cronström, who epitomizes the essence of a true old-school teacher. Your resolute guidance played a pivotal role in shaping my journey as a scientist.

I would also like to express my sincere gratitude towards the funders, who made these research projects possible, Lund University, the Estonian Ministry of Education and the Royal Physiographic Society.

Igualmente, deseo expresar mi más profundo y cálido agradecimiento a mi familia, especialmente a mis queridos padres Walter y Aleida Villacrez, mis primas Moira y Evelyn Caldas, mi tía Carmen McGuire y a mi tía Nila Paz de Villacrez por su incondicional apoyo y cariño.

Sist men inte minst vill jag tacka min älskade sambo Gabriella för att alltid ha stöttat mig. Ditt oerhörda tålamod, din omänskliga förmåga att aldrig sluta tro på mig och din ovillkorliga kärlek betyder allt för mig.

Populärvetenskaplig Sammanfattning

Första delen i denna avhandling fokuserar på '*Imaging Mass Spectrometry*' (IMS), en analytisk teknik med kartografiska egenskaper. Denna teknik används dock inte för att kartlägga geografiska terränger, utan för att skapa kartor över det kemiska landskapet i biologiska prover, från vävnadssnitt av organ eller tumörer till enskilda celler. Dessa kartor visar med hög precision var olika molekyler, såsom kroppsegna ämnen och läkemedel, finns inom de analyserade proverna, och bidrar på så sätt till en djupare förståelse av såväl biologiska som farmakologiska processer på molekylär nivå.

I denna studie använde vi IMS och en insekthjärna för att studera det antipsykotiska läkemedlet klozapin (CLO) och dess två viktigaste metaboliter, *N*-desmetylklozapin (NDMC) och klozapin-*N*-oxid (CNO). Vårt mål var att förstå benägenheten för dessa ämnen att ta sig igenom blod-hjärnbarriären (BBB) samt deras beteende i hjärnan. Vi valde dessa föreningar av följande skäl. Trots att CLO är det vanligaste antipsykotiska läkemedlet utskrivet, är dess verkningsmekanism inte helt kartlagt. NDMC är intressant eftersom den misstänks vara en aktiv substans, delaktig i CLOs effekter. NDMC har utvärderats i kliniska tester men påvisade ingen farmakologisk effekt, något som tros bero på en begränsad förmåga att penetrera BBB. Vad gäller CNO, har den använts flitigt inom neurovetenskap som ett slags fjärrkontroll för att aktivera manipulerade hjärnceller. Dess användning bygger dock på antagandet att den enkelt kan ta sig in i hjärnan och inte genomgår förändringar. Våra IMS-kartor över insektshjärnan visar att CLO effektivt kan passera BBB och fördelar sig jämnt över hela hjärnan. Väl där omvandlas den till NDMC, vars distribution i stort sett matchar CLOs. Däremot, när NDMC administreras direkt, uppvisar den både en inskränkt förmåga att passera BBB och fördela sig hjärnan. Gällande CNO, indikerar våra kartor att den stöter på svårigheter att passera BBB och att den dessutom omvandlas till både CLO och NDMC inne i hjärnan. Våra resultat ifrågasätter användandet av CNO inom neurovetenskap och tyder på att NDMCs begränsade förmåga att penetrera BBB förmodligen är orsaken till dess bristande effekt som läkemedel. För övrigt framhäver denna studie också användbarheten av vår IMS/insekthjärnplattform för farmakologisk och neurovetenskaplig forskning.

I den andra delen i denna avhandling har en metod för att producera vicinala aminohydroxider, ett vanligt förekommande arrangemang i såväl läkemedel som naturliga föreningar, framgångsrikt utvecklats. Detta lyckades vi med genom att tillämpa asymmetrisk överförings hydrogenering på *anti*-α-amido-β-hydroxil estrar som under våra utvecklade betingelser genomgick dynamisk kinetisk resolution. I denna andra del presenteras också våra framsteg i tillverkningen av Aspidophylline A, en förening som återfinns i en oleanderväxtart och som har potentialen att göra resistenta cancerceller mottagliga för behandling. Även om vi inte lyckades fullborda vår syntes har våra ansträngningar satt oss på en lovande väg mot att uppnå detta mål.

Popular Scientific Summary

The first part of this thesis focuses on 'Imaging Mass Spectrometry' (IMS), an analytical technique with cartographic capabilities. However, this technique is not used to map geographical terrains; instead, it is employed to create maps of the chemical landscape within biological samples, ranging from tissue sections from organs or tumours to individual cells. These maps show with high precision where molecules (*e.g.*, endogenous substances and drugs) are located within the analysed samples, contributing to a deeper understanding of both biological and pharmacological processes at the molecular level.

In this study, we used IMS and an insect brain to investigate the antipsychotic drug clozapine (CLO) and its two main metabolites, *N*-desmethylclozapine (NDMC) and clozapine-*N*-oxide (CNO). Our goal was to understand the propensity of these drugs to cross the blood-brain barrier (BBB) and their behaviour in the brain. We selected these drugs for the following reasons. Although CLO ranks as the top antipsychotic of choice, its mechanism of action is not fully understood. NDMC is of interest because it is suspected to be an active substance involved in CLO's effects. NDMC has been evaluated in a clinical trial but showed no effect compared to placebo. It was hypothesised that this ineffectiveness was due to its limited ability to cross the BBB. As for CNO, it has been widely used in neuroscience as a kind of remote control to activate manipulated brain cells. However, its use relies on the assumption that it can easily enter the brain without undergoing changes. Our IMS maps reveal that CLO has a good ability to cross the BBB and is distributed evenly throughout the brain. Once inside, it transforms into NDMC, whose distribution matches that of CLO. However, when NDMC is administered directly, it struggles to cross the BBB and displays also a limited neural distribution. Regarding CNO, our maps show that it has difficulties crossing the BBB and also transforms into both CLO and NDMC inside the brain. Our results question the use of CNO in neuroscience and suggest that NDMC's limited ability to penetrate the BBB is likely the reason for its ineffectiveness as a drug. Furthermore, this study highlights the applicability of our IMS/insect brain platform for pharmacological and neuroscience research.

In the second part of this thesis, a method for producing vicinal amino alcohols, a common arrangement in both pharmaceuticals and natural compounds, has been successfully developed. We achieved this by applying a process known as asymmetric transfer hydrogenation on compounds undergoing dynamic kinetic resolution. In this second part, we also present our progress in the synthesis of Aspidophylline A, a compound found in an oleander species with the potential to make resistant cancer cells responsive to treatment. Although we did not complete our synthesis, our efforts have placed us on a promising path toward achieving this goal.

Resumen Divulgativo

La primera parte de esta tesis se centra en '*Imaging Mass Spectrometry*' (IMS), una herramienta analítica con capacidades cartográficas. Sin embargo, esta técnica no se utiliza para mapear terrenos geográficos, está orientada a crear mapas del paisaje químico en muestras biológicas, desde secciones de tejido de órganos o tumores hasta células individuales. Estos mapas muestran con alta precisión la ubicación de moléculas, así como sustancias endógenas y medicamentos, dentro de las muestras analizadas y contribuye a una comprensión más profunda de los procesos biológicos y farmacológicos a nivel molecular.

En este estudio, utilizamos IMS y un cerebro de insecto para investigar el antipsicótico clozapina (CLO) y sus dos principales metabolitos, *N*-desmetilclozapina (NDMC) y clozapina-*N*-óxido (CNO). Nuestro objetivo era entender cómo estos compuestos cruzan la barrera hematoencefálica (BBB) y cómo se comportan en el cerebro. Elegimos estos medicamentos por las siguientes razones A pesar de que CLO es el antipsicótico más recetado, todavía no se comprende completamente su mecanismo de acción. NDMC es de interés porque se sospecha que es una sustancia activa involucrada en los efectos de CLO. NDMC ha sido evaluado como medicamento, pero no mostró efecto. Se cree que esto se debe a su limitada capacidad para cruzar la BBB. En cuanto a CNO, se ha utilizado ampliamente en neurociencia como un tipo de control remoto para activar neuronas manipuladas. Sin embargo, su uso se basa en la suposición de que puede ingresar fácilmente al cerebro y no sufre cambios. Nuestros mapas revelan que CLO tiene una buena capacidad para cruzar la BBB y se distribuye de manera uniforme en todo el cerebro. Una vez dentro, se transforma en NDMC, cuya distribución se asemeja a la de CLO. Sin embargo, cuando se administra NDMC directamente, tiene dificultades para cruzar la BBB y tiene una distribución limitada. En cuanto a CNO, nuestros mapas muestran que tiene dificultades para cruzar la BBB y también se transforma en CLO y NDMC dentro del cerebro. Nuestros resultados cuestionan el uso de CNO en neurociencia y sugieren que la limitada capacidad de NDMC para penetrar la BBB es probablemente la razón de su falta de eficacia como medicamento. Además, este estudio destaca la aplicabilidad de nuestra plataforma 'IMS/cerebro de insecto' en la investigación farmacológica y neurocientífica.

En la segunda parte de esta tesis, se ha desarrollado con éxito un método para producir aminoalcoholes vicinales, una estructura común tanto en farmacéuticos como en compuestos naturales. Logramos esto aplicando un proceso conocido como hidrogenación asimétrica de transferencia en sinergia con resolución cinética dinámica. En esta segunda parte, también presentamos nuestro progreso en la síntesis de Aspidofilina A, un compuesto natural con el potencial de hacer que células cancerosas resistentes sean receptivas a tratamiento nuevamente. Aunque no completamos nuestra síntesis, nuestros esfuerzos nos han colocado en un camino prometedor hacia la consecución de este objetivo.

Appendix

Material and Methods *(Paper I)*

Chemicals

All chemical used were of analytical reagent grade and purchased from Sigma-Aldrich (Stockholm, Sweden). Ethanol was purchased from Solveco (Rosersberg, Sweden), and acetonitrile was acquired from Fisher Scientific. Chemicals for histology purposes were purchased from Histolab (Gothenburg, Sweden).

Animal Ethics

The studies in this thesis were conducted in accordance with Swedish national legislation and European Community guidelines for animal studies. Experiments were meticulously planned to minimise the number of animals used

Zebrafish

Zebrafish sacrificed for the study were from intercrosses of the wild-type AB strain. A 2 L aquarium containing 1 L water was prepared to host 12 fish. The desired drugs were dissolved in 100% dimethyl sulfoxide to generate stock solutions (10 mM). Properly diluted stock solutions were added to the 2 L aquaria in the amount required to obtain the desired concentration and stirred for 2 minutes for homogeneity purposes. Experiments were initiated when fish were transferred to the drug-prepared aquaria, where they were left to swim freely. After behaviour onset, the fish were removed from the tank and anaesthetised by incubation in ice water for 15 minutes before beginning dissection. The dissection began by lightly patting the fish dry on a paper towel before transfer to the dissection dish. The fish was pinned through the fleshy part of the tail and posterior part of the dorsal fin in order to remove the head with a razor blade. The head was cleaned from as much soft tissue as possible, and the skull was gently broken open. Bones were removed, and the eyes were detached by cutting of the optic nerve. The brain was cleaned before submitted to snap-freezing.

Desert Locust

Insects were obtained from a commercial animal supplier (Petra Aqua, Prague, Czech Republic). Upon arrival, the animals were housed in insect cages supplied by Small-Life Supplies (Peterborough, Great Britain) and adapted to10:14 h Night/Day cycle with a habitat temperature ranging 25−34 °C depending on the animals' distance to the light bulb. Chinese cabbage and wheat bran where used as alimentary source ad libitum and all experiments were conducted 2−3 weeks after adult emergence. Brains were dissected by cutting off the frontal part of the head which later was detached from the cuticle and cleaned from fat and tissue by using fine

forceps. The isolated brains were placed in microwell plate (96U Microwell; Nunc), all containing 250 µL of the drug with the respective concentration of interest dissolved in an insect buffer. The brains were removed from the compound solutions after fixed exposure periods and washed twice in ice-cold insect buffer prior to freezing. The harvested drug treated brains were immediately snap frozen, placed in an Eppendorf tube and kept in a -80 ° freezer until collected for MALDI-IMS experiments.

Snap Freezing

Brain samples from desert locust and zebrafish were collected in an Eppendorf tube to facilitate for freezing procedure. Immediately after collection, prepared tubes are submerged into liquid nitrogen. Snap-freezing is immediate and the tubes where kept submerged for 1 minute to obtain a homogenous frozen specimen. After 1 minute, the tubes are transferred quickly to a Styrofoam box containing dry ice so to safely transfer the tubes to a -80 °C freezer for long-term storage.

MALDI-IMS

To avoid interferences from compounds alien to experiments, all brains were mounted on to the cryostat cutting block using only Millipore water/ice. Brain tissue samples ranging from 8-30 µm thickness were obtained from both treated and untreated specimens at temperature ranging between -12 °C and -20 °C depending on daily humidity conditions. Brain tissues were thaw-mounted onto a MALDI glass slide (Thermo Fischer, Superfrost Ultra Plus, 25 x 75 x 1,0 mm, Germany) for matrix application. Brains not exposed to drugs were also collected and used as controls to obtain zero value tissues used to compare the signal intensities from the drug-treated brains. Thaw-mounted samples were placed in a vacuum chamber for 30-45 minutes to remove condensate formed from atmospheric water. A CHCA matrix solution was prepared with a concentration of 5.0 mg/mL in (1:1) acetonitrile: water and 0.2 % of TFA. An automated pneumatic sprayer (TM-Sprayer, HTX Technologies) was used to uniformly coat brain samples with matrix solution. The nozzle distance between sprayer and sample was fixed to 46 mm, and the spraying temperature was stabilized at 95 °C. The matrix was sprayed (18 passes) over the tissue sections at a nozzle linear velocity of 700 mm/min and a flow rate set to 0.1 ml/min with a nitrogen pressure permanent at 10 psi. An intermission time of 10 s was pre-set in between each pass in order to give time for the sample to dry completely (*i.e*. let the matrix solvent evaporate) before the next pass. The matrix-treated glass slide had a yellow/whitish frosted appearance when all passes where completed. MALDI-IMS data analyses were performed on a MALDI LTQ Orbitrap XL mass spectrometer (Thermo Fisher Scientific, Bremen, Germany). Ten laser shots at 14 µJ were used to ionize each pixel examined and entire brain tissue sample were scanned with a spatial resolution of 50 µm. Full scans in profile mode, mass acquisition ranging from m/z 200 to 400, were obtained in Orbitrap positive polarity. The following scan event were set to produce collision-induced

dissociation (CID) fragmentation MS/MS spectra, mass ranging from m/z 250 to 320 and analysed using a linear ion trap in positive polarity.

Imaging Data Analysis

Molecular images of drug distribution were generated using ImageQuestTM software (Thermo Fisher Scientific, San José, CA) from the MS raw files. CLO, NDMC, CNO parent ions and their corresponding fragments ions (m/z; CLO 270.167, NDMC 270.167, CNO 299.167) were extracted to determine their localization within tissue sections. Screen shots of the distribution for CLO (m/z 327.138), NDMC (m/z 313.123) and CNO (m/z 343.134) parent ions and of their respective fragment ions were obtained. The scale of the colour pattern in the generated images was used to estimate the relative abundance of a drug within a tissue sample.

Histological staining

After performed IMS experiment, matrix coated sample slides were submerged in 70 % ethanol until most of the matrix was dissolved. The slides were then submerged in 90 % ethanol for 5 minutes before being immersed in 4 % phosphate-buffered formaldehyde for 30 min and then washed under running distilled water for 5 s. The fixed samples were immersed in Mayer's for 5 minutes, followed by water bluing for 10 minutes. Further staining was achieved by submerging the slides in an eosin solution followed by a wash with deionized water. The slides were then dipped in 70 % ethanol for 30 seconds, in 90 % ethanol for 1 minute, and later in 99 % dehydrated ethanol for 1 min. Finally, the slides were submerged in four different xylene baths for 1 minute in each bath. The stained slides were protracted by applying Pertex® to a cover slip and gluing together slide and cover slip. [159]

Histological Analysis

The cover-slipped H&E-stained slides were optically examined (Mirax Midi Slide Scanner, Zeiss, Germany) to take non-detailed image for the selection of regions of interest to be scanned at high resolution. The files were opened in Aperio ImageScope Viewer v12.1 (Leica Biosystems Imaging Inc., Vista, CA) where detailed images were taken and saved as *.tiff files.

References

(1) Villacrez, M. Towards the Total Synthesis of Aspidophylline A and Stereoselective Syntehsis of Amino Alcohols Lund University, Media-Tryck, 2016.

(2) Stone, J. Functional neurological disorders: the neurological assessment as treatment. *Pract Neurol* **2016**, *16* (1), 7-17. DOI: 10.1136/practneurol-2015-001241 From NLM.

(3) Preskorn, S. H. CNS drug development. Part I: The early period of CNS drugs. *J Psychiatr Pract* **2010**, *16* (5), 334-339. DOI: 10.1097/01.pra.0000388628.44405.c0 From NLM.

(4) Preskorn, S. H. CNS drug development: Part II: Advances from the 1960s to the 1990s. *J Psychiatr Pract* **2010**, *16* (6), 413-415. DOI: 10.1097/01.pra.0000390760.12204.99 From NLM.

(5) Pangalos, M. N.; Schechter, L. E.; Hurko, O. Drug development for CNS disorders: strategies for balancing risk and reducing attrition. *Nat Rev Drug Discov* **2007**, *6* (7), 521-532. DOI: 10.1038/nrd2094 From NLM.

(6) Garattini, S.; Bertele, V. Efficacy, safety and cost of new drugs acting on the central nervous system. *Eur J Clin Pharmacol* **2003**, *59* (1), 79-84. DOI: 10.1007/s00228-003-0569-3 From NLM.

(7) Palmer, A. M.; Stephenson, F. A. CNS drug discovery: challenges and solutions. *Drug News Perspect* **2005**, *18* (1), 51-57. From NLM.

(8) Chow, B. W.; Gu, C. The molecular constituents of the blood-brain barrier. *Trends Neurosci* **2015**, *38* (10), 598-608. DOI: 10.1016/j.tins.2015.08.003 From NLM.

(9) Achar, A.; Myers, R.; Ghosh, C. Drug Delivery Challenges in Brain Disorders across the Blood-Brain Barrier: Novel Methods and Future Considerations for Improved Therapy. *Biomedicines* **2021**, *9* (12). DOI: 10.3390/biomedicines9121834 From NLM.

(10) Pardridge, W. M. The blood-brain barrier: bottleneck in brain drug development. *NeuroRx* **2005**, *2* (1), 3-14. DOI: 10.1602/neurorx.2.1.3 From NLM.

(11) Loryan, I.; Sinha, V.; Mackie, C.; Van Peer, A.; Drinkenburg, W.; Vermeulen, A.; Morrison, D.; Monshouwer, M.; Heald, D.; Hammarlund-Udenaes, M. Mechanistic understanding of brain drug disposition to optimize the selection of potential neurotherapeutics in drug discovery. *Pharm Res* **2014**, *31* (8), 2203-2219. DOI: 10.1007/s11095-014-1319-1 From NLM.

(12) Reichel, A. Pharmacokinetics of CNS Penetration. In *Blood-Brain Barrier in Drug Discovery*, 2015; pp 5-41.

(13) Mankoff, D. A.; Farwell, M. D.; Clark, A. S.; Pryma, D. A. Making Molecular Imaging a Clinical Tool for Precision Oncology: A Review. *JAMA Oncol* **2017**, *3* (5), 695-701. DOI: 10.1001/jamaoncol.2016.5084 From NLM.

(14) Incoronato, M.; Grimaldi, A. M.; Cavaliere, C.; Inglese, M.; Mirabelli, P.; Monti, S.; Ferbo, U.; Nicolai, E.; Soricelli, A.; Catalano, O. A.; et al. Relationship between functional imaging and immunohistochemical markers and prediction of breast cancer subtype: a PET/MRI study. *Eur J Nucl Med Mol Imaging* **2018**, *45* (10), 1680-1693. DOI: 10.1007/s00259-018-4010-7 From NLM.

(15) Stumpf, W. E. Drugs in the brain--cellular imaging with receptor microscopic autoradiography. *Prog Histochem Cytochem* **2012**, *47* (1), 1-26. DOI: 10.1016/j.proghi.2011.12.001 From NLM.

(16) Ban, W.; You, Y.; Yang, Z. Imaging Technologies for Cerebral Pharmacokinetic Studies: Progress and Perspectives. *Biomedicines* **2022**, *10* (10). DOI: 10.3390/biomedicines10102447 From NLM.

(17) Prideaux, B.; Stoeckli, M. Mass spectrometry imaging for drug distribution studies. *J Proteomics* **2012**, *75* (16), 4999-5013. DOI: 10.1016/j.jprot.2012.07.028 From NLM.

(18) Cobice, D. F.; Goodwin, R. J.; Andren, P. E.; Nilsson, A.; Mackay, C. L.; Andrew, R. Future technology insight: mass spectrometry imaging as a tool in drug research and development. *Br J Pharmacol* **2015**, *172* (13), 3266-3283. DOI: 10.1111/bph.13135 From NLM.

(19) Goodwin, R. J. A.; Takats, Z.; Bunch, J. A Critical and Concise Review of Mass Spectrometry Applied to Imaging in Drug Discovery. *SLAS Discovery* **2020**, *25* (9), 963-976. DOI: https://doi.org/10.1177/2472555220941843.

(20) Shariatgorji, M.; Svenningsson, P.; Andrén, P. E. Mass Spectrometry Imaging, an Emerging Technology in Neuropsychopharmacology. *Neuropsychopharmacology* **2014**, *39* (1), 34-49. DOI: 10.1038/npp.2013.215.

(21) Schnackenberg, L. K.; Thorn, D. A.; Barnette, D.; Jones, E. E. MALDI imaging mass spectrometry: an emerging tool in neurology. *Metab Brain Dis* **2022**, *37* (1), 105-121. DOI: 10.1007/s11011-021-00797-2 From NLM.

(22) Hanrieder, J.; Phan, N. T.; Kurczy, M. E.; Ewing, A. G. Imaging mass spectrometry in neuroscience. *ACS Chem Neurosci* **2013**, *4* (5), 666-679. DOI: 10.1021/cn400053c From NLM.

(23) Liu, G.-X.; Li, Z.-L.; Lin, S.-Y.; Wang, Q.; Luo, Z.-Y.; Wu, K.; Zhou, Y.-L.; Ning, Y.-P. Mapping metabolite change in the mouse brain after esketamine injection by ambient mass spectrometry imaging and metabolomics. *Frontiers in Psychiatry* **2023**, *14*, Original Research. DOI: 10.3389/fpsyt.2023.1109344.

(24) Liu, X.; Ide, J. L.; Norton, I.; Marchionni, M. A.; Ebling, M. C.; Wang, L. Y.; Davis, E.; Sauvageot, C. M.; Kesari, S.; Kellersberger, K. A.; et al. Molecular imaging of drug transit through the blood-brain barrier with MALDI mass spectrometry imaging. *Scientific Reports* **2013**, *3* (1), 2859. DOI: 10.1038/srep02859.

(25) Castellino, S.; Groseclose, M. R.; Sigafoos, J.; Wagner, D.; de Serres, M.; Polli, J. W.; Romach, E.; Myer, J.; Hamilton, B. Central nervous system disposition and metabolism of Fosdevirine (GSK2248761), a non-nucleoside reverse transcriptase inhibitor: an LC-MS and Matrix-assisted laser desorption/ionization imaging MS investigation into central nervous system toxicity. *Chem Res Toxicol* **2013**, *26* (2), 241-251. DOI: 10.1021/tx3004196 From NLM.

(26) Hatton, S. N.; Huynh, K. H.; Bonilha, L.; Abela, E.; Alhusaini, S.; Altmann, A.; Alvim, M. K. M.; Balachandra, A. R.; Bartolini, E.; Bender, B.; et al. White matter abnormalities across different epilepsy syndromes in adults: an ENIGMA-Epilepsy study. *Brain* **2020**, *143* (8), 2454-2473. DOI: 10.1093/brain/awaa200 From NLM.

(27) Rončević, A.; Koruga, N.; Soldo Koruga, A.; Debeljak, Ž.; Rončević, R.; Turk, T.; Kretić, D.; Rotim, T.; Krivdić Dupan, Z.; Troha, D.; et al. MALDI Imaging Mass Spectrometry of High-Grade Gliomas: A Review of Recent Progress and Future Perspective. *Current Issues in Molecular Biology* **2023**, *45* (2), 838-851.

(28) Spruill, M. L.; Maletic-Savatic, M.; Martin, H.; Li, F.; Liu, X. Spatial analysis of drug absorption, distribution, metabolism, and toxicology using mass spectrometry imaging. *Biochem Pharmacol* **2022**, *201*, 115080. DOI: 10.1016/j.bcp.2022.115080 From NLM.

(29) Washburn, H.; Wiley, H.; Rock, S. Mass Spectrometer as Analytical Tool. *Industrial & Engineering Chemistry Analytical Edition* **1943**, *15* (9), 541-547. DOI: 10.1021/i560121a001.

(30) Dilmetz, B. A.; Lee, Y.-R.; Condina, M. R.; Briggs, M.; Young, C.; Desire, C. T.; Klingler-Hoffmann, M.; Hoffmann, P. Novel technical developments in mass spectrometry imaging in 2020: A mini review. *Analytical Science Advances* **2021**, *2* (3-4), 225-237. DOI: https://doi.org/10.1002/ansa.202000176.

(31) Swales, J. G.; Hamm, G.; Clench, M. R.; Goodwin, R. J. A. Mass spectrometry imaging and its application in pharmaceutical research and development: A concise review. *International Journal of Mass Spectrometry* **2019**, *437*, 99-112. DOI: https://doi.org/10.1016/j.ijms.2018.02.007.

(32) Nilsson, A.; Goodwin, R. J. A.; Shariatgorji, M.; Vallianatou, T.; Webborn, P. J. H.; Andrén, P. E. Mass Spectrometry Imaging in Drug Development. *Analytical Chemistry* **2015**, *87* (3), 1437-1455. DOI: 10.1021/ac504734s.

(33) Römpp, A.; Spengler, B. Mass spectrometry imaging with high resolution in mass and space. *Histochem Cell Biol* **2013**, *139* (6), 759-783. DOI: 10.1007/s00418-013-1097-6 PubMed.

(34) Jones, O. R.; Perks, R. M.; Abraham, C. J.; Telle, H. H.; Oakley, A. E. A Comparison of the Techniques of Secondary Ion Mass Spectrometry and Resonance Ionization Mass Spectrometry for the Analysis of Potentially Toxic Element Accumulation in Neural Tissue. *Rapid Communications in Mass Spectrometry* **1997**, *11* (2), 179-183. DOI: 10.1002/(SICI)1097-0231(19970131)11:2<179::AID-RCM757>3.0.CO;2-# (acccessed 2020/02/27).

(35) Gu, H.; Ma, K.; Zhao, W.; Qiu, L.; Xu, W. A general purpose MALDI matrix for the analyses of small organic, peptide and protein molecules. *Analyst* **2021**, *146* (12), 4080-4086. DOI: 10.1039/d1an00474c From NLM.

(36) Francese, S.; Dani, F. R.; Traldi, P.; Mastrobuoni, G.; Pieraccini, G.; Moneti, G. MALDI mass spectrometry imaging, from its origins up to today: the state of the art. *Comb Chem High Throughput Screen* **2009**, *12* (2), 156-174. DOI: 10.2174/138620709787315454 From NLM.

(37) Muddiman, D. C.; Bakhtiar, R.; Hofstadler, S. A.; Smith, R. D. Matrix-Assisted Laser Desorption/Ionization Mass Spectrometry. Instrumentation and Applications. *Journal of Chemical Education* **1997**, *74* (11), 1288. DOI: 10.1021/ed074p1288.

(38) Lee, C.; Ni, C. K. Soft Matrix-Assisted Laser Desorption/Ionization for Labile Glycoconjugates. *J Am Soc Mass Spectrom* **2019**, *30* (8), 1455-1463. DOI: 10.1007/s13361-019-02208-4 From NLM.

(39) Schnackenberg, L. K.; Thorn, D. A.; Barnette, D.; Jones, E. E. MALDI imaging mass spectrometry: an emerging tool in neurology. *Metabolic Brain Disease* **2022**, *37* (1), 105-121. DOI: 10.1007/s11011-021-00797-2.

(40) Castellino, S.; Groseclose, M. R.; Wagner, D. MALDI imaging mass spectrometry: bridging biology and chemistry in drug development. *Bioanalysis* **2011**, *3* (21), 2427-2441. DOI: 10.4155/bio.11.232 (acccessed 2023/09/16).

(41) McDonald, W. S.; Jones, E. E.; Wojciak, J. M.; Drake, R. R.; Sabbadini, R. A.; Harris, N. G. Matrix-Assisted Laser Desorption Ionization Mapping of Lysophosphatidic Acid Changes after Traumatic Brain Injury and the Relationship to Cellular Pathology. *Am J Pathol* **2018**, *188* (8), 1779-1793. DOI: 10.1016/j.ajpath.2018.05.005 From NLM.

(42) Sparvero, L. J.; Amoscato, A. A.; Dixon, C. E.; Long, J. B.; Kochanek, P. M.; Pitt, B. R.; Bayır, H.; Kagan, V. E. Mapping of phospholipids by MALDI imaging (MALDI-MSI): realities and expectations. *Chemistry and Physics of Lipids* **2012**, *165* (5), 545-562. DOI: https://doi.org/10.1016/j.chemphyslip.2012.06.001.

(43) Granborg, J. R.; Handler, A. M.; Janfelt, C. Mass spectrometry imaging in drug distribution and drug metabolism studies – Principles, applications and perspectives. *TrAC Trends in Analytical Chemistry* **2022**, *146*, 116482. DOI: https://doi.org/10.1016/j.trac.2021.116482.

(44) Vallianatou, T.; Strittmatter, N.; Nilsson, A.; Shariatgorji, M.; Hamm, G.; Pereira, M.; Källback, P.; Svenningsson, P.; Karlgren, M.; Goodwin, R. J. A.; et al. A mass spectrometry imaging approach for investigating how drug-drug interactions influence drug blood-brain barrier permeability. *Neuroimage* **2018**, *172*, 808-816. DOI: 10.1016/j.neuroimage.2018.01.013 From NLM.

(45) Shariatgorji, R.; Nilsson, A.; Strittmatter, N.; Vallianatou, T.; Zhang, X.; Svenningsson, P.; Goodwin, R. J. A.; Andrén, P. E. Bromopyrylium Derivatization Facilitates Identification by Mass Spectrometry Imaging of Monoamine Neurotransmitters and Small Molecule Neuroactive Compounds. *J Am Soc Mass Spectrom* **2020**, *31* (12), 2553-2557. DOI: 10.1021/jasms.0c00166 From NLM.

(46) li, W.; Liu, H.; Jiang, H.; Wang, C.; Guo, Y.; Sun, Y.; Zhao, X.; Xiong, X.; Zhang, X.; Zhang, K.; et al. (S)-Oxiracetam is the Active Ingredient in Oxiracetam that Alleviates the Cognitive Impairment Induced by Chronic Cerebral Hypoperfusion in Rats. *Scientific Reports* **2017**, *7* (1), 10052. DOI: 10.1038/s41598-017-10283-4.

(47) Giacomotto, J.; Ségalat, L. High-throughput screening and small animal models, where are we? *Br J Pharmacol* **2010**, *160* (2), 204-216. DOI: 10.1111/j.1476-5381.2010.00725.x From NLM.

(48) Meshalkina, D. A.; Song, C.; Kalueff, A. V. Better lab animal models for translational neuroscience research and CNS drug development. *Lab Animal* **2017**, *46* (4), 91-92. DOI: 10.1038/laban.1236.

(49) Salick, M. R.; Lubeck, E.; Riesselman, A.; Kaykas, A. The future of cerebral organoids in drug discovery. *Seminars in Cell & Developmental Biology* **2021**, *111*, 67-73. DOI: https://doi.org/10.1016/j.semcdb.2020.05.024.

(50) Al-Qadi, S.; Schiøtt, M.; Hansen, S. H.; Nielsen, P. A.; Badolo, L. An invertebrate model for CNS drug discovery: Transcriptomic and functional analysis of a mammalian P-glycoprotein ortholog. *Biochim Biophys Acta* **2015**, *1850* (12), 2439-2451. DOI: 10.1016/j.bbagen.2015.09.002 From NLM.

(51) Tello, J. A.; Williams, H. E.; Eppler, R. M.; Steinhilb, M. L.; Khanna, M. Animal Models of Neurodegenerative Disease: Recent Advances in Fly Highlight Innovative Approaches to Drug Discovery. *Frontiers in Molecular Neuroscience* **2022**, *15*, Review. DOI: 10.3389/fnmol.2022.883358.

(52) Seabrooks, L.; Hu, L. Insects: an underrepresented resource for the discovery of biologically active natural products. *Acta Pharm Sin B* **2017**, *7* (4), 409-426. DOI: 10.1016/j.apsb.2017.05.001 PubMed.

(53) Wang, Y.; Moussian, B.; Schaeffeler, E.; Schwab, M.; Nies, A. T. The fruit fly Drosophila melanogaster as an innovative preclinical ADME model for solute carrier membrane transporters, with consequences for pharmacology and drug therapy. *Drug Discovery Today* **2018**, *23* (10), 1746-1760. DOI: https://doi.org/10.1016/j.drudis.2018.06.002.

(54) Matsumoto, Y. Facilitating Drug Discovery in Human Disease Models Using Insects. *Biol Pharm Bull* **2020**, *43* (2), 216-220. DOI: 10.1248/bpb.b19-00834 From NLM.

(55) Adams, M. M.; Kafaligonul, H. Zebrafish-A Model Organism for Studying the Neurobiological Mechanisms Underlying Cognitive Brain Aging and Use of Potential Interventions. *Front Cell Dev Biol* **2018**, *6*, 135-135. DOI: 10.3389/fcell.2018.00135 PubMed.

(56) Keller, E. T.; Murtha, J. M. The use of mature zebrafish (Danio rerio) as a model for human aging and disease. *Comparative Biochemistry and Physiology Part C: Toxicology & Pharmacology* **2004**, *138* (3), 335-341. DOI: https://doi.org/10.1016/j.cca.2004.04.001.

(57) Carlson, S. D.; Juang, J. L.; Hilgers, S. L.; Garment, M. B. Blood barriers of the insect. *Annu Rev Entomol* **2000**, *45*, 151-174. DOI: 10.1146/annurev.ento.45.1.151 From NLM.

(58) Hindle, S. J.; Bainton, R. J. Barrier mechanisms in the Drosophila blood-brain barrier. *Front Neurosci* **2014**, *8*, 414. DOI: 10.3389/fnins.2014.00414 From NLM.

(59) Mayer, F.; Mayer, N.; Chinn, L.; Pinsonneault, R. L.; Kroetz, D.; Bainton, R. J. Evolutionary Conservation of Vertebrate Blood–Brain Barrier Chemoprotective Mechanisms in Drosophila. *The Journal of Neuroscience* **2009**, *29* (11), 3538-3550. DOI: 10.1523/jneurosci.5564-08.2009.

(60) Li, Y.; Chen, T.; Miao, X.; Yi, X.; Wang, X.; Zhao, H.; Lee, S. M.-Y.; Zheng, Y. Zebrafish: A promising in vivo model for assessing the delivery of natural products, fluorescence dyes and drugs across the blood-brain barrier. *Pharmacological Research* **2017**, *125*, 246-257. DOI: https://doi.org/10.1016/j.phrs.2017.08.017.

(61) Zeng, A.; Ye, T.; Cao, D.; Huang, X.; Yang, Y.; Chen, X.; Xie, Y.; Yao, S.; Zhao, C. Identify a Blood-Brain Barrier Penetrating Drug-TNB using Zebrafish Orthotopic Glioblastoma Xenograft Model. *Scientific Reports* **2017**, *7* (1), 14372. DOI: 10.1038/s41598-017-14766-2.

(62) O'Brown, N. M.; Megason, S. G.; Gu, C. Suppression of transcytosis regulates zebrafish blood-brain barrier development. *bioRxiv* **2019**, 596221. DOI: 10.1101/596221.

(63) Lichtneckert, R.; Reichert, H. Insights into the urbilaterian brain: conserved genetic patterning mechanisms in insect and vertebrate brain development. *Heredity (Edinb)* **2005**, *94* (5), 465-477. DOI: 10.1038/sj.hdy.6800664 From NLM.

(64) Verlinden, H. Dopamine signalling in locusts and other insects. *Insect Biochem Mol Biol* **2018**, *97*, 40-52. DOI: 10.1016/j.ibmb.2018.04.005 From NLM.

(65) Bauknecht, P.; Jékely, G. Ancient coexistence of norepinephrine, tyramine, and octopamine signaling in bilaterians. *BMC Biol* **2017**, *15* (1), 6. DOI: 10.1186/s12915-016-0341-7 From NLM.

(66) Hellman, K.; Aadal Nielsen, P.; Ek, F.; Olsson, R. An ex Vivo Model for Evaluating Blood–Brain Barrier Permeability, Efflux, and Drug Metabolism. *ACS Chemical Neuroscience* **2016**, *7* (5), 668-680. DOI: 10.1021/acschemneuro.6b00024.

(67) Huber, R.; Panksepp, J. B.; Nathaniel, T.; Alcaro, A.; Panksepp, J. Drug-sensitive reward in crayfish: An invertebrate model system for the study of SEEKING, reward, addiction, and withdrawal. *Neuroscience & Biobehavioral Reviews* **2011**, *35* (9), 1847-1853. DOI: https://doi.org/10.1016/j.neubiorev.2010.12.008.

(68) Panula, P.; Chen, Y. C.; Priyadarshini, M.; Kudo, H.; Semenova, S.; Sundvik, M.; Sallinen, V. The comparative neuroanatomy and neurochemistry of zebrafish CNS systems of relevance to human neuropsychiatric diseases. *Neurobiol Dis* **2010**, *40* (1), 46-57. DOI: 10.1016/j.nbd.2010.05.010 From NLM.

(69) Jones, L. J.; McCutcheon, J. E.; Young, A. M.; Norton, W. H. Neurochemical measurements in the zebrafish brain. *Front Behav Neurosci* **2015**, *9*, 246. DOI: 10.3389/fnbeh.2015.00246 From NLM.

(70) Ahkin Chin Tai, J. K.; Horzmann, K. A.; Franco, J.; Jannasch, A. S.; Cooper, B. R.; Freeman, J. L. Developmental atrazine exposure in zebrafish produces the same major metabolites as mammals along with altered behavioral outcomes. *Neurotoxicol Teratol* **2021**, *85*, 106971. DOI: 10.1016/j.ntt.2021.106971 From NLM.

(71) Egeth, M. Behavioral Responses to Light by Headless Anesthetized Drosophila Melanogaster. *Perception* **2011**, *40* (2), 247-248. DOI: 10.1068/p6850.

(72) Spieth, H. T. Drosophilid mating behaviour: The behaviour of decapitated females. *Animal Behaviour* **1966**, *14* (2), 226-235. DOI: https://doi.org/10.1016/S0003-3472(66)80076-3.

(73) Mikani, A.; Wang, Q. S.; Takeda, M. Brain-midgut short neuropeptide F mechanism that inhibits digestive activity of the American cockroach, Periplaneta americana upon starvation. *Peptides* **2012**, *34* (1), 135-144. DOI: 10.1016/j.peptides.2011.10.028 From NLM.

(74) Park, N.-j.; Kamble, S. T. Decapitation Impacting Effect of Topically Applied Chlorpyrifos on Acetylcholinesterase and General Esterases in Susceptible and Resistant German Cockroaches (Dictyoptera: Blattellidae). *Journal of Economic Entomology* **2001**, *94* (2), 499-505. DOI: 10.1603/0022-0493-94.2.499 (acccessed 9/21/2023).

(75) Andersson, O.; Badisco, L.; Hansen, A. H.; Hansen, S. H.; Hellman, K.; Nielsen, P. A.; Olsen, L. R.; Verdonck, R.; Abbott, N. J.; Vanden Broeck, J.; et al. Characterization of a novel brain barrier ex vivo insect-based P-glycoprotein screening model. *Pharmacology Research & Perspectives* **2014**, *2* (4), e00050-n/a. DOI: 10.1002/prp2.50.

(76) Andersson, O.; Hansen, S. H.; Hellman, K.; Olsen, L. R.; Andersson, G.; Badolo, L.; Svenstrup, N.; Nielsen, P. A. The Grasshopper: A Novel Model for Assessing Vertebrate Brain Uptake. *Journal of Pharmacology and Experimental Therapeutics* **2013**, *346* (2), 211-218. DOI: 10.1124/jpet.113.205476.

(77) Thorn, C. F.; Müller, D. J.; Altman, R. B.; Klein, T. E. PharmGKB summary: clozapine pathway, pharmacokinetics. *Pharmacogenet Genomics* **2018**, *28* (9), 214-222. DOI: 10.1097/FPC.0000000000000347 PubMed.

(78) Markram, H. Seven challenges for neuroscience. *Funct Neurol* **2013**, *28* (3), 145-151. DOI: 10.11138/FNeur/2013.28.3.144 PubMed.

(79) Landhuis, E. Neuroscience: Big brain, big data. *Nature* **2017**, *541* (7638), 559-561. DOI: 10.1038/541559a.

(80) Maze, I.; Shen, L.; Zhang, B.; Garcia, B. A.; Shao, N.; Mitchell, A.; Sun, H.; Akbarian, S.; Allis, C. D.; Nestler, E. J. Analytical tools and current challenges in the modern era of neuroepigenomics. *Nat Neurosci* **2014**, *17* (11), 1476-1490. DOI: 10.1038/nn.3816 From NLM.

(81) Danon, J. J.; Reekie, T. A.; Kassiou, M. Challenges and Opportunities in Central Nervous System Drug Discovery. *Trends in Chemistry* **2019**, *1* (6), 612-624. DOI: https://doi.org/10.1016/j.trechm.2019.04.009.

(82) Gribkoff, V. K.; Kaczmarek, L. K. The need for new approaches in CNS drug discovery: Why drugs have failed, and what can be done to improve outcomes. *Neuropharmacology* **2017**, *120*, 11-19. DOI: 10.1016/j.neuropharm.2016.03.021 From NLM.

(83) Markou, A.; Chiamulera, C.; Geyer, M. A.; Tricklebank, M.; Steckler, T. Removing Obstacles in Neuroscience Drug Discovery: The Future Path for Animal Models. *Neuropsychopharmacology* **2009**, *34* (1), 74-89. DOI: 10.1038/npp.2008.173.

(84) Arias, D.; Saxena, S.; Verguet, S. Quantifying the global burden of mental disorders and their economic value. *EClinicalMedicine* **2022**, *54*, 101675. DOI: 10.1016/j.eclinm.2022.101675 From NLM.

(85) Lally, J.; MacCabe, J. H. Antipsychotic medication in schizophrenia: a review. *Br Med Bull* **2015**, *114* (1), 169-179. DOI: 10.1093/bmb/ldv017 From NLM.

(86) Tost, H.; Alam, T.; Meyer-Lindenberg, A. Dopamine and psychosis: theory, pathomechanisms and intermediate phenotypes. *Neurosci Biobehav Rev* **2010**, *34* (5), 689-700. DOI: 10.1016/j.neubiorev.2009.06.005 PubMed.

(87) Seeman, P. Clozapine, a fast-off-D2 antipsychotic. *ACS Chem Neurosci* **2014**, *5* (1), 24-29. DOI: 10.1021/cn400189s From NLM.

(88) Raedler, T. J.; Tandon, R. Cholinergic mechanisms in schizophrenia: Current concepts. *Current Psychosis & Therapeutics Reports* **2006**, *4* (1), 20-26. DOI: 10.1007/BF02629410.

(89) Burstein, E. S.; Ma, J.; Wong, S.; Gao, Y.; Pham, E.; Knapp, A. E.; Nash, N. R.; Olsson, R.; Davis, R. E.; Hacksell, U.; et al. Intrinsic Efficacy of Antipsychotics at Human D₂, D₃, and D₄ Dopamine Receptors: Identification of the Clozapine Metabolite N-Desmethylclozapine as a D₂/D₃ Partial Agonist. *Journal of Pharmacology and Experimental Therapeutics* **2005**, *315* (3), 1278-1287. DOI: 10.1124/jpet.105.092155.

(90) Manvich, D. F.; Webster, K. A.; Foster, S. L.; Farrell, M. S.; Ritchie, J. C.; Porter, J. H.; Weinshenker, D. The DREADD agonist clozapine N-oxide (CNO) is reverse-metabolized to clozapine and produces clozapine-like interoceptive stimulus effects in rats and mice. *Scientific Reports* **2018**, *8* (1), 3840. DOI: 10.1038/s41598-018-22116-z.

(91) Zhu, H.; Roth, Bryan L. Silencing Synapses with DREADDs. *Neuron* **2014**, *82* (4), 723-725. DOI: https://doi.org/10.1016/j.neuron.2014.05.002.

(92) Roth, B. L. DREADDs for Neuroscientists. *Neuron* **2016**, *89* (4), 683-694. DOI: 10.1016/j.neuron.2016.01.040 (acccessed 2020/03/28).

(93) Smith, K. S.; Bucci, D. J.; Luikart, B. W.; Mahler, S. V. DREADDS: Use and application in behavioral neuroscience. *Behav Neurosci* **2016**, *130* (2), 137-155. DOI: 10.1037/bne0000135 PubMed.

(94) Goodwin, R. J. A.; Lang, A. M.; Allingham, H.; Borén, M.; Pitt, A. R. Stopping the clock on proteomic degradation by heat treatment at the point of tissue excision. *PROTEOMICS* **2010**, *10* (9), 1751-1761. DOI: 10.1002/pmic.200900641 (acccessed 2020/03/01).

(95) Schulz, S.; Becker, M.; Groseclose, M. R.; Schadt, S.; Hopf, C. Advanced MALDI mass spectrometry imaging in pharmaceutical research and drug development. *Current Opinion in Biotechnology* **2019**, *55*, 51-59. DOI: https://doi.org/10.1016/j.copbio.2018.08.003.

(96) Nishidate, M.; Hayashi, M.; Aikawa, H.; Tanaka, K.; Nakada, N.; Miura, S.-i.; Ryu, S.; Higashi, T.; Ikarashi, Y.; Fujiwara, Y.; et al. Applications of MALDI mass spectrometry imaging for pharmacokinetic studies during drug development. *Drug Metabolism and Pharmacokinetics* **2019**, *34* (4), 209-216. DOI: https://doi.org/10.1016/j.dmpk.2019.04.006.

(97) Wang, D.; Astruc, D. The Golden Age of Transfer Hydrogenation. *Chemical Reviews* **2015**, *115* (13), 6621-6686. DOI: 10.1021/acs.chemrev.5b00203.

(98) Cummings, S. P.; Le, T.-N.; Fernandez, G. E.; Quiambao, L. G.; Stokes, B. J. Tetrahydroxydiboron-Mediated Palladium-Catalyzed Transfer Hydrogenation and Deuteriation of Alkenes and Alkynes Using Water as the Stoichiometric H or D Atom Donor. *Journal of the American Chemical Society* **2016**, *138* (19), 6107-6110. DOI: 10.1021/jacs.6b02132.

(99) Yoshimura, M.; Tanaka, S.; Kitamura, M. Recent topics in catalytic asymmetric hydrogenation of ketones. *Tetrahedron Letters* **2014**, *55* (27), 3635-3640. DOI: http://dx.doi.org/10.1016/j.tetlet.2014.04.129.

(100) Wang, Y.-Q.; Lu, S.-M.; Zhou, Y.-G. Palladium-Catalyzed Asymmetric Hydrogenation of Functionalized Ketones. *Organic Letters* **2005**, *7* (15), 3235-3238. DOI: 10.1021/ol051007u.

(101) Ide, M. S.; Hao, B.; Neurock, M.; Davis, R. J. Mechanistic Insights on the Hydrogenation of α,β-Unsaturated Ketones and Aldehydes to Unsaturated Alcohols over Metal Catalysts. *ACS Catalysis* **2012**, *2* (4), 671-683. DOI: 10.1021/cs200567z.

(102) Rueping, M.; Sugiono, E.; Azap, C.; Theissmann, T.; Bolte, M. Enantioselective Brønsted Acid Catalyzed Transfer Hydrogenation: Organocatalytic Reduction of Imines. *Organic Letters* **2005**, *7* (17), 3781-3783. DOI: 10.1021/ol0515964.

(103) Zhu, C.; Saito, K.; Yamanaka, M.; Akiyama, T. Benzothiazoline: Versatile Hydrogen Donor for Organocatalytic Transfer Hydrogenation. *Accounts of Chemical Research* **2015**, *48* (2), 388-398. DOI: 10.1021/ar500414x.

(104) Zhao, Q.; Wen, J.; Tan, R.; Huang, K.; Metola, P.; Wang, R.; Anslyn, E. V.; Zhang, X. Rhodium-Catalyzed Asymmetric Hydrogenation of Unprotected NH Imines Assisted by a Thiourea. *Angewandte Chemie International Edition* **2014**, *53* (32), 8467-8470. DOI: 10.1002/anie.201404570.

(105) Blacker, A. J. Enantioselective Transfer Hydrogenation. In *The Handbook of Homogeneous Hydrogenation*, Wiley-VCH Verlag GmbH, 2008; pp 1215-1244.

(106) Amoa, K. Catalytic Hydrogenation of Maleic Acid at Moderate Pressures. *Journal of Chemical Education* **2007**, *84* (12), 1948. DOI: 10.1021/ed084p1948.

(107) Yamakawa, M.; Ito, H.; Noyori, R. The Metal−Ligand Bifunctional Catalysis: A Theoretical Study on the Ruthenium(II)-Catalyzed Hydrogen Transfer between Alcohols and Carbonyl Compounds. *Journal of the American Chemical Society* **2000**, *122* (7), 1466-1478. DOI: 10.1021/ja991638h.

(108) Ohkuma, T.; Tsutsumi, K.; Utsumi, N.; Arai, N.; Noyori, R.; Murata, K. Asymmetric Hydrogenation of α-Chloro Aromatic Ketones Catalyzed by η6-Arene/TsDPEN−Ruthenium(II) Complexes. *Organic Letters* **2007**, *9* (2), 255-257. DOI: 10.1021/ol062661s.

(109) Arai, N.; Satoh, H.; Utsumi, N.; Murata, K.; Tsutsumi, K.; Ohkuma, T. Asymmetric Hydrogenation of Alkynyl Ketones with the η6-Arene/TsDPEN–Ruthenium(II) Catalyst. *Organic Letters* **2013**, *15* (12), 3030-3033. DOI: 10.1021/ol4012184.

(110) Chen, Y.-C.; Xue, D.; Deng, J.-G.; Cui, X.; Zhu, J.; Jiang, Y.-Z. Efficient asymmetric transfer hydrogenation of activated olefins catalyzed by ruthenium amido complexes. *Tetrahedron Letters* **2004**, *45* (7), 1555-1558. DOI: http://dx.doi.org/10.1016/j.tetlet.2003.12.057.

(111) Noyori, R.; Hashiguchi, S. Asymmetric Transfer Hydrogenation Catalyzed by Chiral Ruthenium Complexes. *Accounts of Chemical Research* **1997**, *30* (2), 97-102. DOI: 10.1021/ar9502341.

(112) Gladiali, S.; Alberico, E. Asymmetric transfer hydrogenation: chiral ligands and applications. *Chemical Society Reviews* **2006**, *35* (3), 226-236, 10.1039/B513396C. DOI: 10.1039/B513396C.

(113) Seashore-Ludlow, B.; Villo, P.; Häcker, C.; Somfai, P. Enantioselective Synthesis of anti-β-Hydroxy-α-amido Esters via Transfer Hydrogenation. *Organic Letters* **2010**, *12* (22), 5274-5277. DOI: 10.1021/ol102323k.

(114) Seashore-Ludlow, B.; Villo, P.; Somfai, P. Enantioselective Synthesis of anti-β-Hydroxy-α-Amido Esters by Asymmetric Transfer Hydrogenation in Emulsions. *Chemistry – A European Journal* **2012**, *18* (23), 7219-7223. DOI: 10.1002/chem.201103739.

(115) Seashore-Ludlow, B.; Saint-Dizier, F.; Somfai, P. Asymmetric Transfer Hydrogenation Coupled with Dynamic Kinetic Resolution in Water: Synthesis of anti-β-Hydroxy-α-amino Acid Derivatives. *Organic Letters* **2012**, *14* (24), 6334-6337. DOI: 10.1021/ol303115v.

(116) Limanto, J.; Krska, S. W.; Dorner, B. T.; Vazquez, E.; Yoshikawa, N.; Tan, L. Dynamic Kinetic Resolution: Asymmetric Transfer Hydrogenation of α-Alkyl-Substituted β-Ketoamides. *Organic Letters* **2010**, *12* (3), 512-515. DOI: 10.1021/ol902715d.

(117) Cartigny, D.; Püntener, K.; Ayad, T.; Scalone, M.; Ratovelomanana-Vidal, V. Highly Diastereo- and Enantioselective Synthesis of Monodifferentiated syn-1,2-Diol Derivatives through Asymmetric Transfer Hydrogenation via Dynamic Kinetic Resolution. *Organic Letters* **2010**, *12* (17), 3788-3791. DOI: 10.1021/ol101451s.

(118) Mohar, B.; Valleix, A.; Desmurs, J.-R.; Felemez, M.; Wagner, A.; Mioskowski, C. Highly enantioselective synthesis via dynamic kinetic resolution under transfer hydrogenation using Ru([small eta]6-arene)-N-perfluorosulfonyl-1,2-diamine catalysts: a first insight into the relationship of the ligand's pKa and the catalyst activity. *Chemical Communications* **2001**, (24), 2572-2573, 10.1039/B107822B. DOI: 10.1039/B107822B.

(119) Son, S.-M.; Lee, H.-K. Dynamic Kinetic Resolution-Based Asymmetric Transfer Hydrogenation of 2-Benzoylmorpholinones and Its Use in Concise Stereoselective Synthesis of All Four Stereoisomers of the Antidepressant Reboxetine. *The Journal of Organic Chemistry* **2013**, *78* (17), 8396-8404. DOI: 10.1021/jo401102d.

(120) Eustache, F.; Dalko, P. I.; Cossy, J. Enantioselective Monoreduction of 2-Alkyl-1,3-diketones Mediated by Chiral Ruthenium Catalysts. Dynamic Kinetic Resolution. *Organic Letters* **2002**, *4* (8), 1263-1265. DOI: 10.1021/ol025527q.

(121) Eustache, F.; Dalko, P. I.; Cossy, J. Enantioselective monoreduction of 2-alkyl 1,3-diketones using chiral ruthenium catalysts. Synthesis of the C14□C25 fragment of bafilomycin A1. *Tetrahedron Letters* **2003**, *44* (49), 8823-8826. DOI: http://dx.doi.org/10.1016/j.tetlet.2003.09.192.

(122) Cossy, J.; Eustache, F.; Dalko, P. I. Ruthenium-catalyzed asymmetric reduction of 1,3-diketones using transfer hydrogenation. *Tetrahedron Letters* **2001**, *42* (30), 5005-5007. DOI: http://dx.doi.org/10.1016/S0040-4039(01)00906-6.

(123) Koike, T.; Murata, K.; Ikariya, T. Stereoselective Synthesis of Optically Active α-Hydroxy Ketones and anti-1,2-Diols via Asymmetric Transfer Hydrogenation of Unsymmetrically Substituted 1,2-Diketones. *Organic Letters* **2000**, *2* (24), 3833-3836. DOI: 10.1021/ol0002572.

(124) Murata, K.; Okano, K.; Miyagi, M.; Iwane, H.; Noyori, R.; Ikariya, T. A Practical Stereoselective Synthesis of Chiral Hydrobenzoins via Asymmetric Transfer Hydrogenation of Benzils. *Organic Letters* **1999**, *1* (7), 1119-1121. DOI: 10.1021/ol990226a.

(125) Corbett, M. T.; Johnson, J. S. Diametric Stereocontrol in Dynamic Catalytic Reduction of Racemic Acyl Phosphonates: Divergence from α-Keto Ester Congeners. *Journal of the American Chemical Society* **2013**, *135* (2), 594-597. DOI: 10.1021/ja310980q.

(126) Fernández, R.; Ros, A.; Magriz, A.; Dietrich, H.; Lassaletta, J. M. Enantioselective synthesis of cis-α-substituted cycloalkanols and trans-cycloalkyl amines thereof. *Tetrahedron* **2007**, *63* (29), 6755-6763. DOI: http://dx.doi.org/10.1016/j.tet.2007.04.075.

(127) Ros, A.; Magriz, A.; Dietrich, H.; Lassaletta, J. M.; Fernández, R. Stereoselective synthesis of syn β-hydroxy cycloalkane carboxylates: transfer hydrogenation of cyclic β-keto esters via dynamic kinetic resolution. *Tetrahedron* **2007**, *63* (32), 7532-7537. DOI: http://dx.doi.org/10.1016/j.tet.2007.05.058.

(128) Alcock, N. J.; Mann, I.; Peach, P.; Wills, M. Dynamic kinetic resolution–asymmetric transfer hydrogenation of 1-aryl-substituted cyclic ketones. *Tetrahedron: Asymmetry* **2002**, *13* (22), 2485-2490. DOI: http://dx.doi.org/10.1016/S0957-4166(02)00648-1.

(129) Ding, Z.; Yang, J.; Wang, T.; Shen, Z.; Zhang, Y. Dynamic kinetic resolution of [small beta]-keto sulfones via asymmetric transfer hydrogenation. *Chemical Communications* **2009**, (5), 571-573, 10.1039/B818257D. DOI: 10.1039/B818257D.

(130) Goodman, C. G.; Do, D. T.; Johnson, J. S. Asymmetric Synthesis of anti-β-Amino-α-Hydroxy Esters via Dynamic Kinetic Resolution of β-Amino-α-Keto Esters. *Organic Letters* **2013**, *15* (10), 2446-2449. DOI: 10.1021/ol4009206.

(131) Villacrez, M.; Somfai, P. Enantioselective synthesis of anti-β-amido-α-hydroxy esters via asymmetric transfer hydrogenation coupled with dynamic kinetic resolution. *Tetrahedron Letters* **2013**, *54* (38), 5266-5268. DOI: http://dx.doi.org/10.1016/j.tetlet.2013.07.100.

(132) Rich, D. H.; Moon, B. J.; Harbeson, S. Inhibition of aminopeptidases by amastatin and bestatin derivatives. Effect of inhibitor structure on slow-binding processes. *J Med Chem* **1984**, *27* (4), 417-422. DOI: 10.1021/jm00370a001.

(133) DeMattei, J. A.; Leanna, M. R.; Li, W.; Nichols, P. J.; Rasmussen, M. W.; Morton, H. E. An Efficient Synthesis of the Taxane-Derived Anticancer Agent ABT-271. *The Journal of Organic Chemistry* **2001**, *66* (10), 3330-3337. DOI: 10.1021/jo0057203.

(134) Leanna, M. R.; DeMattei, J. A.; Li, W.; Nichols, P. J.; Rasmussen, M.; Morton, H. E. Synthesis of the C-13 Side Chain Precursors of the 9-Dihydrotaxane Analogue ABT-271. *Organic Letters* **2000**, *2* (23), 3627-3630. DOI: 10.1021/ol006508o.

(135) Feske, B. D.; Kaluzna, I. A.; Stewart, J. D. Enantiodivergent, Biocatalytic Routes to Both Taxol Side Chain Antipodes. *The Journal of Organic Chemistry* **2005**, *70* (23), 9654-9657. DOI: 10.1021/jo0516077.

(136) Patel, R. N.; Banerjee, A.; Howell, J. M.; McNamee, C. G.; Brozozowski, D.; Mirfakhrae, D.; Nanduri, V.; Thottathil, J. K.; Szarka, L. J. Microbial synthesis of (2R,3S)-(−)-N-benzoyl-3-phenyl isoserine ethyl ester-a taxol side-chain synthon. *Tetrahedron: Asymmetry* **1993**, *4* (9), 2069-2084. DOI: http://dx.doi.org/10.1016/S0957-4166(00)82256-9.

(137) Commerçon, A.; Bézard, D.; Bernard, F.; Bourzat, J. D. Improved protection and esterification of a precursor of the taxotere® and taxol side chains. *Tetrahedron Letters* **1992**, *33* (36), 5185-5188. DOI: http://dx.doi.org/10.1016/S0040-4039(00)79128-3.

(138) Pravst, I.; Zupan, M.; Stavber, S. Directed regioselectivity of bromination of ketones with NBS: solvent-free conditions versus water. *Tetrahedron Letters* **2006**, *47* (27), 4707-4710. DOI: http://dx.doi.org/10.1016/j.tetlet.2006.04.119.

(139) Palamini, P.; Allouche, E. M. D.; Waser, J. Iron-Catalyzed Synthesis of α-Azido α-Amino Esters via the Alkylazidation of Alkenes. *Organic Letters* **2023**. DOI: 10.1021/acs.orglett.3c02153.

(140) Steward, K. M.; Corbett, M. T.; Goodman, C. G.; Johnson, J. S. Asymmetric Synthesis of Diverse Glycolic Acid Scaffolds via Dynamic Kinetic Resolution of α-Keto Esters. *Journal of the American Chemical Society* **2012**, *134* (49), 20197-20206. DOI: 10.1021/ja3102709.

(141) Steward, K. M.; Johnson, J. S. Catalytic Nucleophilic Glyoxylation of Aldehydes. *Organic Letters* **2010**, *12* (12), 2864-2867. DOI: 10.1021/ol100996w.

(142) Seashore-Ludlow, B.; Somfai, P. Domino Carbopalladation−Carbonylation: Generating Quaternary Stereocenters while Controlling β-Hydride Elimination. *Organic Letters* **2010**, *12* (17), 3732-3735. DOI: 10.1021/ol1009703.

(143) Seashore-Ludlow, B.; Danielsson, J.; Somfai, P. Domino Carbopalladation-Carbonylation: Investigation of Substrate Scope. *Advanced Synthesis & Catalysis* **2012**, *354* (1), 205-216. DOI: 10.1002/adsc.201100678.

(144) Subramaniam, G.; Hiraku, O.; Hayashi, M.; Koyano, T.; Komiyama, K.; Kam, T.-S. Biologically Active Aspidofractinine, Rhazinilam, Akuammiline, and Vincorine Alkaloids from Kopsia. *Journal of Natural Products* **2007**, *70* (11), 1783-1789. DOI: 10.1021/np0703747.

(145) Olofsson, B.; Somfai, P. Divergent Synthesis of d-erythro-Sphingosine, l-threo-Sphingosine, and Their Regioisomers. *The Journal of Organic Chemistry* **2003**, *68* (6), 2514-2517. DOI: 10.1021/jo0268254.

(146) Koizumi, H.; Yokoshima, S.; Fukuyama, T. Total Synthesis of (−)-Morphine. *Chemistry – An Asian Journal* **2010**, *5* (10), 2192-2198. DOI: 10.1002/asia.201000458.

(147) Lippstreu, J. J.; Straub, B. F. Mechanism of Enyne Metathesis Catalyzed by Grubbs Ruthenium−Carbene Complexes: A DFT Study. *Journal of the American Chemical Society* **2005**, *127* (20), 7444-7457. DOI: 10.1021/ja042622g.

(148) Rosillo, M.; Domínguez, G.; Casarrubios, L.; Amador, U.; Pérez-Castells, J. Tandem Enyne Metathesis-Diels−Alder Reaction for Construction of Natural Product Frameworks. *The Journal of Organic Chemistry* **2004**, *69* (6), 2084-2093. DOI: 10.1021/jo0356311.

(149) Clark, D. A.; Kulkarni, A. A.; Kalbarczyk, K.; Schertzer, B.; Diver, S. T. Tandem Enyne Metathesis and Claisen Rearrangement: A Versatile Approach to Conjugated Dienes of Variable Substitution Patterns. *Journal of the American Chemical Society* **2006**, *128* (49), 15632-15636. DOI: 10.1021/ja063132m.

(150) Kulkarni, A. A.; Diver, S. T. Cycloheptadiene Ring Synthesis by Tandem Intermolecular Enyne Metathesis. *Organic Letters* **2003**, *5* (19), 3463-3466. DOI: 10.1021/ol035246y.

(151) Peppers, B. P.; Kulkarni, A. A.; Diver, S. T. Functional Group Scope in the Methylene-Free, Tandem Enyne Metathesis. *Organic Letters* **2006**, *8* (12), 2539-2542. DOI: 10.1021/ol060727d.

(152) Nishimura, M.; Minakata, S.; Thongchant, S.; Ryu, I.; Komatsu, M. Selective [2+1] aziridination of conjugated dienes with a nitridomanganese complex: a new route to alkenylaziridines. *Tetrahedron Letters* **2000**, *41* (36), 7089-7092. DOI: http://dx.doi.org/10.1016/S0040-4039(00)01219-3.

(153) Yin, W.; Kabir, M. S.; Wang, Z.; Rallapalli, S. K.; Ma, J.; Cook, J. M. Enantiospecific Total Synthesis of the Important Biogenetic Intermediates along the Ajmaline Pathway, (+)-Polyneuridine and (+)-Polyneuridine Aldehyde, as well as 16-Epivellosimine and Macusine A. *The Journal of Organic Chemistry* **2010**, *75* (10), 3339-3349. DOI: 10.1021/jo100279w.

(154) Pei, Y.; Brade, K.; Brulé, E.; Hagberg, L.; Lake, F.; Moberg, C. A General Method for the Preparation of Chiral TREN Derivatives. *European Journal of Organic Chemistry* **2005**, *2005* (13), 2835-2840. DOI: 10.1002/ejoc.200500094.

(155) Hashmi, A. S. K.; Häffner, T.; Yang, W.; Pankajakshan, S.; Schäfer, S.; Schultes, L.; Rominger, F.; Frey, W. Gold Catalysis: Non-Spirocyclic Intermediates in the Conversion of Furanynes by the Formal Insertion of an Alkyne into an Aryl–Alkyl C□C Single Bond. *Chemistry – A European Journal* **2012**, *18* (34), 10480-10486. DOI: 10.1002/chem.201200306.

(156) M. Gardiner, J.; R. Loyns, C. Synthesis of novel 1-, 1,4- and 1,7-substituted 2-mercapto- and 2-methylmercapto- benzimidazoles: Acyclic analogues of the HIV-1 RT inhibitor, TIBO. *Tetrahedron* **1995**, *51* (42), 11515-11530. DOI: http://dx.doi.org/10.1016/0040-4020(95)00751-S.

(157) Tuthill, P. A.; Seida, P. R.; Barker, W.; Cassel, J. A.; Belanger, S.; DeHaven, R. N.; Koblish, M.; Gottshall, S. L.; Little, P. J.; DeHaven-Hudkins, D. L.; et al. Azepinone as a conformational constraint in the design of κ-opioid receptor agonists. *Bioorganic & Medicinal Chemistry Letters* **2004**, *14* (22), 5693-5697. DOI: http://dx.doi.org/10.1016/j.bmcl.2004.08.041.

(158) Smith, M. W.; Snyder, S. A. A Concise Total Synthesis of (+)-Scholarisine A Empowered by a Unique C–H Arylation. *Journal of the American Chemical Society* **2013**, *135* (35), 12964-12967. DOI: 10.1021/ja406546k.

(159) Connell, J. J.; Sugihara, Y.; Török, S.; Döme, B.; Tóvári, J.; Fehniger, T. E.; Marko-Varga, G.; Végvári, Á. Localization of sunitinib in in vivo animal and in vitro experimental models by MALDI mass spectrometry imaging. *Analytical and Bioanalytical Chemistry* **2015**, *407* (8), 2245-2253, journal article. DOI: 10.1007/s00216-014-8350-2.

Paper I

ACS Chemical Neuroscience Cite This: ACS Chem. Neurosci. 2018, 9, 1994−2000

Letter

pubs.acs.org/chemneuro

Evaluation of Drug Exposure and Metabolism in Locust and Zebrafish Brains Using Mass Spectrometry Imaging

Marvin Villacrez,[†] Karin Hellman,[†] Tatsuya Ono,[‡] Yutaka Sugihara,[‡] Melinda Rezeli,[‡] Fredrik Ek,[†] Gyorgy Marko-Varga,[‡] and Roger Olsson*[,†]

[†]Chemical Biology & Therapeutics group, Department of Experimental Medical Science, Lund University, S-22184 Lund, Sweden

[‡]Division of Clinical Protein Science and Imaging, Department of Experimental Medical Science, Lund University, S-22184 Lund, Sweden

Supporting Information

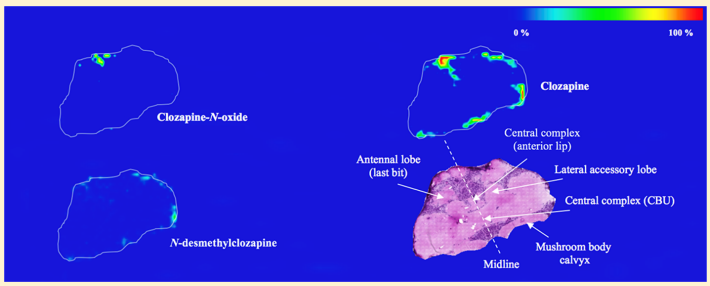

ABSTRACT: Studying how and where drugs are metabolized in the brain is challenging. In an entire organism, peripheral metabolism produces many of the same metabolites as those in the brain, and many of these metabolites can cross the blood-brain barrier from the periphery, thus making the relative contributions of hepatic and brain metabolism difficult to study in vivo. In addition, drugs and metabolites contained in ventricles and in the residual blood of capillaries in the brain may overestimate drugs' and metabolites' concentrations in the brain. In this study, we examine locusts and zebrafish using matrix assisted laser desorption ionization mass spectrometry imaging to study brain metabolism and distribution. These animal models are cost-effective and ethically sound for initial drug development studies.

KEYWORDS: *Mass spectrometry imaging, blood-brain barrier, drug metabolism, clozapine, zebrafish, Locust*

The human brain is the most complex and heterogeneous organ. In drug discovery for the central nervous system (CNS), the focus has been on if drugs reach the brain or not and not on the drugs' destiny within the brain.[1,2] Drug metabolism in the brain has largely been ignored during the drug discovery process based on the assumption that drug metabolism is negligible compared to the metabolism in the liver. However, the main metabolizing enzymes, cytochrome P450 enzymes (CYPs), can reach concentrations comparable with the ones found in the liver because of compartmentalization to specific cells.[3,4] Thus, cell-specific drug metabolism can generate significant effects if metabolites are generated in the vicinity of their site of biological action.[5] A detrimental implication of this is the bioactivation of xenobiotics to toxic metabolites, for instance, the pesticide chlorpyrifos causes neurological effects in humans once oxidized to chlorpyrifos oxon by P450 2B.[6] In blood and liver chlorpyrifos oxon is reactive, quickly inactivated and is unlikely to reach the brain, suggesting that the direct transformation in the brain is the reason for brain toxicity.[7,8] Hence, metabolites formed in the liver that are either reactive or unable to reach or penetrate the blood-brain barrier (BBB) can still be formed directly in the brain.

In search of alternative animal models that can be efficiently used in early drug discovery to evaluate the drug activity and pharmacokinetic properties of potential drugs and toxins in the central nervous system, we focus on zebrafish, *Danio rerio*, and the desert locust, *Schistocerca gregaria*. We recently reported on an ex vivo model based on the desert locust that examines BBB permeability, efflux, drug metabolism, and free fraction of the drug in brain.[9] As in vertebrates, the insect brain has conserved essential mechanisms for CNS protection, i.e., requirements for tightness and control of elements entering the brain.[10] Moreover, it has been shown that the insect brain barrier contains various transporter proteins, including a homologue to the vertebrate P-glycoprotein (P-gp).[11] One of the functions of

Special Issue: Model Systems in Neuroscience

Received: November 20, 2017
Accepted: January 12, 2018
Published: January 19, 2018

DOI: 10.1021/acschemneuro.7b00459
ACS Chem. Neurosci. 2018, 9, 1994−2000

CYPs in the brain is about cell-specific synthesis of endogenous neurochemicals, and because mammals and invertebrates share a plethora of neurotransmitters, it is likely that they share endogenous synthetic pathways of several neurochemicals.[12] Using the locust ex vivo model to analyze drug metabolism, drug−drug interactions, BBB permeability, efflux by P-gp, and free fraction of the drug, we showed that most findings correlated well with data in the literature for mammals; however, we found that clozapine-*N*-oxide (CNO) is not a highly BBB permeant compound as previously been stated.[13] This finding was of particular interest, as it was a clear discrepancy between the results reported from mammals and the findings in the ex vivo insect model at the time. However, it has recently been established that CNO is a P-gp substrate and not a highly BBB permeant compound in nonhuman primates and rodents; this finding corroborates results from the insect brain.[14,15]

Previously, using the locust ex vivo model, we initially focused on evaluating the BBB penetration of clozapine (CLO) and CLO's major metabolite, *N*-desmethylclozapine (NDMC) (Scheme 1). The reason for this was that the pharmacology of

Scheme 1. Our Previous Experiments Support the Observation That Biotransformation Occurs between CLO and CNO While NDMC Appears to Act As a Metabolic Sink

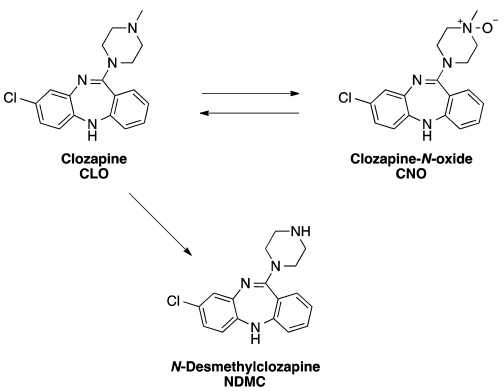

NDMC was introduced as the missing link to explain the unique efficacy of CLO to improve cognition and negative symptoms in the treatment of patients with schizophrenia.[16] However, in a phase IIb trial for the treatment of schizophrenia, NDMC failed to show improved efficacy compared to placebo at two doses. One hypothesis for NDMC's lack of efficacy in the trial was that replacing the *N*-methyl with hydrogen, that is, adding a hydrogen bond donor, decreased the BBB penetration. Using the locust ex-vivo model revealed that CLO penetrated the BBB better than NDMC did, but only with a modest factor of about two. The results also showed that NDMC was formed in the brain from CLO, and the other metabolite, CNO, was preferentially detected in the solution immersing the incubated brain, thus indicating that CNO was formed but was transported out of the brain into the solution. Another explanation of CLO's unique profile could be the combination of pharmacology from CLO and the formed NDMC and their distributions in the brain. Albeit far from a human brain, the locust brain could provide an illustrative picture of BBB penetration, metabolism and distribution in the brain. The locust ex vivo model uses controlled in-vitro-like exposure conditions that provide a direct comparison of chemical compounds and thus no interference from peripherally formed metabolites or residues in the vascularity and ventricles.

The ex vivo locust model could be regarded as a black box, meaning that the model can determine whether metabolism has taken place but cannot determine where metabolism has occurred in the brain nor the resulting distribution of the drugs and their metabolites. Recently, matrix assisted laser desorption ionization (MALDI) mass spectrometry imaging (MSI) has entered the field of tissue-based research and proved itself to be a powerful technique to study drug transit and metabolism. This label-free technique can distinguish between parent drugs and parent-derived metabolites based on molecular weights and fragmentation patterns and thereby provide a spatial distribution of drug and metabolites.[17,18] MALDI MSI complements autoradiography and positron emission tomographyand has the advantage of not requiring specific labeling.[19]

In a methodology paper, CLO and NDMC were analyzed using MALDI MSI, and the method demonstrated a sufficient spatial resolution and sensitivity to reveal the distribution of drugs in rat brain tissue samples. Further, the results of CLO distribution in rat brain sections obtained using the MALDI MSI method were consistent with those obtained by autoradiography.[20] Still, no studies have been reported that link drug BBB penetration and metabolism (excluding peripheral metabolism) in the brain using MALDI MSI. Herein, we report on the combination of MALDI MSI and an ex vivo model for the study of the metabolism and distribution of the atypical antipsychotic drug CLO and its major metabolites, NDMC and CNO, as shown in Scheme 1. This model illustrates the fate of a drug after penetration of the BBB, emphasizes distribution and metabolism and distinguishes drug and drug-derived metabolites by generating an ion intensity map of a brain tissue sample.

In the locust ex vivo model, the brain is dissected from the insect and placed in a well containing the test compound of interest. After incubation with the drug, the brain was snap frozen with dry ice and stored at −78 °C for no more than 3 days, as time of storage had an impact with respect to sample degradation. This is probably because of changes in cell morphology and endogenous enzymatic degradation of the analytes of interest.[18] Following the freezing process, the brains were sectioned using a freezing microtome; however, the critical MALDI MSI sample preparation steps of freezing, mounting and cutting were difficult because of the size of the insect brain, which was no more than a fraction of a pinhead (1.5*1.5* 0.7 mm^3). Due to the small brain size, significant deformation of the brain was difficult to avoid throughout the freezing process, and it was difficult to achieve an accurate sample orientation in the process of sectioning. To adequately manage the sample orientation, an optimum cutting temperature polymer was experimented with at an initial stage of the study but was soon abandoned due to ion suppression. Consequently, after harvesting of the brain, the freezing part was performed meticulously to minimize shape deformation, and the brain was sectioned by attachment to the cryomicrotome chuck by only applying Millipore water/ice as the adherent medium. Sectioning of the mounted brain was performed at 14 μm at different microtome atmosphere temperatures, which were selected depending on daily humidity conditions; this issue also probably stems from brain size.

DOI: 10.1021/acschemneuro.7b00459
ACS Chem. Neurosci. 2018, 9, 1994−2000

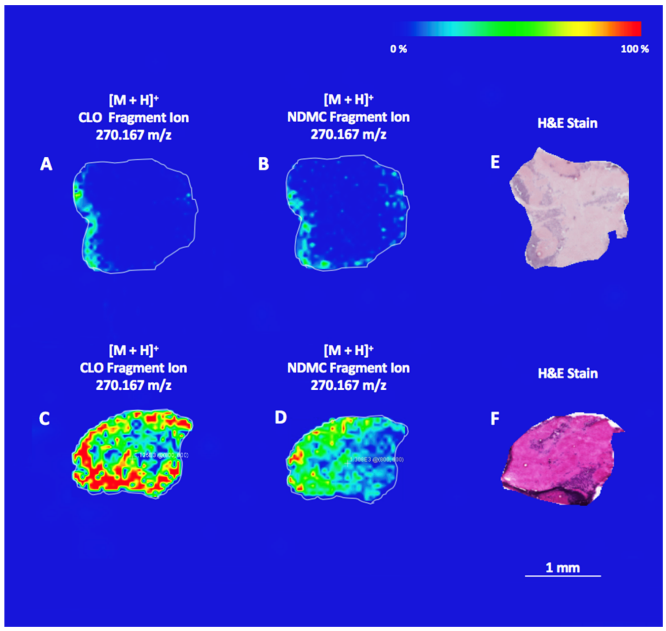

Figure 1. MS/MS MALDI MSI images for incubation of brains with CLO. Administrated CLO at an incubation time of 15 min (A) shows limited diffusion into the brain but a clear metabolization to NDMC (B). Incubation with CLO for 45 min (C) reveals distributions of CLO throughout the entire brain section as well as widespread distribution of NDMC (D). H&E staining was performed for the analyzed tissue samples (E) and (F). Color coded gradient bar shows relative concentrations of the analyzed compound. Scale bar = 1 mm.

Choosing an inadequate working temperature resulted in destroyed tissue slices because of sample rolling complications concurrently with the cutting instance, a result from supporting embedding medium absence. Before analysis in MALDI MSI and data acquisition, the matrix selection was guided by a previous study conducted on Africanized honeybee brains in which α-cyano-4-hydroxycinnamic acid (CHCA) was the matrix of choice. CHCA provided better ionization compared to sinapic acid (SA) and 2,5-dihydroxybenzoic acid (DHB), which are the two most common matrixes in MALDI MSI studies.[21,22] The results for the brain tissue experiments are presented by generating MS/MS ion intensity maps with a spatial resolution of 50 μm, product of collision induced dissociation (CID) fragmentation in a mass range from m/z 250 to 320 where the major ion fragments for all three drugs were to be found (m/z 270.167 for CLO as wells as for NDMC and m/z 299.167 for CNO, in accordance with a fragmentation study of CLO, NDMC and CNO[23]). In addition, the Supporting Information contains MS and MS/MS spectra for drug and its metabolites for early metal plate experiments as well as for brain experiments. The ion intensity maps presented in forthcoming figures are all bordered with a white line which depicts the actual brain tissue region. After MALDI MSI analysis, the matrix was removed and the tissue samples were stained with hematoxylin and eosin (H&E) to clearly demonstrate that drug signals arise from desert locust brain tissues. Overlays between MALDI images and H&E pictures are also presented in the Supporting Information.

CLO and NDMC were separately incubated with an isolated locust brain for 15 and 45 min, and the test solutions were set to 3 μM for both drugs; the concentration was determined based on our previous studies. The distribution and metabolism for CLO incubated brains were analyzed by MALDI MSI, and the results are presented in Figure 1. As shown in Figure 1A, the ion intensity maps illustrate that CLO has a limited penetration depth through the BBB after 15 min of incubation, but although CLO has modest permeability, the metabolism of CLO to NDMC, as shown in Figure 1B, is clearly seen, but CNO could not be detected in any case. Alongside this observation, small amounts of NDMC were found where CLO appeared to be absent; this could be an indication of fast metabolism in certain areas of the brain. Brains incubated with CLO for 45 min showed a distribution of CLO throughout the brain tissue sample with the highest relative concentration of CLO along the edges; this was most likely the consequence of diffusion rates after penetration through the BBB (Figure 1C). High relative concentrations of CLO could also be found along specific compartments of the brain. However, the distribution of CLO is not only existent throughout the entire brain sample after 45 min, but the NDMC that derives from CLO metabolism is also equally distributed, with the highest relative concentrations of NDMC being closest to the edges, as shown in Figure 1D. The H&E stained tissues for respective MALDI MSI runs are presented in Figure 1E, F. As for CNO, our previous LC-MS experiments of CLO exposed that CNO was only present in a fraction of the concentrations of CLO and NDMC in the same experimental conditions as those used in the current study. The absence of CNO in the generated MALDI MSI images does not per se mean that the metabolite is not generated in the brain, but this could be the outcome of

DOI: 10.1021/acschemneuro.7b00459
ACS Chem. Neurosci. 2018, 9, 1994−2000

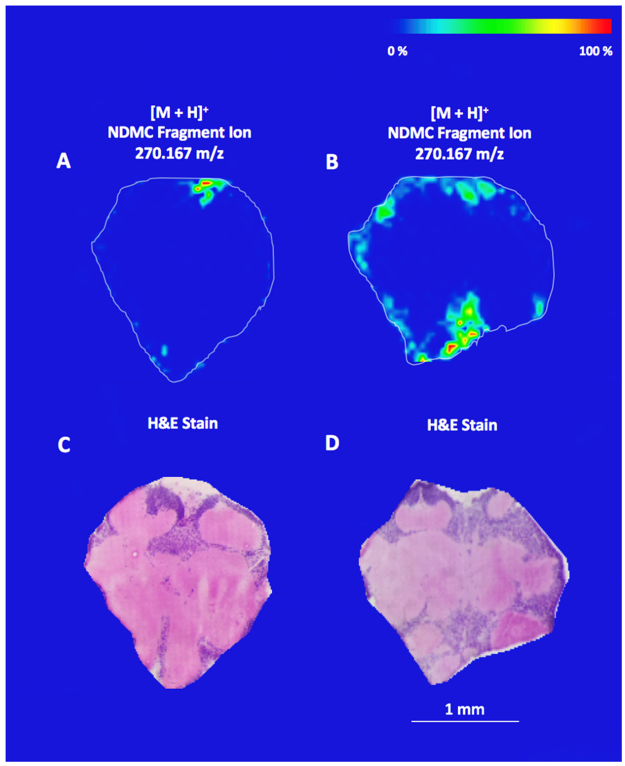

Figure 2. Brains incubated with NDMC for 15 min (A) depict a limited penetration of the drug trough the BBB. Extending the incubation time to 45 min (B) reveals that NDMC clearly penetrates through the BBB. H&E staining was performed for the analyzed tissue samples (C) and (D). Color coded gradient bar shows relative concentrations of the analyzed compound. Scale bar = 1 mm.

the low abundance of this metabolite, which is suppressed by the relative high concentrations of CLO and NDMC. To further study the distribution of CLO and its major metabolites, incubation with NDMC at 15 and 45 min was also conducted, as shown in Figure 2, and, as expected, neither CLO nor CNO were detected. Incubating with NDMC for 15 min (Figure 2A) indicates that this drug also has a limited and similar distribution as CLO for this time frame. However, for the NDMC 45 min setup (Figure 2B), a more limited distribution of NDMC compared to the CLO 45 min setup was seen. This observation corroborates the notion that NDMC has more polar features than CLO due to its additional hydrogen bonding potential. The analyzed brain samples were treated with H&E staining methodology (Figure 2C, D).

Finally, in experiments conducted with CNO, incubation occurred for 45 min and the concentration was initially set to 3 μM, but it was later increased to 10 μM because neither the drug nor the metabolites, CLO and NDMC, were observed at the lower of the concentrations. This is also probably the result of poor CNO permeation into the brain due to its more polar characteristics. This observation correlates well with that of our previous study and indicates that CNO is a P-gp substrate. Nevertheless, incubation with 10 μM for 45 min, as presented in Figure 3, shows, even if modest, permeability of CNO (Figure 3A) into the insect brain and formation of both CLO (Figure 3B) and NDMC (Figure 3C), indicating that CNO is not an inert compound toward metabolism in the brain. The analyzed brain sample was finally treated with H&E staining methodology (Figure 3D).

Zebrafish is an emerging animal model for evaluating in vivo activity, but to position zebrafish as a complement or an alternative to mammalian studies it is necessary to be able to conduct predictive pharmacokinetic−pharmacodynamics (PK−PD) modeling in zebrafish.[24−26] Thus, the quality of bioanalysis in zebrafish must at least reach a level comparable with what is done in rodents to facilitate transitions between animal models. Recently, MALDI MSI on whole zebrafish larvae revealed that cocaine accumulates in their eyes.[27] The finding indicated that central nervous system drugs must be properly assessed when using waterborne drug exposure and that whole fish bioanalysis of zebrafish larvae is not predictive for brain concentrations. However, proper PK−PD modeling in adult zebrafish drug concentrations and distribution in the brains is important.

Adult zebrafish in a shoal of 10 were treated with waterborne CLO (10 μM); initially, the shoal remained fairly evenly distributed in the bottom-half of the tank, but after a few minutes, individual fish started to demonstrate fast, repetitive movements between the surface and the bottom of the tank. This behavior culminated in that after 10 min of exposure, all fish in the shoal were constantly at the top of the tank and were

DOI: 10.1021/acschemneuro.7b00459
ACS Chem. Neurosci. 2018, 9, 1994−2000

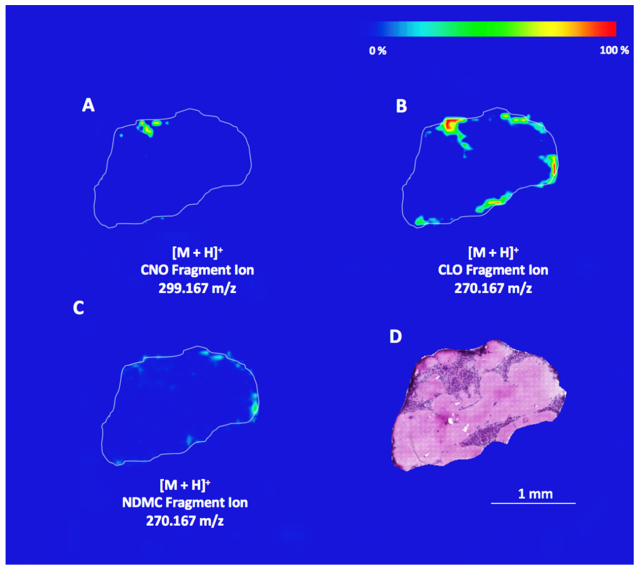

Figure 3. Only a scarce amount of CNO was observed after 45 min of incubation at 10 μM (A). This may be the consequence of fast biotransformation to CLO (B), which metabolized to NDMC, (C) but the limited penetration depth of all three compounds implies that CNO has a poor ability to cross the BBB. Staining with H&E of the analyzed tissue (D) was performed after MALDI MSI was conducted. Color coded gradient bar shows relative concentrations of the analyzed compound. Scale bar = 1 mm.

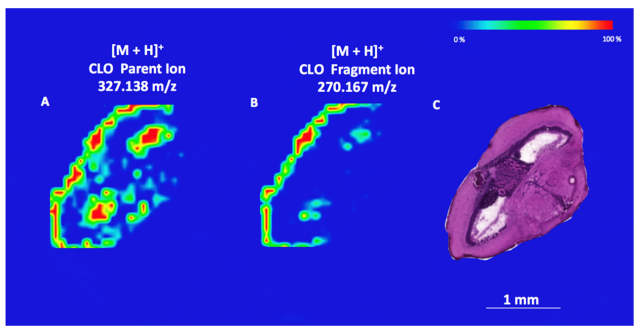

Figure 4. Zebrafish exposed to 10 μM CLO for 10 min. CLO parent ion (A) and major fragment ion (B) found in MALDI MSI. Correlating the MALDI ion intensity maps with H&E histology stains uncovers that CLO seems to be more abundant around the ventricular system, the periventricular gray zone and the optic tectum. Color coded gradient bar shows relative concentrations of the analyzed compound. Scale bar = 1 mm.

repeatedly breaching the surface, thus displaying intense activity. Meanwhile, the controls, which were in a matched shoal in a tank placed beside the CLO-treated shoal, showed no such activity and remained gathered in the shoal. In humans, there is a relationship between CLO dose and occurrence of CLO-induced side effects, such electroencephalogram abnormalities and seizures, which may occur due to anticholinergic effects.[28,29] This phenotype was not seen in adult zebrafish during waterborne exposure with CLO's metabolite, NDMC (10 μM). The observed behavioral changes were used as an indication of in vivo activity and verified sufficient exposure of CLO. After behavior onset, the fish were sacrificed by cooling prior to decapitation, and the brains were isolated, snap frozen in liquid nitrogen and stored at −78 °C. CLO distribution in the brain was analyzed using MALDI MSI (Figure 4). High concentrations of CLO were seen in the ventricular and vascular systems, the periventricular gray zone and the optic tectum. This highlights the importance of a proper technique for bioanalysis of specific brain areas. MALDI MSI can show the distribution of drugs with a high level of detail in zebrafish and, importantly, separate between drug exposure in tissue and in vascularity. There is a risk that traditional bioanalysis of brain content using homogenized whole tissue would have overestimated the brain exposure. The use of MALDI MSI to correlate drug exposure with molecular responses and behavior for detailed PK−PD modeling in zebrafish is ongoing.

DOI: 10.1021/acschemneuro.7b00459
ACS Chem. Neurosci. 2018, 9, 1994−2000

METHODS

CLO, NDMC, and CNO were analytical reagent grade. The matrix CHCA and trifluoroacetic acid (TFA) were purchased from Sigma-Aldrich (Stockholm, Sweden). Ethanol was purchased from Solveco (Rosersberg, Sweden), and acetonitrile was acquired from Fisher Scientific. Chemicals for histology purposes were purchased from Histolab (Gothenburg, Sweden).

The desert locusts used in the present study were tended to according to our previous work (Hellman et al).[9] Brains were removed from the cuticle, dissected free from fatty tissue, and placed in a microwell plate with the drug of interest dissolved in an insect buffer. The harvested drug treated brains were immediately snap frozen, placed in an Eppendorf tube and saved in a −80 °C freezer where they remained stored until they were collected to perform the MALDI MSI experiments. Samples were placed in the cutting cryo-microtome chamber at −20 °C (Leica CM1950 Cryostat, Nussloch, Germany) for 10 min before cutting. To avoid polymer interference, in mass spectra, originating from optimal cutting temperature media, the brains were mounted on the cutting block using Millipore water/ice. Transverse brain sections were obtained from both treated and untreated specimens at varying temperatures to a thickness of 14 μm and attached onto the MALDI glass slide (Thermo Fischer, Superfrost Ultra Plus, 25 × 75 × 1.0 mm^3, Germany) by means of thaw mounting. Untreated brains were used as controls to obtain a zero value, which was used to compare the signal intensities from the drug-treated brains. Following the freezing process, brains were placed in a vacuum chamber for 30 min in order to remove condensate produced from atmospheric water. The matrix CHCA solution was made with a concentration of 5.0 mg/mL in (1:1) acetonitrile:water and 0.2% of TFA. An automated pneumatic sprayer (TM-Sprayer, HTX Technologies) was used to deposit the matrix solution over the dried brain tissue samples. The nozzle distance was 46 mm, and the spraying temperature was set to 95 °C. Following, the reagent was sprayed (18 passes) over the tissue sections at a linear velocity of 700 mm/min with a flow rate set to 0.1 mL/min and a nitrogen pressure set at 10 psi. After each pass, a holding time of 10 s was preset on the spraying machine to give time for the sample to dry completely before the next pass was about to start. The slide had a yellow/whitish frosted appearance when the deposition of matrix was completed.

The mass spectrometry imaging data acquisition was performed on a MALDI LTQ Orbitrap XL mass spectrometer (Thermo Fisher Scientific, Bremen, Germany) by applying a method that employed 10 laser shots at 14 μJ. The tissue surface was sampled with a spatial resolution of 50 μm. Full scans in profile mode in a mass ranging from m/z 200 to 400 were initially generated in the Orbitrap in positive polarity. The following scan event that produced collision-induced dissociation (CID) fragmentation MS/MS spectra in a mass ranging from m/z 250 to 320 performed in the linear ion trap in positive polarity.

Molecular images of the drug distribution in dessert locust were generated and analyzed using ImageQuestTM software (Thermo Fisher Scientific, San José, CA) from the raw MS raw files. CLO, NDMC, and CNO parent ions and their corresponding fragments ions (m/z 270.167 for CLO as well as for NDMC and m/z 299.167 for CNO) were extracted to determine their localization within the tissue sections. Screenshots were taken of the distribution of CLO (m/z 327.138), NDMC (m/z 313.123) and CNO (m/z 343.134) parent ions and of their fragment ions. The scale of the color patterns in the generated images was used to estimate the relative abundance of a drug within a tissue sample.

H&E staining was used to compare the histochemical method result data obtained with some of the imaging experiments, and histological structures were attained according to methodology published in previous work.[30]

ASSOCIATED CONTENT

Supporting Information

The Supporting Information is available free of charge on the ACS Publications website at DOI: 10.1021/acschemneuro.7b00459.

MALDI MS/MS spectra (FTMS and ITMS) of CLO, NDMC, and CNO; overlays between H&E images and corresponding ion intensity maps (PDF)

AUTHOR INFORMATION

Corresponding Author

*E-mail: roger.olsson@med.lu.se.

ORCID

Melinda Rezeli: 0000-0003-4373-5616

Roger Olsson: 0000-0002-7107-3472

Author Contributions

R.O. and G.M.V designed the study. K.H. performed brain dissections and drug incubations. M.V. performed CLO, NDMC and CNO MALDI studies, H&E histology and analyzed data. Y.S. and T.O. performed CLO MALDI studies and corresponding H&E histology. R.O. and M.V. drafted the manuscript, F.E., G.M.V., T.O., K.H., Y.S., M.W. and R.O conducted critical revision of the manuscript. M.R. sustained mass spectrometry assistance.

Funding

We thank the Swedish Research Council for funding, grants (2015-03296) and (2016-05863) and Lund University for generous financial support. This work was also supported by grants from the National Research Foundation of Korea, funded by the government of the Republic of Korea.

Notes

The authors declare no competing financial interest.

ACKNOWLEDGMENTS

The authors are thankful to Stanley Heinze for his expertise and advice regarding locust anatomy and Alexander Rappensberger for technical expertise.

REFERENCES

(1) Pardridge, W. M. (2005) The Blood-Brain Barrier: Bottleneck in Brain Drug Development. *NeuroRx 2*, 3−14.

(2) Alavijeh, M. S., Chishty, M., Qaiser, M. Z., and Palmer, A. M. (2005) Drug Metabolism and Pharmacokinetics, the Blood-Brain Barrier, and Central Nervous System Drug Discovery. *NeuroRx 2*, 554−571.

(3) Meyer, R. P., and Gehlhaus, M. (2010) A role for CYP in the drug−hormone crosstalk of the brain. *Expert Opin. Drug Metab. Toxicol. 6*, 675−687.

(4) Miksys, S., and Tyndale, R. F. (2013) 2011 CCNP Heinz Lehmann Award paper: Cytochrome P450−mediated drug metabolism in the brain. *Journal of Psychiatry & Neuroscience: JPN 38*, 152−163.

(5) Agarwal, V., Kommaddi, R. P., Valli, K., Ryder, D., Hyde, T. M., Kleinman, J. E., Strobel, H. W., and Ravindranath, V. (2008) Drug Metabolism in Human Brain: High Levels of Cytochrome P4503A43 in Brain and Metabolism of Anti-Anxiety Drug Alprazolam to Its Active Metabolite. *PLoS One 3*, e2337.

(6) García-Suástegui, W. A., Ramos-Chávez, L. A., Rubio-Osornio, M., Calvillo-Velasco, M., Atzin-Méndez, J. A., Guevara, J., and Silva-Adaya, D. (2017) The Role of CYP2E1 in the Drug Metabolism or Bioactivation in the Brain. *Oxid. Med. Cell. Longevity 2017*, 4680732.

DOI: 10.1021/acschemneuro.7b00459
ACS Chem. Neurosci. 2018, 9, 1994−2000

(7) Khokhar, J. Y., and Tyndale, R. F. (2012) Rat Brain CYP2B-Enzymatic Activation of Chlorpyrifos to the Oxon Mediates Cholinergic Neurotoxicity. *Toxicol. Sci. 126*, 325−335.
(8) Khokhar, J. Y., and Tyndale, R. F. (2014) Intracerebroventricularly and Systemically Delivered Inhibitor of Brain CYP2B (C8-Xanthate), Even Following Chlorpyrifos Exposure, Reduces Chlorpyrifos Activation and Toxicity in Male Rats. *Toxicol. Sci. 140*, 49−60.
(9) Hellman, K., Aadal Nielsen, P., Ek, F., and Olsson, R. (2016) An ex Vivo Model for Evaluating Blood−Brain Barrier Permeability, Efflux, and Drug Metabolism. *ACS Chem. Neurosci. 7*, 668−680.
(10) Andersson, O., Hansen, S. H., Hellman, K., Olsen, L. R., Andersson, G., Badolo, L., Svenstrup, N., and Nielsen, P. A. (2013) The Grasshopper: A Novel Model for Assessing Vertebrate Brain Uptake. *J. Pharmacol. Exp. Ther. 346*, 211−218.
(11) Andersson, O., Badisco, L., Hansen, A. H., Hansen, S. H., Hellman, K., Nielsen, P. A., Olsen, L. R., Verdonck, R., Abbott, N. J., Vanden Broeck, J., and Andersson, G. (2014) Characterization of a novel brain barrier ex vivo insect-based P-glycoprotein screening model. *Pharmacol. Res. Perspect. 2*, e00050.
(12) Huber, R., Panksepp, J. B., Nathaniel, T., Alcaro, A., and Panksepp, J. (2011) Drug-sensitive reward in crayfish: An invertebrate model system for the study of SEEKING, reward, addiction, and withdrawal. *Neurosci. Biobehav. Rev. 35*, 1847−1853.
(13) Alexander, G. M., Rogan, S. C., Abbas, A. I., Armbruster, B. N., Pei, Y., Allen, J. A., Nonneman, R. J., Hartmann, J., Moy, S. S., Nicolelis, M. A., McNamara, J. O., and Roth, B. L. (2009) Remote Control of Neuronal Activity in Transgenic Mice Expressing Evolved G Protein-Coupled Receptors. *Neuron 63*, 27−39.
(14) Raper, J., Morrison, R. D., Daniels, J. S., Howell, L., Bachevalier, J., Wichmann, T., and Galvan, A. (2017) Metabolism and Distribution of Clozapine-N-oxide: Implications for Nonhuman Primate Chemogenetics. *ACS Chem. Neurosci. 8*, 1570−1576.
(15) Gomez, J. L., Bonaventura, J., Lesniak, W., Mathews, W. B., Sysa-Shah, P., Rodriguez, L. A., Ellis, R. J., Richie, C. T., Harvey, B. K., Dannals, R. F., Pomper, M. G., Bonci, A., and Michaelides, M. (2017) Chemogenetics revealed: DREADD occupancy and activation via converted clozapine. *Science 357*, 503.
(16) Mendoza, M. C., and Lindenmayer, J. P. (2009) N-Desmethylclozapine: Is There Evidence for its Antipsychotic Potential? *Clin. Neuropharmacol. 32*, 154−157.
(17) Castellino, S., Groseclose, M. R., and Wagner, D. (2011) MALDI imaging mass spectrometry: bridging biology and chemistry in drug development. *Bioanalysis 3*, 2427−2441.
(18) Norris, J. L., and Caprioli, R. M. (2013) Analysis of Tissue Specimens by Matrix-Assisted Laser Desorption/Ionization Imaging Mass Spectrometry in Biological and Clinical Research. *Chem. Rev. 113*, 2309−2342.
(19) Amstalden van Hove, E. R., Smith, D. F., and Heeren, R. M. A. (2010) A concise review of mass spectrometry imaging. *J. Chromatogr. A 1217*, 3946−3954.
(20) Hsieh, Y., Casale, R., Fukuda, E., Chen, J., Knemeyer, I., Wingate, J., Morrison, R., and Korfmacher, W. (2006) Matrix-assisted laser desorption/ionization imaging mass spectrometry for direct measurement of clozapine in rat brain tissue. *Rapid Commun. Mass Spectrom. 20*, 965−972.
(21) Pratavieira, M., da Silva Menegasso, A. R., Garcia, A. M. C., dos Santos, D. S., Gomes, P. C., Malaspina, O., and Palma, M. S. (2014) MALDI Imaging Analysis of Neuropeptides in the Africanized Honeybee (Apis mellifera) Brain: Effect of Ontogeny. *J. Proteome Res. 13*, 3054−3064.
(22) Angel, P. M., and Caprioli, R. M. (2013) Matrix-Assisted Laser Desorption Ionization Imaging Mass Spectrometry: In Situ Molecular Mapping. *Biochemistry 52*, 3818.
(23) Skibiński, R., Trawiński, J., Komsta, Ł., and Bajda, K. (2016) Characterization of forced degradation products of clozapine by LC-DAD/ESI-Q-TOF. *J. Pharm. Biomed. Anal. 131*, 272−280.
(24) Best, J. D., and Alderton, W. K. (2008) Zebrafish: An in vivo model for the study of neurological diseases. *Neuropsychiatr. Dis. Treat. 4*, 567−576.
(25) Vargas, R., Jóhannesdóttir, I. P., Sigurgeirsson, B., Porsteinsson, H., and Karlsson, K. Æ. (2011) The zebrafish brain in research and teaching: a simple in vivo and in vitro model for the study of spontaneous neural activity. *Adv. Physiol. Educ. 35*, 188.
(26) Kantae, V., Krekels, E. H. J., Ordas, A., González, O., van Wijk, R. C., Harms, A. C., Racz, P. I., van der Graaf, P. H., Spaink, H. P., and Hankemeier, T. (2016) Pharmacokinetic Modeling of Paracetamol Uptake and Clearance in Zebrafish Larvae: Expanding the Allometric Scale in Vertebrates with Five Orders of Magnitude. *Zebrafish 13*, 504−510.
(27) Kirla, K. T., Groh, K. J., Steuer, A. E., Poetzsch, M., Banote, R. K., Stadnicka-Michalak, J., Eggen, R. I. L., Schirmer, K., and Kraemer, T. (2016) From the Cover: Zebrafish Larvae Are Insensitive to Stimulation by Cocaine: Importance of Exposure Route and Toxicokinetics. *Toxicol. Sci. 154*, 183−193.
(28) Goyal, N., Praharaj, S. K., Desarkar, P., and Nizamie, H. (2011) Electroencephalographic Abnormalities in Clozapine-Treated Patients: A Cross-Sectional Study. *Psychiatry Invest. 8*, 372−376.
(29) Kikuchi, Y. S., Sato, W., Ataka, K., Yagisawa, K., Omori, Y., Kanbayashi, T., and Shimizu, T. (2014) Clozapine-induced seizures, electroencephalography abnormalities, and clinical responses in Japanese patients with schizophrenia. *Neuropsychiatr. Dis. Treat. 10*, 1973−1978.
(30) Connell, J. J., Sugihara, Y., Török, S., Döme, B., Tóvári, J., Fehniger, T. E., Marko-Varga, G., and Végvári, Á. (2015) Localization of sunitinib in in vivo animal and in vitro experimental models by MALDI mass spectrometry imaging. *Anal. Bioanal. Chem. 407*, 2245−2253.

DOI: 10.1021/acschemneuro.7b00459
ACS Chem. Neurosci. 2018, 9, 1994−2000

Paper II

Tetrahedron Letters 54 (2013) 5266–5268

Contents lists available at SciVerse ScienceDirect

Tetrahedron Letters

journal homepage: www.elsevier.com/locate/tetlet

Enantioselective synthesis of *anti*-β-amido-α-hydroxy esters via asymmetric transfer hydrogenation coupled with dynamic kinetic resolution

Marvin Villacrez [a], Peter Somfai [a,b,*]

[a] Centre for Analysis and Synthesis, Lund University, PO Box 124, 221 00 Lund, Sweden
[b] Institute of Technology, University of Tartu, Nooruse 1, 504 41 Tartu, Estonia

ARTICLE INFO

Article history:
Received 18 June 2013
Revised 6 July 2013
Accepted 19 July 2013
Available online 27 July 2013

Keywords:
Dynamic kinetic resolution
Asymmetric transfer hydrogenation
Ruthenium
Enantioselective
1,2-Amino alcohols

ABSTRACT

The asymmetric transfer hydrogenation of β-amido-α-keto esters providing the corresponding *anti*-β-amido-α-hydroxy esters via dynamic kinetic resolution is reported. The use of a commercially available, or simply prepared, chiral ruthenium catalyst results in good yields as well as high diastereoselectivities and enantioselectivities.

The β-amino-α-hydroxy ester functionality, and the related vicinal amino alcohol moiety, are found in a variety of biologically active natural products.[1] The importance of 1,2-amino alcohols is also well recognized in asymmetric synthesis, where the need for chiral auxiliaries and ligands is continuously increasing.[2] Not surprisingly, the asymmetric synthesis of these structures has received considerable attention.[3]

It has been shown that asymmetric transfer hydrogenation (ATH) coupled with dynamic kinetic resolution (DKR)[4] can be applied to the formation of α-substituted-β-hydroxy esters.[5] In addition, we have previously shown that ATH/DKR of α-amido-β-keto esters **1** offers an efficient entry to *anti*-α-amido-β-hydroxy esters (Scheme 1).[6] This strategy relies on the stereochemical lability of the α-stereocenter in **1**, allowing for two stereocenters to be introduced in the asymmetric reduction. The β-amido-α-hydroxy ester **4** could, in theory, be obtained from **3** using a similar ATH/DKR approach, thus accessing the regioisomeric amino alcohol derivatives. The realization of such a strategy would depend on the rate of racemization of the β-stereocenter in substrate **3**, which must be faster than the rate of transfer hydrogenation. Although this kinetic scenario is indeed operating in the ATH/DKR of ester **1**, it is not obvious that it should also hold true for regioisomer **3**, in which the rate of racemization would be expected to be lower than that in **1**.

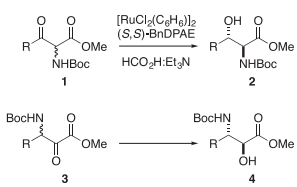

Scheme 1.

In an elegant study, Johnson and co-workers demonstrated that β-alkyl-substituted α-keto esters can be reduced using ATH/DKR to the corresponding β-alkyl-substituted α-hydroxy esters in high yield, distereoselectivity, and enantioselectivity, thus lending considerable support for the proposed conversion of ketone **3** into amido alcohol **4**.[7] More recently, the Johnson group reported the asymmetric synthesis of compound **4** from **3** using an asymmetric transfer hydrogenation coupled with kinetic resolution,[8] which prompted us to report our findings in this area. Herein, we report our results on the enantioselective synthesis of *anti*-β-amido-α-hydroxy esters via ATH/DKR.

We began our investigation of the ATH/DKR of β-amido-α-keto-esters by subjecting substrate **5a**[9] and $[RuCl_2(cymene)]_2$ to a series of 1,2-diphenylethane-1,2-diamine (DPEN) and 2-amino-1,2-diphenylethanol (DPAE) derived chiral ligands in DMF using

* Corresponding author. Tel.: +46 70 6936377; fax: +46 46 2228209.
E-mail address: peter.somfai@chem.lu.se (P. Somfai).

0040-4039/$ - see front matter © 2013 Elsevier Ltd. All rights reserved.
http://dx.doi.org/10.1016/j.tetlet.2013.07.100

Table 1
Asymmetric transfer hydrogenation of **5a**[a]

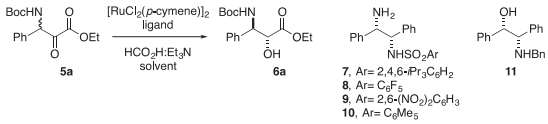

Entry	Ligand	Solvent	Yield[b] (%)	Time (h)	dr[b]	er[c]
1	**7**	DMF	95	1	>20:1	94:6
2	**8**[d]	DMF	95	1	>20:1	95:5
3	**9**	DMF	73	5	>20:1	78:22
4	**10**	DMF	97	1	>20:1	81:19
5	**11**	DMF	88	0.5	>20:1	83:17
6	**8**[d]	Toluene	90	1	>20:1	90:10
7	**8**[d]	DMSO	94	1	>20:1	94:6
8	**8**[d]	Et_3N:HCO_2H (2:5)	93	1	>20:1	92:8
9[e]	**8**[d]	H_2O:CH_2Cl_2	95	1	3:1	n.d.[f]

[a] Reactions performed by heating $[Ru(cymene)Cl_2]_2$ (0.05 equiv) and the ligand (0.15 equiv) in 2-propanol (*c* 0.1 M) at 80 °C for 1 h. After cooling to rt the solvent was removed and the catalyst was added to a solution of **5a** (1 equiv, *c* 0.1 M) and HCO_2H/Et_3N (5:2, 5 equiv).
[b] Yield and dr determined by ^1H NMR spectroscopy of the crude reaction mixture.
[c] Determined by chiral HPLC analysis of the crude reaction mixture.
[d] Commercially available RuCl[(*R*,*R*)-FsDPEN](*p*-cymene) was used.
[e] Reaction was performed using emulsion conditions, see Ref. 6b.
[f] Not determined.

Table 2
Substrate scope of the ATH/DKR reaction[a]

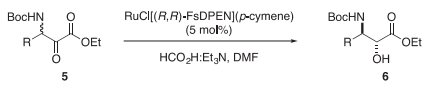

Entry	**5**, R=	Yield[b] (%)	Time (h)	er[c]
1	**a**, Ph	95	1	95:5
2	**b**, *p*-$MeOC_6H_4$	96	1	98:2
3	**c**, *p*-MeC_6H_4	96	1	94:6
4	**d**, *p*-FC_6H_4	89	2	99:1
5	**e**,*o*-BrC_6H_4	78	2	94:6
6	**f**, *m*-BrC_6H_4	68	2	62:38
7	**g**, 3-Thienyl	92	1	94:6

[a] To a solution of the substrate (1 equiv) in DMF (*c* 0.1 M) was added RuCl[(*R*,*R*)-FsDPEN](*p*-cymene) (5 mol %) and HCOOH/Et_3N (5:2, 5 equiv), and the resultant mixture was stirred at rt for the indicated time.
[b] Yield and dr (>20:1 in each case) determined by ^1H NMR spectroscopy of the crude reaction mixture.
[c] Determined by chiral HPLC analysis of the crude reaction mixture.

HCO_2H:Et_3N as the reducing agent (Table 1, entries 1–5). In all cases the corresponding β-amido-α-hydroxy ester **6a** was obtained in good yield and excellent diastereoselectivity, favouring the *anti* diastereomer.[10] The optimal conditions used the pentafluorinated DPEN derivative **8** as ligand, affording **6a** in 95:5 er (Table 1, entry 2).[11] Next, the influence of changing the solvent on the reaction outcome was investigated, but solvents other than DMF resulted in inferior results (entries 2 and 6–9). Several aspects of this reaction are noteworthy. Compared to the ATH/DKR of the regioisomeric α-amido-β-keto esters, which normally take 1–7 days to reach completion, the present transfer hydrogenation of **5a** reached completion within 1 h when conducted in DMF and using chiral ligand **8** (entry 2). This difference in reactivity is perhaps due to the increased electrophilicity of the α-carbonyl carbon in **5a** compared to that of the regioisomeric β-carbonyl derivative, resulting in a faster reduction. It was also noted that the dr of the reaction decreased upon prolonged reaction time, going from dr >20:1 (*anti*:*syn*) when the reaction was terminated after 1 h to 3:1 (*anti*:*syn*) when it was allowed to stand overnight. It is believed that this is the result of epimerization of the α-stereocenter under the reaction conditions and that the dr obtained after prolonged reaction times represents the equilibrium value under the present conditions. Furthermore, **6a** was not stable during purification by flash chromatography on silica gel resulting in a 40–50% isolated yield, compared to 95% yield as determined by ^1H NMR spectroscopy of the crude reaction mixture using an internal standard.

With the optimized conditions in hand the scope of the reaction was examined and the performance of several aromatic substrates **5a–g** was investigated (Table 2).[12] Both electron-rich (entries 2 and 3) and electron-poor (entry 4) aromatics performed well, affording the corresponding *anti*-amino alcohols as the only detectable diastereomer in good yields and high er. Somewhat surprisingly, the *m*-bromo derivative **5f** was reduced with only modest er, while the corresponding *o*-bromo compound **5e** yielded amino alcohol **6e** in high er. It was also noted that the heteroaromatic substrate **5g** was tolerated under the reaction conditions, affording **6g** in good yield and selectivity.

In conclusion, a rapid and straightforward diastereo- and enantioselective synthesis of *anti*-β-amido-α-hydroxy esters via ATH/DKR of the corresponding β-amido-α-keto esters has been developed. The present protocol makes use of a commercially available ligand–catalyst complex, thus making it easy and operationally straightforward to perform.

Acknowledgment

The authors would like to thank Lund University and the Estonian Ministry of Education (project no. SF0180073s08) for funding.

References and notes

1. (a) Ager, D. J.; Prakash, I.; Schaad, D. R. *Chem. Rev.* **1996**, *96*, 835–876; (b) Bergmeier, S. C. *Tetrahedron* **2000**, *56*, 2561–2576; (c) Karjalainen, O. K.; Koskinen, A. M. P. *Org. Biomol. Chem.* **2012**, *10*, 4311–4326.
2. (a) Seyden-Penne, J. *Chiral Auxiliaries and Ligands in Asymmetric Synthesis*; Wiley: New York, 1995; (b) Boto, A.; Romero-Estudillo, I. *Org. Lett.* **2011**, *13*, 3426–3429.

3. (a) Tao, B.; Schlingloff, G.; Sharpless, K. B. *Tetrahedron Lett.* **1998**, *39*, 2507–2510; (b) Shivani; Pujala, B.; Chakraborti, A. K. *J. Org. Chem.* **2006**, *72*, 3713–3722.
4. Pellissier, H. *Tetrahedron* **2003**, *59*, 8291–8327.
5. (a) Makino, K.; Iwasaki, M.; Hamada, Y. *Org. Lett.* **2006**, *8*, 4573–4576; (b) Makino, K.; Goto, T.; Hiroki, Y.; Hamada, Y. *Tetrahedron: Asymmetry* **2008**, *19*, 2816–2828; (c) Hamada, Y.; Koseki, Y.; Fujii, T.; Maeda, T.; Hibino, T.; Makino, K. *Chem. Commun.* **2008**, 6206–6208; (d) Hamada, Y.; Makino, K. Stereoselective Synthesis of *anti*-β-Hydroxy-α-Amino Acids Using *anti*-Selective Asymmetric Hydrogenation In *Asymmetric Synthesis and Application of α-Amino Acids*; American Chemical Society, 2009; Vol. 1009, pp 227–238.
6. (a) Seashore-Ludlow, B.; Häcker, C.; Somfai, P. *Org. Lett.* **2010**, *12*, 5274–5277; (b) Seashore-Ludlow, B.; Saint-Dizier, F.; Somfai, P. *Org. Lett.* **2012**, *14*, 6334–6337; (c) Seashore-Ludlow, B.; Villo, P.; Somfai, P. *Chem. Eur. J.* **2012**, *18*, 7219–7223.
7. Steward, K. M.; Corbett, M. T.; Goodman, C. G.; Johnson, J. S. *J. Am. Chem. Soc.* **2012**, *134*, 20197–20206.
8. Goodman, C. G.; Do, D. T.; Johnson, J. S. *Org. Lett.* **2013**, *15*, 2446–2449.
9. Compounds **5a–g** were prepared according to known procedures, see: Zhao, Y.; Jiang, N.; Chen, S.; Peng, C.; Zhang, X.; Zou, Y.; Zhang, S.; Wang, J. *Tetrahedron* **2005**, *61*, 6546–6552.
10. The relative stereochemistry was determined by conversion into the corresponding oxazolidinone and ^{1}H NMR analysis of the relevant *J* coupling values. See: Tomasini, C.; Vecchione, A. *Org. Lett.* **1999**, *1*, 2153–2156.
11. The absolute stereochemistry of **6a** was determined by comparing its optical rotation, $[\alpha]_D^{25}$ −82 (*c* 0.3, $CHCl_3$), with literature data, $[\alpha]_D^{25}$ −81.5 (*c* 0.3, $CHCl_3$); see Ref. 8.
12. *Typical experimental procedure:* Reduction of **5a**: A solution of **5a** (30 mg, 0.1 mmol) in DMF (1 mL) was transferred to a vial containing RuCl[(*R*,*R*)-FsDPEN](*p*-cymene) (3.5 mg, 4.9 μmol) After stirring for 10 min, HCO_2H/Et_3N (40 μL, 0.5 mmol) was added. Upon completion of the reaction, the mixture was diluted with Et_2O (5 mL) and H_2O (5 mL), the phases were separated and the aqueous layer was extracted with Et_2O (3 × 5 mL). The organic phase was dried (Na_2SO_4) and concentrated. ^{1}H NMR analysis of the crude reaction mixture indicated a 95% yield (2-methoxynaphthalene as the internal standard). The residue was purified by flash chromatography (15% EtOAc:heptane) to give **6a** as a white solid (20 mg, 65%). ^{1}H NMR (400 MHz, $CDCl_3$): δ 7.34–7.23 (m, 5H), 5.62–5.60 (d, *J* = 8.5 Hz, 1H), 5.12–5.10 (d, *J* = 8.5 Hz, 1H), 4.58 (br s, 1H), 4.19–4.07 (m, 2H), 2.90–2.89 (d, *J* = 6.7 Hz, 1H), 1.43 (s, 9H), 1.26–1.23 (t, *J* = 7.15 Hz, 3H); ^{13}C NMR (100 MHz, $CDCl_3$): δ 172.0, 153.5, 130.1, 128.1, 129.7, 76.9, 73.1, 62.3, 55.5, 28.3, 14.1.

Manuscript I

A Rapid Construction of an Advanced Tricyclic Intermediate for the Total Synthesis of Aspidophylline A

Marvin Villacrez, Tessie Borg, Virendra Kumbar, Peter Somfai*

Centre for Analysis and Synthesis, Lund University, P.O. Box 124, 221 00 Lund, Sweden

Abstract: *A rapid access to A/B/C ring system in aspidophylline A is presented. The synthesis features i) an aziridination of a cyclic 1,3-diene, ii) a regioselective aminolysis of an aziridine, and iii) an intramolecular Heck reaction to accomplish the tricyclic scaffold.*

Key words: aspidophylline A, indole alkaloid, aziridination, Natural product, akuammiline, monoterpene

For decades, indole alkaloids of natural origin have constituted a group of substances offering great interest to synthetic organic chemists and hence driving the development of novel and innovative methodology within the field of total synthesis.[1] One of these indole alkaloids, aspidophylline A (**1**), was isolated in 2007 by Kam and co-workers from the Malayan *Kopsia Singaporensis* and was shown to reverse drug resistance in cancer resistant cells (Figure 1)[2]. Aspidophylline A belongs to the family of akuammiline monoterpene indole alkaloids which also includes other polycyclic natural compounds such as vincorine[3] (**2**), strictamine[4, 5] (**3**), and scholarisine A[5] (**4**) *inter alia,* figure 1.[6]

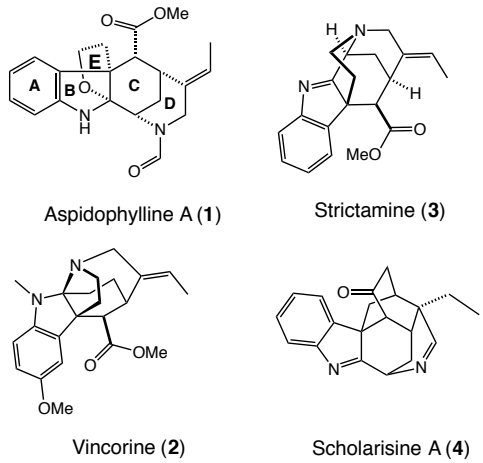

Figure 1: Members of the family of akuammiline monoterpene indole alkaloids.

A noteworthy feature of aspidophylline A is the intricate pentacyclic framework that incorporates a [3.3.1] bicycle with five contiguous stereogenic centres, one of which is an all-carbon quaternary one. Due to its attractive molecular architecture and promising biological activity, three total syntheses and one approach to the pentacyclic core of (**1**) have been reported to date[7]. The first total synthesis of (**1**) was accomplished by Garg and co-wokers in 2011. Their route proceeded in 18 steps and implicated an elegant late-stage interrupted Fisher indolization as the key step to install the furoindoline motif and accomplish the complete pentacyclic framework of compound 1[8]. In 2014, the two remaining approaches for the total synthesis of (**1)** were published. The synthetic route by Ma and colleagues featured an intramolecular oxidative coupling to generate a tetracyclic A/B/C/E ring system, followed by a nickel-mediated cyclization to introduce the remaining D ring.[9] The approach by Zhu and co-workers involved an intramolecular azidoalkoxylation of an enecarbamate yielding the A/B/C/E ring system, similar to the one used in the Ma approach.[6] Completion of the synthesis was achieved by using an intramolecular Michael reaction to install the remaining D ring. In addition, an approach to the pentacyclic core of **1** was developed by Shi and co-workers in 2013.[10]

Herein, we wish to report the development of a 5-step route to the tricyclic A/B/C ring system **8** which is an important intermediate in our ongoing studies towards the total synthesis of **1**. We planned to assemble compound **8** through an intramolecular Heck reaction of diamine **7**, which, in turn, should be available from aziridine 6 by a regio- and stereoselective aminolysis reaction. Finally, intermediate **(6)** was predicted to be derived from the 1,3-diene **(5)** by a regioselective aziridination on the least substituted double bond.

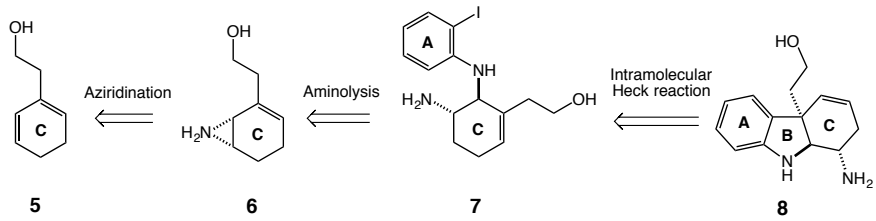

Scheme 1: Retrosynthetic analysis of the tricyclic scaffold **8**.

We launched our synthesis by the elaboration of the conjugated diene **11** (Scheme 2), which was accessible by employing a tandem enyne metathesis procedure developed by Diver and co-workers[11]. The synthesis was conducted by the slow addition of compound **10** to Grubbs second generation catalyst and 1,5-cyclooctadiene. The protected alkyne **10** was formed by treating commercially available alcohol **9** with NaH and TBSCl.

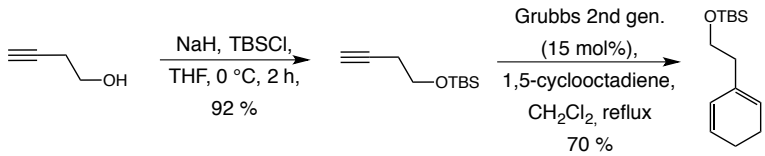

Scheme 2: Synthesis of conjugated diene **11**.

Having assembled the desired conjugated diene **11**, we turned our attention to construction of the aziridine intermediate **13** by applying chemistry developed by Komatsu[12] and co-workers (Scheme 3).[12] This olefin aziridination reaction was performed by means of nitridomanganese complex **12** which afforded insertion of the nitrogen into the least substituted double bond, *i.e.* the bond expected to possess the lowest reactivity towards metal-nitrene complexes. However, no regioisomer of **13** was found in the crude reaction product. The modest yield of 48 % could be the result of a [4+1] nitrene insertion, believed to compete with the anticipated [2+1] insertion. The ring opening reaction of aziridine **13** with *o*-iodoaniline in DMF at 75 °C turned out to be a successful transformation offering quantitative yields of *trans*-diamine **14**.[13] The completion of A/B/C system was then accomplished by using an intramolecular Heck reaction, affording compound **15** in good yield.[14]

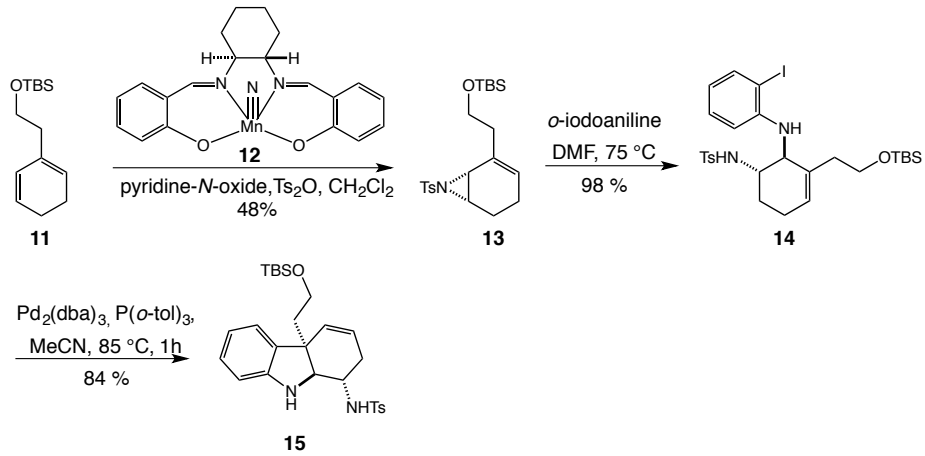

Scheme 3: Completion of the synthesis of compound **15**.

In conclusion, we have developed a 5 step route to the A/B/C tricyclic scaffold **15** present in aspidophylline A (**1**). Key features in our approach is the straightforward installation of the correct relative stereochemistry of **15** through the regioselective opening of aziridine **13**. It also provides rapid access to an advanced intermediate for the studies towards aspidophylline A (**1**). The total synthesis of **1** by using this strategy is actively being pursued in our laboratories.

(1) Bandini, M.; Eichholzer, A. Catalytic Functionalization of Indoles in a New Dimension. *Angewandte Chemie International Edition* **2009**, *48* (51), 9608-9644. DOI: 10.1002/anie.200901843.
(2) Subramaniam, G.; Hiraku, O.; Hayashi, M.; Koyano, T.; Komiyama, K.; Kam, T.-S. Biologically Active Aspidofractinine, Rhazinilam, Akuammiline, and Vincorine Alkaloids from Kopsia. *Journal of Natural Products* **2007**, *70* (11), 1783-1789. DOI: 10.1021/np0703747.
(3) Zi, W.; Xie, W.; Ma, D. Total Synthesis of Akuammiline Alkaloid (−)-Vincorine via Intramolecular Oxidative Coupling. *Journal of the American Chemical Society* **2012**, *134* (22), 9126-9129. DOI: 10.1021/ja303602f.
(4) Ahmad, Y.; Fatima, K.; Atta ur, R.; Occolowitz, J. L.; Solheim, B. A.; Clardy, J.; Garnick, R. L.; Le Quesne, P. W. Structure and absolute configuration of strictamine and strictalamine from Rhazya stricta. Stereochemistry of the Picralima alkaloids. *Journal of the American Chemical Society* **1977**, *99* (6), 1943-1946. DOI: 10.1021/ja00448a041.
(5) Smith, M. W.; Snyder, S. A. A Concise Total Synthesis of (+)-Scholarisine A Empowered by a Unique C–H Arylation. *Journal of the American Chemical Society* **2013**, *135* (35), 12964-12967. DOI: 10.1021/ja406546k.
(6) Ren, W.; Wang, Q.; Zhu, J. Total Synthesis of (±)-Aspidophylline A. *Angewandte Chemie International Edition* **2014**, *53* (7), 1818-1821. DOI: 10.1002/anie.201310929.
(7) Smith, J. M.; Moreno, J.; Boal, B. W.; Garg, N. K. Cascade Reactions: A Driving Force in Akuammiline Alkaloid Total Synthesis. *Angewandte Chemie International Edition* **2015**, *54* (2), 400-412. DOI: https://doi.org/10.1002/anie.201406866.
(8) Zu, L.; Boal, B. W.; Garg, N. K. Total Synthesis of (±)-Aspidophylline A. *Journal of the American Chemical Society* **2011**, *133* (23), 8877-8879. DOI: 10.1021/ja203227q.
(9) Teng, M.; Zi, W.; Ma, D. Total Synthesis of the Monoterpenoid Indole Alkaloid (±)-Aspidophylline A. *Angewandte Chemie International Edition* **2014**, *53* (7), 1814-1817. DOI: 10.1002/anie.201310928.

(10) Li, Q.; Li, G.; Ma, S.; Feng, P.; Shi, Y. An Approach to the Skeleton of Aspidophylline A. *Organic Letters* **2013**, *15* (11), 2601-2603. DOI: 10.1021/ol4007713.
(11) Peppers, B. P.; Kulkarni, A. A.; Diver, S. T. Functional Group Scope in the Methylene-Free, Tandem Enyne Metathesis. *Organic Letters* **2006**, *8* (12), 2539-2542. DOI: 10.1021/ol060727d.
(12) Nishimura, M.; Minakata, S.; Thongchant, S.; Ryu, I.; Komatsu, M. Selective [2+1] aziridination of conjugated dienes with a nitridomanganese complex: a new route to alkenylaziridines. *Tetrahedron Letters* **2000**, *41* (36), 7089-7092. DOI: http://dx.doi.org/10.1016/S0040-4039(00)01219-3.
(13) Olofsson, B.; Somfai, P. Divergent Synthesis of d-erythro-Sphingosine, l-threo-Sphingosine, and Their Regioisomers. *The Journal of Organic Chemistry* **2003**, *68* (6), 2514-2517. DOI: 10.1021/jo0268254.
(14) Koizumi, H.; Yokoshima, S.; Fukuyama, T. Total Synthesis of (−)-Morphine. *Chemistry – An Asian Journal* **2010**, *5* (10), 2192-2198. DOI: 10.1002/asia.201000458.

An Organic Chemistry Odyssey

MARVIN VILLACREZ, originally from Huacho, Peru, found a sanctuary amidst the picturesque landscapes of Söderåsen in Billesholm during his early childhood. It was the legacy of Carl von Linné and the abundant natural wonders surrounding him, that ignited his passion for natural sciences. After earning a master's degree in organic chemistry under the guidance of Professor K. Wärnmark at Lund University, he had the privilege to pursue doctoral studies under the esteemed Professor P. Somfai. Later, he had the fortune of conducting multidisciplinary research in Professor R. Olsson's laboratory, delving into the realms of organic chemistry, neuroscience, pharmacology, and analytical techniques.

This thesis condenses my doctoral studies and comprises two parts. In the initial segment, the gold standard antipsychotic, clozapine, is studied in an isolated brain. Our research revolves around the revolutionary mapping technique of Imaging Mass Spectrometry, which is capable of generating detailed maps of the chemical landscape within biological samples.

The second part of this thesis presents an efficient approach for the asymmetric synthesis of vicinal amino alcohols and our attempts towards the total synthesis of the natural product Aspidophylline A.

Printed by Media-Tryck, Lund 2024 NORDIC SWAN ECOLABEL 3041 0903

LUND UNIVERSITY

ISBN 978-91-8096-034-2

Centre for Analysis and Synthesis
Department of Chemistry
Faculty of Science
Lund University

9 789180 960342